研究成果報告書

一般研究集会（課題番号：2023WS-05）

「スロー地震から海溝型地震へのプロセスの理解と地震災害軽減を目指して」

令和　5　年　9　月　13～15　日

東京大学　伊藤謝恩ホール

【 報告書 】

令和　６ 年　６月　７日

一般研究集会（ 課題番号 ： 2023WS-05 ）

京都大学防災研究所長　殿

［申請者（研究代表者)］

氏　　名　：北　佐枝子

職　　名　：主任研究員

所属機関名：国立研究開発法人　建築研究所

下記のとおり、研究集会の実施結果について報告します。

記

集会名：　スロー地震から海溝型地震へのプロセスの理解と地震災害軽減を目指して

主催者名：　※共催の場合

研究代表者：北　佐枝子

所属機関名：国立研究開発法人　建築研究所

所内担当者名：伊藤 喜宏

開催日：令和　5　年　9　月　13～15　日

開催場所：東京大学　伊藤謝恩ホール

参加者数：229 名

・大学院生の参加形態　［ 口頭発表, ポスター発表, 聴講, 運営補助 ］

研究及び教育への波及効果について

国際研究集会において、将来の発生が予測される南海トラフ巨大地震の本震と周囲で発生するスロー地震との関連性について、同様に発生が予測される関東地震に関する研究成果について最新の知見を共有することができた。特に、国内外の観測・調査・実験・技術開発・理論・モデリングについて、地震学・測地学・地質学・物理学分野など、幅広くかつ学際的な視点で議論を行右ことができた。研究集会は英語で行われ、大学院生・若手研究者・外国出身の若手研究者からも積極的な発言が得られた。若手研究者らの多くは、令和３年 10 月より採択された学術変革領域研究(A)「Slow-to-Fast 地震学」に分担者・研究協力者として参加しており、彼らの人的ネットワーク構築に際して本研究集会と関連イベントが大きく貢献した。また、大学院生や若手研究者からは、研究者間の交流促進についての積極的な提言が相次ぎ、研究集会がポストコロナの研究コミュニティーの活性化に貢献しており、来年以後にも期待したいとの意見が寄せられた。

研究集会報告

(1)目的

将来の南海トラフ巨大地震等の発生を見据え、海溝型巨大地震とスロー地震の関係について最先端の研究成果を持ち寄り、今後のスロー地震・海溝型地震研究の方向性や、研究成果の減災への活用について議論し、共通認識を得ることを目的とする。科研費学術変革領域研究（A)「Slow-to-Fast 地震学」および東大地震研とも共催し、特にダイバーシティー推進や次世代育成を意識して国内外から参加者を募り、地震学・測地学・地質学・物理学・情報科学などの分野を横断し、集中的に知見を議論する。

(2)成果のまとめ

本研究集会では、科研費学術変革領域研究（A)「Slow-to-Fast 地震学」の参画者及び国内外の幅広い分野の研究者が集った。海溝型巨大地震とスロー地震との関係性に関する議論の高度化、巨大地震災害の軽減のための研究成果の活用への議論、今後の課題の抽出などがなされた。特に、上記研究プロジェクトの中間評価を控え、今後どのように若手の研究活動を促進方策について様々な世代間での意見交換が積極的になされた。旅費申請に関しては、特にダイバーシティ推進を意識した上で分野融合に長けた外国人研究者を招聘し、人的ネットワークの拡充などの中長期的な波及効果を狙ったが、集会では若手の積極的な活動・発言が見受けられた。会議はオンライン上でも同時公開され他ため、参加者の裾野がより広い国内外に広がることが可能となった。今回の集会をもとに、世界をリードする国際的な地震研究コミュニティの発展が期待される。

(3)プログラム

別紙1

(4)研究成果の公表

研究集会の概要やアブストラクトについては，以下のサイトから参照・ダウンロード可能となっている.

日本語　https://sites.google.com/view/slow2fast-earthquake-workshop/japanese

英語　https://sites.google.com/view/slow2fast-earthquake-workshop/english

また、別紙2を参照されたい

(5)参加者名簿

別紙3

M~7 inland earthquakes at anomalously deep focal depth and their relationship with seismic velocity and attenuation structure beneath Hidaka collision zone, northern Japan

Saeko Kita[1,2]

[1]IISEE, Building Research Institute (BRI), National Research and Development agency
[2]National Graduate Institute for Policy Studies (GRIPS)

In northern Japan, a Kuril forearc sliver migrates westward and collapses with the Northeastern Japan arc beneath the south-central Hokkaido, making a Hidaka collision zone. In this region, M~7 inland earthquakes occurred repeatedly at a recurrence interval of approximately 40 years. Depths of the mainshocks are located at depths of 20-40 km, though D90 is ~15km [Omuralieva et al. 2012] beneath the Japan archipelago. In order to reveal a cause of these anomalously deep and large inland earthquakes, detailed seismic velocity and attenuation structures were imaged beneath Hokkaido, by merging waveform data from a dense permanent seismic network with those from a very dense temporary network.

Inhomogeneous seismic velocity and attenuation structures are clearly imaged beneath the south-central Hokkaido. A broad low-Qp and low-V zone is located at depths of 0–60km to the west of the Hidaka main thrust. The fault planes of the 1970 M6.7 and 1982 M7.1 earthquakes are located at the edges of this broad low-Qp and low-V zone. The images of velocity structure have high resolution (~10 km), indicating that several smaller-scale high-velocity zones are located at depths of 0–35 km and distributed at the deeper extension of geological boundaries. The clearest high-velocity zone is located beneath the Hidaka metamorphic belt and is in contact with the eastern edge of the broad low-velocity zone. The boundary between the clearest high-velocity and the broad low-velocity zones corresponds to the fault plane of the 1970 M 6.7 Hidaka earthquake. The western boundary of another small high-velocity zone, at depths of 20 to 30 km within the broad low-velocity zone, corresponds to the fault plane of the 1982 M 7.1 Urakawa-oki earthquake.

The mainshock and its aftershocks of the 2018 M 6.7 Hokkaido Iburi-Tobu inland earthquake are located at depths of 10 to 40 km within the lower crust of the anomalous deep and thickened crust near the uppermost mantle material intrusions in the northwestern edge of this Hidaka collision zone. Like the two previous M~7 events, the aftershocks of this event appear to be distributed in the deeper extension of the Ishikari-teichi-toen fault zone. The aftershock alignment is located at the western edge of the high-attenuation (low-Qp) and low-V zone.

These observations suggest that these three large and anomalously deep inland earthquakes occurred at sharp material boundaries (maybe roots of fault system) under a NE-SW compressional stress field caused by the arc-arc collision process. Based on a comparison with heat flow studies [Tanaka 2004], these M~7 events and their aftershocks with anomalously depth focal depths could be caused by the locally lower temperature in south-central Hokkaido.

References: Kita (2019, EPS); Kita et al. (2012, JGR); Kita et al. (2014, JGR)

Geofluid behavior prior to 2018 Hokkaido eastern Iburi earthquake based on groundwater geochemistry

Zahra Zandvakili[1], Yoshiro Nishio[1], Yuji Sano[1]

[1]Marine Core Research Institute, Kochi University

Geofluids are known to be involved in large earthquakes. However, our understanding of the behavior of fluids in the subsurface prior to the actual occurrence of a major earthquake is extremely limited. Geophysical information such as seismic wave velocity structure and electrical conductivity is extremely useful for understanding the distribution of subsurface fluids over a wide area, and is the primary method used in subsurface fluid studies. However, it is not suitable for detecting time-series changes in fluid volume within a limited area, such as geofluid behavior before a large earthquake. On the other hand, geochemical observation of groundwater is effective in identifying the origin of fluids and may reveal traces of mixing of fluids of different origins before a large earthquake. Thus, knowledge from geophysical and geochemical observations can compensate for each other's weaknesses and provide a higher level of understanding of the behavior of geofluids prior to major earthquakes. However, it is extremely difficult to routinely observe groundwater geochemistry prior to a large earthquake. Using commercially available bottled drinking water, Tsunogai and Wakita (1995) revealed an increase in chloride ion concentrations in groundwater before the M7.2 1995 Kobe earthquake. Using a similar approach, Sano and his group have focused on the isotopic composition of volatile elements such as hydrogen, oxygen, and carbon in groundwater prior to several major earthquakes (Sano et al., 2020, Onda et al., 2018). Among the reports of Sano group, Sano et al. (2020) point out that changes in carbon isotope ratios observed a few months before the M6.7 earthquake in eastern Hokkaido, Japan, in 2018, may have caused the influx of carbon dioxide into groundwater. To further explore the origin of the CO_2-fluid that entered the groundwater prior to this 2018 eastern Hokkaido earthquake, we examined time-series changes in the isotopic ratios of the nonvolatile elements Li and Sr, which are leading indicators of the origin of the fluid in the groundwater. The results of this study indicate that the CO_2 injected into the groundwater near the epicenter before the earthquake, as revealed by Sano et al. (2020), was not accompanied by water originating from deep underground.

Searching for Very Low Frequency Earthquakes (VLFE) around Western Kuril Trench

Novia Anggraini[1], Hiroaki Takahashi[1]

[1]Institute of Seismology and Volcanology, Hokkaido University

Very Low Frequency Earthquake (VLFE) is one kind of slow earthquake that occurs dominantly in a transition zone between a seismogenic zone and a stable sliding zone and has frequency of 0.02-0.05 Hz. This slow slip has been detected in subduction zones in Japan, such as around Ryukyu Trench, Nankai Trough, and Japan Trench. Meanwhile, around Kuril Trench, activity was detected in the southern part of the trench, around Tokachi (Asano, et al., 2008). Recently, Baba et al., (2020) tried to detect the activity in the other part of the trench which is around Nemuro but the detections were dominated by false detections. In this study, we try to check the detection catalog of Baba et al., 2020 for duration from March 2007 to July 2018 to find the activity of VLFE around the western Kuril Trench. The waveforms are generated from F-net stations located on the Pacific coast of Japan and 5 additional distant stations from IRIS. Then, resampled one sample per second, and filtered by a bandpass filter with a frequency of 0.02-0.05 Hz. The waveforms are checked visually, and the epicenter location is estimated using Particle Motion plot. Initially, we obtained six candidates for VLFE. However, after checking the probability of this event being a surface wave, no VLFE was found. This indicates that the activity of VLFE in this area is low. In addition, the existence of a strongly coupled area also supports the difficulty in detecting VLFE around this area. We plan to continue to check another catalog, which is from NIED, recorded from June 2003 to June 2023.

Acknowledgement We would like to express our gratitude to Satoru Baba (JAMSTEC), Yusuke Yamashita (Kyoto University), and Youichi Asano (NIED) for providing us with the catalogs and waveforms.

The interplay between fast and slow earthquakes and its relation with fluid pressure cycling in a collisional mountain belt

Kate Huihsuan Chen[1], Wei Peng[1], I-Chu Hua[1], Satoshi Ide[2],
Chien-Chih Chen[3], Yaru-Hsu[4]
[1]Dept. of Earth Sciences, National Taiwan Normal Univ.,
[2]Dep. EPS, Univ. Tokyo, [3]Dept. of Earth Sciences, National Central Univ., [4]Institute of Earth Sciences, Academia Sinica

Slow earthquakes are part of the spectrum of aseismic processes that release tectonic stress at greater depth. Their episodic occurrence in subduction zones has been regarded as an important indicator for stress and fluid pressure cycling. Whether the characteristics of fluid generation and migration is different at different tectonic regimes, and how do they influence earthquake cycle however, remain elusive. The active collisional mountain belt in Taiwan provides a unique opportunity to study the association between fluid-flow system and their impact on various earthquake behavior. Using the catalogs of repeating earthquakes, swarm events (fast earthquakes), and tectonic tremors (slow earthquakes) in Taiwan, we attempt to characterize their periodic behavior and spatiotemporal association. Beneath the southern Central Range where the earthquake swarms and tectonic tremors actively occurred at the depth of < 15 km and 15-45 km separately, the repeating events are found to mostly belong to burst-type sequence with extremely short recurrence intervals. In addition, during the earthquake swarms we also observed the low frequency (1-4 Hz) events that are usually interpreted to reflect flow-induced resonance of fluid-filled cracks.

Here, we explore to what extent the wide range of fault slip behaviors (seismic to aseismic events) can be explained by fluids pressure cycling. As the significant seasonal variation peaking in the spring of each year apparent in both the tremor and swarm catalogs, we found 61% tremors and 70% swarm events taking place at the lower ground water level. This is contradictory with opposite clamping effect of hydrological/tidal stresses on thrust faulting (tremor) and normal faulting (swarm) slips. We therefore, suggest that the deep fluids from prograde metamorphic dehydration reactions due to subduction of continental crust of Eurasia is the necessary mechanism for weakening the fault zones at greater depth, which then enables the seasonal hydrological and tidal forcing to have effect on seismic and aseismic activity.

Tectonic tremors in Taiwan, 2012-2022

Satoshi Ide[1] and Kate Huihsuan Chen[2]

[1]Dept. EPS, Univ. Tokyo, [2]National Taiwan Normal Univ.

Tectonic tremors in Taiwan have been discovered since ~15 years ago, as remotely triggered events (Peng and Chao, 2008; Chao et al., 2010) or ambient activities (Chuang et al., 2014; Idehara et al., 2014). While triggered tremors were distributed widely in Taiwan (Chao et al., 2010), ambient tremors were found to highly concentrate in southern Central Range in a cluster of ~10 km radius (Chuang et al., 2014; Ide et al., 2015; Chao et al., 2017; Aguiar et al., 2017; Chen et al., 2018). Based on focal mechanism (moment tensor) analysis and tidal sensitivity of tremors, Ide et al. (2015) suggested a low-angle thrust motion, while Aguiar et al. (2017) proposed a steeply dipping angle based on location of low-frequency earthquakes. To reconcile the two possible fault geometries, Chen et al. (2018) proposed a mechanical model that reconcile the two possible fault geometries as the high angle structure reflecting the dominance buoyancy forces in the subducted hanging wall, while low angle structure representing the failure in the footwall below the shear zone.
Since 2019, continuous seismological data of Central Weather Bureau (CWB) Seismographic Network (CWBSN) have been available for public. We used the data of CWBSN and Broadband Array in Taiwan for Seismology (BATS) to better monitor the tectonic tremors in Taiwan. In this study, we applied the envelope correlation method of Mizuno and Ide (2019) using continuous horizontal velocity seismograms from all available CWBSM and BATS stations from 2012 to 2022. With a large number of seismic stations used in this study and removal of short-lasted events (< 10 s), we successfully detected about 7000 events with waveforms characteristics similar to the tectonic tremors worldwide. Except for the tremor zone previously observed at southern Central Range, we report the new tremor “hotspots” across the mountain range of the island, over a distance of 200 km. The newly catalogued tremors are clustered into five separate zones at the depth range of 20 to 50 km where no earthquakes are present. They are aligned along the eastern flank of the Central Range and at the northern end of the Hsuehshan Range, indicating a strong connection between tremor generation mechanism and mountain building process. Different from the fluid-rich environment previously established for tremors in southern Central Range, the new tremor zones in northern Taiwan however, are characterized by low Vp/Vs and high Qp/Qs. In addition, the five tremor zones are found to coincide with the spots with high geothermal heat flux, indicating that the temperature effect may be the common mechanism for tremor generation in a mountain belt of Taiwan.

Mud Tectonics and Creeping Faults in SW Taiwan

Kuo-En Ching[1], Shih-Han Hsiao[1], Song-Chuen Chen[2], Pei-Ching Tsai[1], Wu-Lung Chang[3], and Yu-Tsung Lo[3]

[1]Dept. Geomatics, Natl. Cheng Kung Univ., [2]CGS, [3]Dept. Earth Sci., Natl. Central Univ.

The existence of mud tectonics has been proposed in SW Taiwan, but the ongoing activity and its interaction with active faults in dominating the surface deformation patterns are still debated. Additionally, the presence of mud diapirs or mud-cored anticlines in SW Taiwan remains to be confirmed. In this study, we proposed that the mud-cored anticlines are the primary structures in SW Taiwan through the regional geomorphological analysis, seismic reflection profiles and surface vertical velocity field. The reverse faults may develop accompanying with mud-cored anticlines. Positive gravity anomalies caused by the dewatered mudstone identify the mud diapirs on the mud-cored anticlines, which are several kilometers in scale. Then the mud diatremes, which are a few to tens of meters in scale, distributed around the mud-cored anticlines near the ground surface could be identified by the damages to artificial constructions and buildings, electrical resistivity survey, or local geomorphological investigations. Mud volcanoes are likely to form if an abundant fluid supply is within the mud tectonics, and a fault passes through this structure. Geological investigations may not provide clear lithological boundaries, as development of the mud tectonics is primarily controlled by overpressured fluids and gas. However, a significant concentration of scaly fabric may be observed at the boundary of mud diapirs or mud diatremes. According to the comparison of horizontal and vertical velocity fields in SW Taiwan, it is possible to identify the aseismic deformation resulted from the mud tectonics. Furthermore, when the active faults pass through the mud tectonics, active crustal faults in SW Taiwan exhibit creeping or partial creeping behavior due to the fluid and gas supplied by mud tectonics. The fault creeping rates could be up to 15 mm/yr in SW Taiwan. Although the coupling is also inferred at the part of shallow segments of faults, which is usually shallower than 2 km, the energy could be released by slow-slip events. Therefore, although the surface deformation rate in SW Taiwan is high, but the earthquake potential may not be as high as previously anticipated.

Dynamic triggering along the Dead Sea Transform uncovers tremor source physics

Asaf Inbal

Dept. of Geophysics, Tel Aviv University, Israel

The 2023 earthquake pair in southeast Türkiye, which consisted of a M_w7.8 followed by a M_w7.6, dramatically altered the seismicity rates in the Palestine Territories and in Israel. The study area, located about 600 km from the Türkish mainshocks, is mostly affected by the Dead Sea Transform (DST), a major plate boundary accommodating about 5 mm/yr of relative motion between the Sinai sub-plate and the Arabic plate. Yet, abundant aftershocks occurred in the weeks following the mainshocks along structures predominantly located off- the main DST fault trace. I will report on tremor occurring along the DST, and a microearthquake on the Carmel-Fari'a Fault (CFF), both dynamically triggered by the 2023 M_w7.6. Surface waves excited by that mainshock also dynamically triggered a repeating aftershock sequence in the Dead Sea basin. Interestingly, the M_w7.8 did not dynamically trigger earthquakes or tremor in the study area. Thus, non-triggering by the M_w7.8 followed by triggering by the M_w7.6 elucidates the physical mechanism driving remote triggering.

The dynamically triggered tremor location coincides with maxima of long-period velocity gradients, concentrated in the CFF-DST intersection and near a CFF fault-jump. A newly acquired S-wave velocity model for the study area suggests the tremor source, which lies at a depth of about 15 km, is located adjacent to a strong lateral velocity discontinuity. That deep structure may have played a role in promoting tremorgenic fault behavior, for example by focusing of the M_w7.6 Love wave energy onto the tremor source region. Relative to other remotely triggered tremors, the DST tremor is strong and deficient in high-frequency seismic energy. Furthermore, analysis of several triggered tremor episodes from other tectonic environments suggests that tremors spectral fall-off rates are not universal. I will discuss the seismological attributes that may give rise to these observations in the context of two models. In the first, tremor is produced due to inertial vibrations of a frictionally-controlled oscillator, and in the second it is produced by a swarm of Low-Frequency Earthquakes.

Effects of subducting seamount on slow and fast seismicity in the Guerrero Seismic Gap, Mexico

Yoshihiro Ito[1], Shukei Ohyanagi[2], Raymundo Plata-Martinez[3], Ketzallina Flores[2], Yanhan Chen[2], and Kentaro Kuniyoshi[2]

[1]DPRI, Kyoto Univ., [2]Graduate School of Science, Kyoto Univ., [3]JAMSTEC

Understanding the physical properties surrounding faults is fundamental for comprehending the mechanisms of both slow and fast earthquakes. The precise estimation of the spatial distributions of slow and fast earthquakes enables us to compare them based on physical properties, such as velocity and density around the sources, while also considering location errors. Recently, ocean bottom seismometers have played a crucial role in detecting and locating the sources of fast and slow earthquakes beneath the sea. We deployed nine to ten ocean bottom seismometers during two observation periods (2017–2018 and 2018–2019), each lasting one year, in the western part of the Guerrero seismic gap in Mexico. Utilizing a modified envelope correlation method for tectonic tremors (Mizuno and Ide, 2019) and the EQTransformer for fast earthquakes (Mousavi et al., 2020), we successfully detected and located instances of slow and fast seismicity.

We conducted a comparison of the epicenters of the slow and fast earthquakes near the trench with residual gravity data. In previous studies (Basset et al., 2015), residual gravity data have been utilized to interpret the shallow subducting slab's surface, leading to the identification of potential features such as subducting bathymetry. Interestingly, we observed that tectonic tremors were predominantly located around an area with a high residual gravity anomaly, rather than within it. This particular region with the high residual gravity anomaly aligns with the source area of the M6.7 earthquake, characterized by low scaled seismic energy and identified as a small tsunami earthquake (Flores et al., 2018; 2023).

Additionally, the other low-seismicity areas also showed a high residual gravity anomaly. We identified a low-seismicity area of fast earthquakes within a region of low residual gravity anomaly, which was previously proposed as a silent zone by Plata-Martinez et al. (2021). Our results suggest that “standard” fast interplate earthquakes and ordinary slow earthquakes have not occurred in the areas with both high and low residual gravity anomalies. However, tsunami earthquakes are possibly occurring within the high residual gravity area near the trench.

These residual gravity anomalies and their correlation with slow and fast earthquakes are possibly controlled by density or porosity complexities within the accretionary wedge, which, in turn, is feasibly affected by subducting seamounts. Numerical modeling has indicated that the area in front of and above a subducting seamount could have a highly under-consolidated accretionary wedge near the surface (Sun et al., 2020). The under-consolidated wedge with a high-porosity or low-density accretionary wedge may control the occurrence of fast and slow earthquakes, such as tsunami earthquakes, microearthquakes, and tectonic tremors.

Fiber optic sensing experiments in the seafloor and seafloor borehole in the Nankai Trough.

Eiichiro Araki[1], Takashi Yokobiki[1], Yuya Machida[1], Hiroyuki Matsumoto[1], Satoru Baba[1], Shuhei Tsuji[1], Shuhei Nishida[1]

[1]JAMSTEC

We would like to utilize optical fiber sensing technology to observe very broadband phenomena occurring at subducting plate boundaries. We are currently conducting observations using submarine optical fiber cables in the seafloor and preparing to install optical fibers in seafloor boreholes.

In the Nankai Trough, subduction of the Philippine Sea Plate has repeatedly caused large earthquakes. It is now also known that slow earthquakes and slow slip occur at the deeper and shallower side of the plate interface of such large earthquakes. Since the slow phenomena on the shallow side occur beneath the seafloor, seafloor observations are particularly important. In the Nankai Trough, submarine cable observation networks such as DONET have been established. In addition, observations in seafloor boreholes are now established by the IODP. Observations in the vicinity of the shallow subduction interface have revealed repeating slow slip events there. However, such observations are still limited to only a few areas in such as off-Kumano.

Distributed optical fiber sensing can measure strain distribution of optical fiber over nearly 100 km at intervals of 1 m. If we can conduct optical fiber sensing using submarine optical fiber cables that span areas where slow earthquakes and slow slip occur, we would be able to study the evolution of slow slip in the plate interface beneath the seafloor more in detail.

Therefore, we have applied two optical fiber sensing techniques, i.e., DAS and TW-COTDR, to the 120-km cable off Muroto across the Nankai Trough subduction zone, started long-term observations. DAS observation in Muroto cable successfully captured and allowed detailed analysis of low frequency tremors in March, 2022 (Baba et al., 2023). We have improved low-frequency performance of the DAS by ultra stable laser aiming observation of further slow processes like VLFEs (Araki et al., 2022) and now the long-term observation of DAS extends up to 110 km from the shore, well expectable to capture shallow VLFEs nearby the submarine cable.

TW-COTDR observation is considered more suitable for slow slip event observation because the technique is free from the effects of rapid optical phase changes during earthquakes, severely influencing in DAS observation. We performed almost a year continuous test observation by the TW-COTDR in Muroto cable. The very long period (> a day) strain change observed by the TW-COTDR showed significant influences from possible seafloor water temperature fluctuations. We performed installation of seafloor thermometers to confirm the relationship between the seafloor temperature and the apparent long-period strain signals observed by the TW-COTDR. As the temperature effect is severely large (~8 microstrain/degC) in comparison with expected seafloor strain caused by slow slip events (~ a microstrain), we need more efforts to correct for the temperature, or eliminate the effects from the temperature.

Optical fiber installation in deep seafloor boreholes would be a clean solution for such temperature noise. We designed a new seafloor borehole observation system which includes optical fiber for distributed optical fiber sensing as well as borehole fiber optic strainmeter which measures a total length of 200 m long sensing optical fiber, not like 10 cm in TW-COTDR measurements. In the borehole observatory design, we also introduced specifically designed optical fiber cable, which enables separation between strain and strain caused by temperature change. We demonstrated the separation in a test borehole observatory in Kamioka land borehole in March, 2023, which clearly showed separation between strain caused by cement consolidation and cooling of the borehole.

We are scheduled to install the new seafloor borehole observatory in off Kii channel by D/V Chikyu in November 2023. Distributed optical sensing in the seafloor borehole (DAS and TW-COTDR) will be performed during the Chikyu cruise as well as the following cruises by R/V Shinsei-maru by connection of the optical fiber through a ROV to the interrogator abord the ship. A shorter fiber length (~ 5 km including ROV cable to the seafloor) enable us to sample the fiber in the borehole in much finer resolution like 10 cm. DTS (distributed temperature sensing) is also planned during the Shinsei-maru cruise to profile the temperature distribution from the seafloor to the bottom of 500 m deep borehole.

Geological constraints on slip duration and slip rate in exhumed accretionary complexes for a comparison in a scaling law of slow earthquakes

Yoshitaka Hashimoto[1], Makoto Okubo[1], Yohei Hamada[2]

[1]Kochi University, [2]JAMSTEC

It has been discussed for many years about the difficulty in comparison between parameters from geological and geophysical observations. The difficulty can mainly come from the different scales in time and space for their observations. We know that there are some scaling laws in nature. The scaling law can be useful to connect the scale difference between geological and geophysical observations.

Ide et al. (2007) provided a scaling low for slow earthquakes. In the study, the scaling law between slip duration and moment magnitudes of slow earthquakes has a specific slope which is different from that for regular earthquakes. This is a scaling law form the geophysical observations.

In geological observations, slip duration and slip rate of faults have been estimated from a diffusion pattern of the paleomaximum temperature as a function of the distance from the faults. Sakaguchi et al. (2001) found the diffusion patterns of vitrinite reflectance in the cores from Nankai Trough. Fulton et al. (2012) and Hamada et al. (2015) simulated the diffusion processes of heat and the maturation of carbonaceous materials during fault slip. Then they successfully constrained the slip behavior such as slip duration and slip rate. Followed by the studies, estimation of slip behaviors for the faults in exhumed accretionary complexes have conducted using the same methods. In this study, we summarized the slip duration and slip rate estimated from the faults in exhumed accretionary complexes (Hashimoto et al., 2016 and Kawaji et al., 2022) then discussed about their slips using the scaling law for slow earthquakes.

The study areas are Nonokawa formation and Yokonami mélange in the Cretacaous Shimanto Belt. Paleo maximum temperatures of them are about 185˚C and 250˚C, which are the baselines of the calculation of thermal diffusion patterns. The thicnkesses of faults are 3.7 mm and 20 cm for each area. In the Yokonami mélange, the 20 cm fault zone includes the thin slip zone (less than 1 mm). The quartz blocks within the fault zone in the Yokonami mélange show dislocation creeps which suggests that the fault zone had a local heating up to 300˚C.

The distribution of vitrinite reflectance (Ro) as a function of the distance from the center of fault zone was examined. They show normally scattered distribution, decreasing patterns in Ro were identified. Using the decreasing pattern, we constrained slip duration (Tr) and heat generation rate (Q) for each fault. Q is equal to slip rate times effective shear stress. Tr and Q for the fault in the Nonokawa formation were 10^4s and $10^{3.9}$J/m^2/s. For the fault zone in the Yokonami mélange, they were $10^{3.4}$s and $10^{4.3}$ J/m^2/s.

In the scaling law for slow earthquakes, moment magnitude can be converted Q. Therefore, Tr and Q can be compared in the scaling law between geological and geophysical observations. The Tr and Q from the geological observations did fit with the scaling law for slow earthquakes, suggesting that the faults slipped as slow earthquake faults. However, the absolute values are smaller than these from the geophysical observations, which may be caused by a sensitivity of the Ro and a scale of the geological observation.

Physical conditions of magmatic-hydrothermal fracturing in deep crust: Records of subvolcanic deep low-frequency earthquakes?

Masaoki Uno[1], Takumi Nara[1], Diana Mindaleva[1], Tetsuo Kawakami[2], Tatsuro Adachi[3], Fumiko Higashino[2], Noriyoshi Tsuchiya[1,4]

[1]Tohoku Univ., [2]Kyoto Univ., [3]Kyushu Univ., [4]Hachinohe college

Apart from plate boundaries, subvolcanic regions are one of the other active sites of slow earthquakes[e.g., 1,2]. Recent geophysical observations have revealed that subvolcanic deep low-frequency earthquakes (DLFEs) in the lower crust are coupled with volcanic earthquakes in the upper crust, suggesting magmatic/hydrothermal fluid flow triggering the earthquakes[e.g., 2]. Here we represent the occurrences of magmatic dikes and hydrothermal mineral veins in a high-temperature metamorphic terrane[e.g., 3–5], show their mode of fracturing, duration of fluid flow, stress state and fluid pressure during their activities, and discuss their relation to the observed seismic activities.

The study area is a high-temperature metamorphic terrane of Sør Rondane Mountains, East Antarctica. High-angle granitic dikes and/or hornblende±biotite veins commonly occur throughout the survey area. The dikes and veins cut the local gneissosity with extensional or extensional-shear displacements, intrude into the granulite-facies rocks, and form hydrous reaction zones along the dikes and/or veins. Reaction zones are characterized by the replacement of the pyroxenes with amphibole and biotite/phlogopite, representing hydration reactions at 600–750°C and ~0.5 GPa to 0.6–0.8 GPa (i.e., 20–30 km depth).

Within the reaction zones, Cl or F concentrations in apatite, biotite and/or amphibole are high within the dike or veins, and decrease towards the host rock. Reactive transport modeling of Cl or F suggests that the duration of fluid activity was on the order of days to months for the dikes, and hours to weeks for the veins.

These observations suggest that extensional and/or extensional shear fracturing is common during the movement of magmatic fluids in the middle-lower crust. The granitic dikes release excess aqueous fluids, raise the local fluid pressure lasting days to months, and subsequently form hornblende±biotite veins within hours to weeks. These depths (20–30 km), temperature (~700°C), duration of high-pressure fluids (hours to months), and the extensional-shear mode of fracturing observed in these dikes/veins are largely comparable to the depth and characteristic duration of the subvolcanic DLFEs[e.g., 2, 6]. The geological observations strongly support non-double couple mechanisms for crustal fracturing in these regions.

[References]

1: Hasegawa et al. (2005) Tectonophysics
2: Yukutake et al. (2019) GRL
3: Uno et al. (2017) Lithos
4: Mindaleva et al. (2020) Lithos
5: Mindaleva et al. (2023) GRL
6: Kurihara and Obara (2021) JGR

Geological tracers of temporal evolution of fluid flow in high-grade metamorphic rocks related to seismic events in the middle crust.

Diana Mindaleva[1], Masaoki Uno[1], Noriyoshi Tsuchiya[1]

[1] Grad. School of Environmental Studies, Tohoku Univ.

Fluid flow in the Earth's crust modifies rock properties and can trigger earthquakes. However, limitations in quantifying fluid volumes and infiltration timescales, along with gaps in understanding time-integrated fluid fluxes from geological specimens and their implications on seismic activity, persist. This study aims to bridge these gaps by integrating fluid infiltration timescales with transport properties from metamorphic reaction zones to understand the fluid flux during crustal fracturing and its influence on controlling seismic/aseismic events.
This study focuses on fluid flow through fractures and fluid-rock reaction zones, specifically in relation to low-magnitude fracturing events like tremors and low-frequency earthquakes. Understanding fluid flow enables the calculation of seismic moment and cumulative magnitude associated with potential seismic/aseismic events.
By analyzing amphibolite-facies fluid-rock reaction zones, the duration of fluid infiltration and time-integrated fluid fluxes are approximated. The findings suggest that flow along a single fracture is compatible with non-volcanic tremor and low-frequency earthquakes. Rapid fluid infiltration (~10 h) occurs due to crustal fracturing and permeability evolution from low- to highly-permeable rocks (~10^{-9}–10^{-8} m^2). We also discuss fluid composition, entrapment process and fluid transport based on evidence from fluid inclusions.
Estimates are made for perpendicular time-integrated fluid fluxes towards fractures and overall fluid flux through the reaction zone. Using reactive-transport modeling and thermodynamic analyses, fluid volumes are determined. Time-integrated fluid flux through the fracture results in $10^{3\text{-}6}$ m^3/m^2. The lower range is similar to the fluxes through the upper crustal fracture zones (~$10^{3\text{-}4}$ m^3/m^2), while the almost whole range is comparable to the contact metamorphism zone (~$10^{2\text{-}5}$ m^3/m^2).
We used the approach introduced by McGarr in 1976, utilizing fluid volumes and shear modulus to estimate cumulative seismic moment. Additionally, we constrain the magnitude using the geometry of a single fracture and make comparisons with two independent methods.
Comparison of fluid volumes transported through fractures with fluid injection experiments provides further insights. Durations of fluid infiltration are compared to durations of slow slip events. Our finding reveals that the transportation of voluminous fluid volumes through a fracture may be related to short seismic/aseismic events such as tremors and LFEs, supported by duration and cumulative magnitude estimates. The findings highlight the importance of single fractures in facilitating voluminous fluid flow and controlling seismic activity in the lower-to-middle crust.

Fluid flow and fluid-rock interactions at shallow mantle wedge

Atsushi Okamoto[1], Kazuki Yoshida[1], Shunya Okino[1], Ryosuke Oyanagi[2]

[1]GSES, Tohoku Univ., [2]Kokushikan Univ.,

The mantle wedge is a unique location where the subducting plate interacts with the overlying mantle, leading to a range of fluid-rock interactions and the transfer of H_2O-CO_2 fluids and elements. In particular, serpentinization and metasomatic reactions play a significant role in influencing fluid pressure and mechanical properties at subduction zone interfaces. However, the relationship between slow earthquakes and fluid-rock interactions is not well understood. In this presentation, we present several geological records of fluid flow and fluid-rock interactions found near the mantle wedge corner and discuss the potential influence on slow earthquakes.

The first example is the antigorite vein networks that developed in hydrated ultramafic rocks in the Oman ophiolite (Yoshida et al., 2023). The Oman ophiolite represents the sequence from the upper crust to the lower crust to the peridotites. These rocks were formed at the mid-ocean ridge and suffered from extensive low-temperature serpentinization, but they also recorded fluid processes at the later stage of subduction zone setting. We analyzed core samples of the crust-mantle transition zones recovered by the Oman Drilling Project. In the samples, antigorite veins that cut the completely serpentinized dunite (lizardite+brucite+magnetite) have brucite-rich reaction zones. The detailed mass balance analysis revealed that these reaction zones were formed by the leaching of silica from the host rocks. By using the coupled thermodynamic and diffusion model, we revealed that the channelized fluid flow was short-lived (2.1×10^{-1} to 1.1×10^{1} years) and had a high fluid flow velocity (2.7×10^{-3} to 4.9×10^{-2} meters second^{-1}). This timescale and fluid flow velocity are similar to the propagation of seismic events in subduction zones related to slow earthquakes. Episodic fluid drainage can result in a decrease in poor fluid pressure, which influences seismicity at the plate boundaries.

The second example is metasomatized serpentinite bodies from the Sanbagawa metamorphic belt in Japan (Okamoto et al., 2021; Okamoto and Oyanagi 2023). The Sanbagawa belt contains numerous ultramafic bodies derived from the mantle wedge, which provide important opportunities to understand the reactions between sediments and the overlying mantle wedge. At the contact between the serpentinite and metasediments, clear reaction zones developed: actinolite + chlorite schists on the side of the serpentinite and chlorite rocks on the sides of the pelitic schists. Talc schists or thin talc vein networks developed within the serpentinite. This suggests that Si transport from the crust to the mantle and Mg transport from the mantle to the crust occur simultaneously (Okamoto and Oyanagi, 2023). Thermodynamic calculations along the subduction zones indicate that the fluid compositions, relative mobility of Si and Mg, and abundances of the sheet silicates (talc versus chlorite) change between the subduction zone geotherms. In addition, the infiltration of CO_2-bearing fluids, if present, effectively causes significant talc formation with the carbonation and dehydration of serpentinites (Okamoto et al. 2021). Our recent experiments on metasomatic reactions at analog crust-mantle boundaries (serpentine/metapelite and peridotite/metapelite) at 500 °C and 1 GPa also indicated the strong effect of CO_2 rather than Si (over 10 times) on talc formation during metasomatism. Talc is a mantle mineral with a low friction coefficient, and its role in earthquakes has been suggested (Hoover et al. 2022).

Metamorphism is a slow process (over 10^3 years) and is treated in the framework of equilibrium thermodynamics. However, the examples presented in this talk and other recent studies have suggested that fluid-mediated metamorphic or metasomatic reactions can be fast relevant to slow earthquakes, which strongly influence the fluid pressure and formation of weak minerals. In particular, fluid composition is important for controlling the reaction types in the source regions of slow earthquakes.

References

Yoshida K, Oyanagi R, Kimura M, Plümper O, Fukuyama M, Okamoto A, 2023. Science Advances, 9, eade6674.
Okamoto A, Oyanagi R, 2023. Progress in Earth and Planetary Science, 10, no. 39.
Okamoto A, Oyanagi R, Yoshida K, Uno M, Shimizu H, Satishkumar M, 2021. Communications Earth & Environment, 2, 151.
Hoover WF, Codit CB, Lindquist, Moser AC, Guevara VE, 2022. Geophysical Research Letters, 49, e2022GL101083.

The potential use of laboratory SSEs as stick-slip precursors in simulated fault gouges

Matt J. Ikari

MARUM Center for Marine Environmental Science and Faculty of Geosciences, University of Bremen, Germany

Since the discovery of geodetically-observed slow slip events (SSEs), the nature of the relationship between SSEs and ordinary earthquakes has become one of the most important questions in earthquake science. Especially intriguing is the observation that SSEs sometimes occur immediately prior to large magnitude earthquakes, within the future rupture patch of the earthquake. Notable examples include the 2011 Tohoku-Oki earthquake in the Japan Trench, and the 2014 Iquique earthquake offshore northern Chile. The timing of these SSEs suggests the possibility that they may have been earthquake precursors.

Here, I report on laboratory friction experiments on simulated fault gouges which show SSEs that exhibit a precursory relationship to fast stick-slip instabilities. The experiments are conducted at room temperature and at low pressure (10 MPa effective normal stress) and under water saturation to simulate the shallow, near-surface portions of major fault zones. A key feature of these experiments is the use of realistically slow driving velocities as low as 5 cm/yr (1.6 nm/s) to simulate natural tectonic forcing. This study focuses on four synthetic fault gouges which exhibited consistent stick-slip: pyrite, hematite, gypsum, and Carrara marble powders.

Preliminary results show that when sheared at 5 cm/yr, the hematite and pyrite gouges exhibit small stress drops and peaks in sliding velocity, interpreted to be SSEs, immediately prior to stick-slips. The hematite gouge shows precursory SSEs with stress drops on the order of 10’s of kPa and peak slip velocities within an order of magnitude of the driving rate, whereas the stick-slips exhibit stress drops of about 1 MPa and peak slip velocities of up to ~1 mm/s. The SSEs occur at shear stresses within 1% of the peak stress and a few hours prior to the stick-slip events, compared to a roughly 1-1.5 day recurrence interval.

The position of SSE occurrence near large stick-slips in both time and shear stress space suggests that they are precursors to stick-slip instabilities. These results also suggest that both slow and fast slip can occur on the same fault patch under the same conditions. However, the mechanism for the precursory SSEs is unclear. Such precursory SSEs were not observed for the gypsum and marble gouges, suggesting that grain characteristics and gouge mineralogy are important. Furthermore, shearing at faster velocities show that the stick-slip stress drops decrease in magnitude, but the precursory slow slip stress drops may increase, which would suggest a time-sensitive mechanism. Further experimentation and analyses of the precursory nature of SSEs and the mechanism behind them is currently ongoing.

High-velocity friction experiments for samples of various size

Hiroyuki Noda[1], Kiyokazu, Oohashi[2]

[1]DPRI, Kyoto Univ., [2]Grad. School of Science and Engineering, Yamaguchi Univ.

There is a large difference in length scale between laboratory and natural large events. Then it is crucial to study the scale effect in friction and evaluate applicability of lab-experiments. It is known that friction decreases dramatically at coseismic slip rate due to frictional heating and various associated physico-chemical effects (e.g., Tsutsumi and Shimamoto, 1997 (TS97); Di Toro et al., 2011). High-velocity friction experiments for centimeter-scale samples showed the dynamic weakening at slip rates V of the order of 0.1 m/s. On the other hand, recent experiments by Yamashita et al. (2015) (Y+15) demonstrated that a large sample with 1.5 m-long and 0.1 m-wide frictional surface showed the dynamic weakening at V of the order of 0.01 m/s, arguing existence of the scale effect on the weakening slip rate V_{w}. Noda (2023) pointed out that it can be explained by concentration of frictional power due to thermoelastic instability (e.g., Dow and Burton, 1972). Heterogeneous thermal expansion of wall rocks of a frictional surface due to heterogeneous normal stress causes unlimited growth of the heterogeneity at $V > V_{\mathrm{cr}}$, where V_{cr} is the critical slip rate proportional to the wavenumber of the heterogeneity. A larger sample hosts heterogeneity of a smaller wavenumber, and thus should weaken at a lower slip rate. In this case, V_w is expected to be inversely proportional to the sample size. Here, we present our preliminary results of high-velocity friction experiments for samples of various size conducted in order to confirm the scale effect and the hypothesis of the thermoelastic instability. We used gabbro of sub-millimeter grain size ("Zimbabwe black") which may be comparable to experiments by TS97 and by Y+15. Because thermal properties of the apparatus matters (Yao et al., 2016), we used the same apparatus that TS97 used, which is now at Yamaguchi University. Width of the frictional surface W is 4.5 mm in TS97, 0.1 m and 11.5 mm in Y+15. So far, we conducted experiments with W of 3 mm and 13.5 mm. The experimental conditions are similar to TS97; the normal stress was kept at 1.5 MPa and successive positive velocity steps of a factor of about 1.5 were applied every about 50 m of slip. The sample with $W = 3$ mm weakened at $V = 0.4$ m/s, while that with $W = 13.5$ mm did at $V = 0.25$ m/s. When plotted together with TS97 and Y+15, V_w ranges for about 2 orders of magnitude. Normalization of the slip rate by V_{cr}, which is inversely proportional to W, reduces this variation to about 1 order of magnitude (Figure). The comparison indicates the existence of the scale effect, reconfirming the discovery by Y+15 and inferring significance of thermoelastic instability although more data is needed.

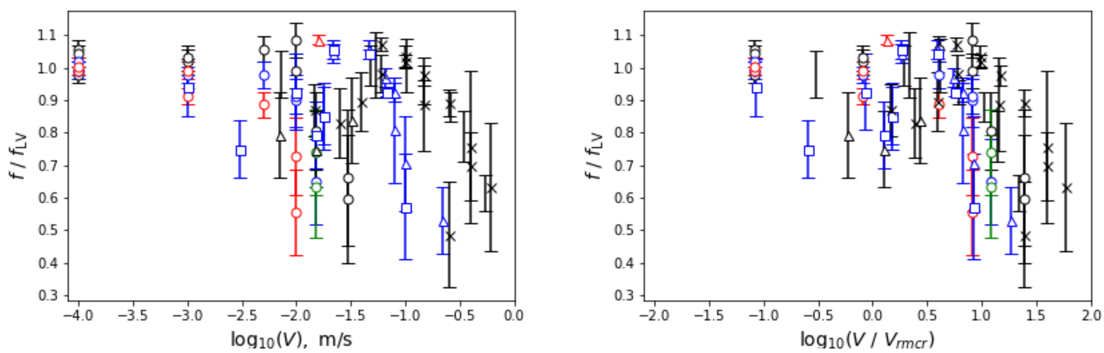

Figure. Normalized friction coefficients by low-velocity values for experiments in this study (x), TS97 (only errorbars), and Y+15 (other symbols) plotted against V (left) and V/V_{cr} (right).

Major fast megathrust earthquake recurrence in the Japan Trench? Long-term (> 17 000 years) perspectives from submarine paleoseismology

Michael Strasser[1], Ken Ikehara[2], Jyh-Jaan Steven Huang[1,3], Takuya Itaki[2], Toshiya Kanamatsu[4], Yoshitaka Nagahashi[5], Yasufumi Satoguchi[6], Jeremy Everest[7], Lena Maeda[8], and the IODP Expedition 386 Science Party[*]

[1]Dept. Geology, Univ. Innsbruck, [2]AIST Geol. Survey Japan, [3]Inst. Oceanography, National Taiwan University, [4] JAMSTEC, Research Institute of Marine Geodynamics, [5] Faculty of Symbiotic Systems Science, Fukushima University, [6] Lake Biwa Museum, [7] British Geological Survey, [8] JAMSTEC MarE3

Our observational understanding of the largest ordinary fast megathrust earthquakes is limited by short historical and instrumental records. These major earthquakes can involve multi-segment ruptures and may break boundaries that were previously considered rupture barriers. Current knowledge suggests different types of recurrence pattern and/or supercycles maintained for such earthquakes. However, even emerging paleoseismic records often do not yet contain enough accurately dated, spatially-well-distributed events to capture the full spectrum of long-term spatiotemporal rupture variability. This limits the validation of proposed conceptual and/or physics-based recurrence models using sound observational data. To address this gap in long-term records of magnitude 9 class earthquakes, such as the Tohoku-Oki earthquake in 2011, International Ocean Discovery Program (IODP) Expedition 386, Japan Trench Paleoseismology, was conducted. The aim of this expedition was to test and further develop submarine paleoseismology techniques to extract signals of megathrust earthquake from geological records preserved in the Japan Trench. Here, we provide an overview of the current state-of-the-art in submarine paleoseismology and present initial findings from IODP coring at 15 sites along the entire Japan Trench. Through these coring activities, we were able to recover continuous, upper Pleistocene (>17000 yrs) to present-day stratigraphic successions in 11 trench-fill basins. These basins act as "natural submarine paleoseismometers" and are expected to have independently recorded past earthquakes. Our results document event-stratigraphic successions that consists of numerous events characterized by different types, facies, properties, composition, and frequency of occurrence. We observe spatial variations in these characteristics across the southern, central, and northern Japan Trench. By analyzing the event stratigraphic expressions and spatiotemporal distribution we aim to identify proxy evidence of giant versus smaller earthquakes versus other driving mechanisms. This will help us to establish long-term high-resolution spatiotemporal earthquake histories.

Focusing on initial results from the central Japan Trench we report (i) good correlation of the three marker event beds in the uppermost, youngest stratigraphic intervals with the established and "calibrated" submarine paleoseismic records of the last 1500 years, and (ii) the occurrence of 10s of older thick beds comprising similar characteristics as event-beds from major historical earthquakes. The resulting continuous paleoseismic record -spanning approximately 17 000 yrs in the central Japan Trench provides long enough observational time series for robust recurrence statistics of different event types recorded in the "natural paleoseismometers". Emerging results offer new long-term perspectives for evaluation and discussion of quasi-periodic to weakly-periodic recurrence of major megathrust earthquakes and, eventually, of the relationship between the spatiotemporal pattern of megathrust earthquakes, plate-boundary interface properties and megathrust slip behavior.

Shallow transient fault slip and frictional instabilities at the Sumatra-Andaman subduction zone

Paola Vannucchi[1,2], Elena Spagnuolo[3], Stefano Aretusini[3], Giulio di Toro[4],

[1]University of Florence, Italy, [2]OGS, Trieste, Italy, [3]INGV, Rome, Italy, [4]University of Padua, Italy

Rupture models of the 2004 Mw 9.2 Sumatra-Andaman EQ imply shallow co-seismic slip that could have even extended close to the trench particularly offshore the northern part of the island of Sumatra. Geophysical imaging of the Sumatran accretionary prism suggested that the shallow plate boundary interface propagates through sediments deposited in the Warton Basin, particularly those near the base of the Nicobar fan and even in pre-fan, pelagic layers. However, imaging was not able to identify the precise location of the frontal megathrust, and three "candidates" for this sediment horizon were proposed in the input section. IODP Exp. 362 sampled these layers to investigate the characteristics of the input material and the factors controlling shallow seismogenic slip potential. We conducted shear stress- and velocity-controlled experiments performed under water depleted, damped, and pressurized conditions in a rotary shear apparatus. These experiments allow us to observe a broad spectrum of slip behaviors that spontaneously occur upon shearing, from aseismic creep to accelerated slip at seismic slip rates (1 m/s), without forcing dynamic weakening as a consequence of the seismic slip rate – i.e. at 1 m/s all materials tend to have a remarkable slip weakening behavior. These tests reveal that although the dynamic weakening behaviour seems similar for all the "candidate" fault materials, the way in which they accumulate and adjust their shear stress differs one from the other, resulting in hererogeneous fault stability characteristics, explained using the energy budget for rupture propagation. Specifically, we identified a pre-fan layer that can accumulate high stress and release it all at once through a fast (>1 m/s) event, behaving like a locked fault patch. Most of the other layers, although still able to accumulate stress, release elastic shear stress both by creeping and also by short-lasting fast (> 0.1 m/s) events, behaving like creeping patches which can accelerate to reach seismic slip rates. These conclusions hold if elastic strain is not released by adjacent weaker lithological units. Deformation features in the lower plate as well as in the prism, and plate flexural bending can all exert a key role in building up elastic stress favoring fault propagation – as well as fault nucleation – in the candidate décollement layer.

Spatiotemporal variation of pore pressure and stress state in the plate subduction zone

Takeshi Tsuji[1], Yusuke Kakiuchi[1], Takashi Tonegawa[2]

[1] Univ. Tokyo, [1] JAMSTEC

To investigate the dynamic behavior of stress or strain state in the Nankai accretionary prism, we estimated the temporal variation of seismic velocity by using cross-correlations of ambient noise recorded by the DONET offshore seismic network. Our findings unveil a distinct reduction in seismic velocity during the earthquake events. These co-seismic velocity drops exhibited a correlation with peak ground velocities recorded at each station, underscoring the role of dynamic stress changes induced by intense ground motions as a primary driver of co-seismic velocity fluctuations. Differences in the sensitivity of seismic velocity changes to peak ground velocity may reflect subsurface conditions at each station, such as geological structure and effective pressure conditions. We also observed a long-term increase in seismic velocities that may reflect tectonic strain accumulation around the Nankai subduction zone. If the long-term increasing trend is related to strain accumulation from plate subduction process, our approach may be useful in monitoring variations of the regional stress state, which is difficult to observe in offshore environments, and may provide vital information for understanding future earthquakes as well as slow earthquake. Our results suggest that ambient noise cross-correlation might be used to monitor the stress state in the Nankai accretionary prism in offshore environments, which would contribute to a better understanding of earthquake processes. Furthermore, we undertake a comparison between the spatiotemporal fluctuations of seismic velocity and the geological structures visualized within seismic reflection profiles, aiming to elucidate both the origins and spatial extents of seismic velocity alterations.

Frontal Thrust ramp-up and slow Earthquakes due to Underthrust of Basement high Relief in the Nankai Trough

G. Kimura[1], K. Shiraishi[1], Y. Nakamura[1], S. Kodaira[1], and G. Fujie[1]

[1] Research Institute for Marine Geodynamics, Japan Agency for Marine-Earth Science and Technology (JAMSTEC)

Recently integrated observations of geophysical-geological surveys in subduction zone, have revealed that the slow earthquakes and tremors repeatedly occur beneath the outer wedge of the forearc. In December 2020 to January 2021, clustered slow-earthquakes and tremors were propagated around the frontal thrust of accretionary wedge in the off-Kumano Nankai Trough, Japan. The frontal thrust ramps up from the basal decollement beneath the accretionary wedge and slips over trench-filling sediment along the landward edge of the Nankai trough floor. Igneous basement of the Philippine Sea Plate beneath the frontal thrust presents high relief, and its northern edge is located just at the ramp-up position of the frontal thrust. Ocean floor topography and geologic structure revealed by a new seismic reflection survey of JAMSTEC in 2022 (Fig. 1) document that the horizontal distance between the northern edge of the high relief of the basement and exit of the front thrust (deformation front) is from ~3200 m to ~ 9600 m and the crestal uplift of the frontal prism is from ~250 m to ~1100 m (Fig. 2). Considering that the relative plate convergence between the upper Amurian Plate of the Nankai forearc and the subducting Philippine Sea Plate is ~6.0 cm/y in ~300-degree direction, the basement high relief has kept jacking up the frontal crest of the wedge by an uplift rate of 2.8~6.5 mm/y for several tens to hundred thousand years in average, which is the same rate of Himalayan foreland. The slow earthquakes and tremors in December 2020 to January 2021 appear a snapshot of “living” Nankai frontal thrust during inter-large seismic period.

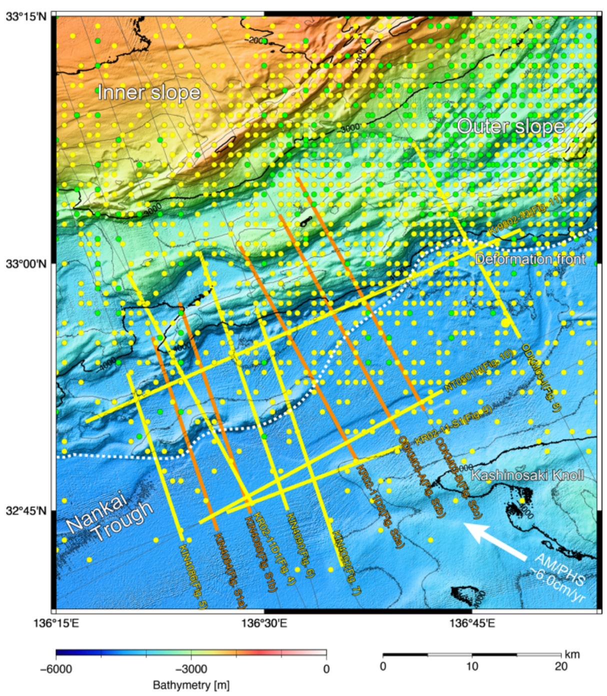

Figure 1. Distribution of very low frequency earthquakes (VLFE: green dot) and tremors (yellow dot) with topography and seismic reflection lines. VLFE: Nakano et al. (2018), Takemura et al. (2019a, 2019b, 2022a, 2022b), tremors: Tamaribuchi et al. (2022), Ogiso and Tamaribuchi (2022)

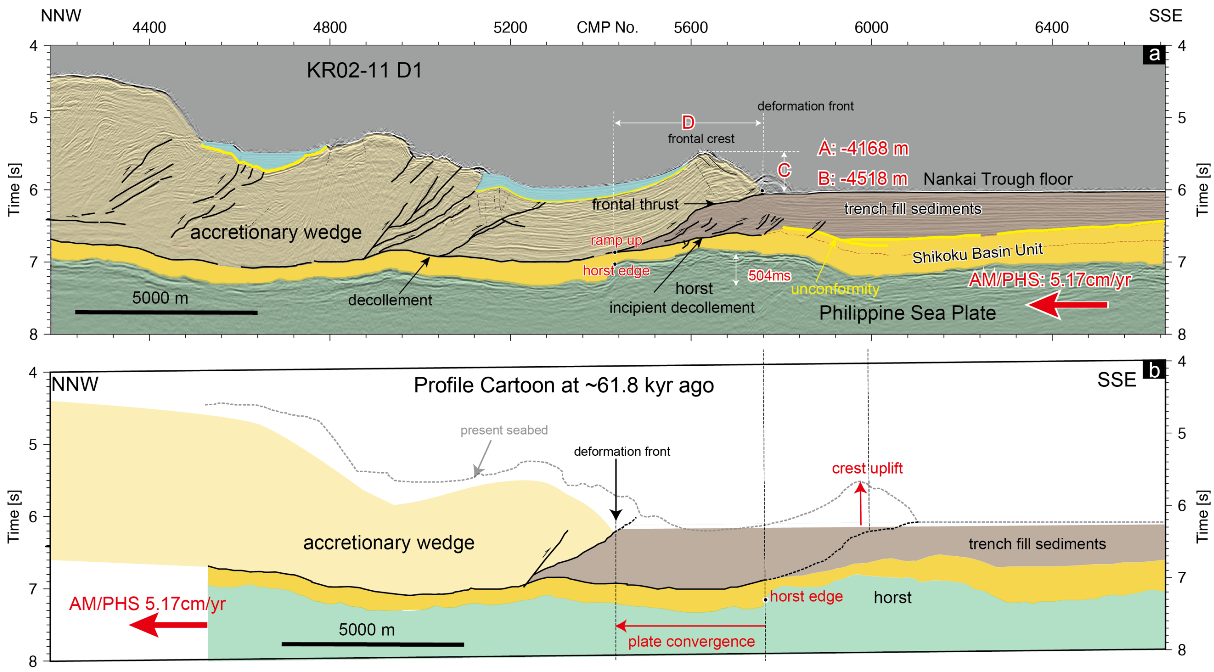

Figure 2. (a) An interpretation of the seismic profile (KR02-11 D1: location in Fig. 1), (b) A profile cartoon at the start age of ~61.8 kyr ago of impingement of basement horst with ramp-up of a new frontal thrust. Note that the deformation front jumped southward with wedge shorten-thickening and a new accretion of trench fill sediments.

References

Nakano et al. (2018). *Progress in Earth and Planetary Science*, *5*(1), 1-17.

Ogiso and Tamaribuchi (2022). *Earth, Planets and Space*, *74*(1), 1-14.

Takemura et al. (2019a). *Geophysical Research Letters*, *46*(8), 4192-4201.

Takemura et al. (2019b). *Geophysical Research Letters, 46*(21), 11830-11840

Takemura et al. (2022a). *Journal of Geophysical Research: Solid Earth*, *127*(3), e2021JB023073

Takemura et al. (2022b). *Geophysical Research Letters*, *49*(11), e2022GL097979.

Tamaribuchi et al. (2022). *Journal of Geophysical Research: Solid Earth*, *127*(8), e2022JB024403.

Preliminary results of R/V Yokosuka YK23-10S cruise: submersible survey along the Shionomisaki submarine canyon in the Nankai Trough

Asuka Yamaguchi[1], Rina Fukuchi[2], Yohei Hamada[3], Hiroaki Koge[4], Kiichiro Kawamura[5], Akira Ijiri [6], Hanaya Okuda[3], Mari Hamahashi[5], Konosuke Terui[1], Takahiro Hosokawa[7], Kanji Tatsumi[6], Juichiro Ashi[1], Takafumi Kasaya[3], Masataka Kinoshita[1], Koji Kameo[8], Yoshimi Kubota[9], Takeshi Tsuji[1], Kazuya Shiraishi[3], Gaku Kimura[3]

[1]Univ. Tokyo, [2]Naruto Univ. of Education, [3]JAMSTEC, [4]GSJ, AIST, [5]Yamaguchi Univ., [6]Kobe Univ., [7]Kochi Univ., [8]Chiba Univ., [9]NMNS, Tokyo

The Nankai Trough is a subduction zone where an accretionary complex is typically developed. The macroscopic features of the forearc region of the Nankai Trough are essential for understanding subduction zone seismogenesis and geodynamics. Based on the results of recent deep-sea drilling and reflection surveys in the Nankai Trough, we conducted seafloor geological surveys and sampling by using the submersible Shinkai 6500, during the R/V Yokosuka YK23-10S cruise (June 15-26, 2023). In this presentation, we report the initial shipboard results of the YK23-10S cruise.

Submersible studies were focused on the Shionomisaki submarine canyon off the Kii peninsula, located near the segment boundary of the Tonankai and Nankai earthquakes. Through five dives during the cruise, we observed mudstones (accretionary prism sediments), conglomerates (slope basin or the lowest part of forearc basin), and sandstone-mudstone alternation layers (forearc basin deposit), and 104 rock samples and 13 cores were recovered. We also conducted temperature measurements using SAHF at 9 points. Three-component magnetometer and subbottom profiler are loaded on Shinkai 6500 and are used to acquire subsurface and geomagnetic features. During sailing observations at and around Shionomisaki submarine canyon, we used shipboard three-component magnetometer, proton magnetometer, multi-beam echo sounding system, and subbottom profiler for geomagnetic, bathymetric, and subsurface observations. Further postcruise research will enable us to elucidate the tectonic evolution of the Nankai accretionary complex and the Kumano Basin, and the nature of the segmental boundary from a material point of view.

Weakening of clayey gouge at intermediate velocities and its potential effect on slow earthquakes

Hanaya Okuda[1], Takehiro Hirose[1], Asuka Yamaguchi[2]

[1]Kochi, JAMSTEC, [2]AORI, Univ. Tokyo

In shallow subduction zones, volcanic glass erupted from arc volcano deposits and subducts along the plate interface. Volcanic glass alters into one of the weakest materials, smectite, with depth. Mixtures of volcanic glass and smectite are common constituents of subducting volcanic ash layer and they sometimes become glide planes for submarine landslides. Despite its potential importance, the understanding of frictional behavior of volcanic glass-smectite mixture is still limited, especially at intermediate velocity conditions. We conducted friction experiments with volcanic glass-smectite mixture under water-pressurized conditions at various velocity conditions. Friction coefficients decreased with smectite content, which is generally consistent with previous studies. At intermediate velocity conditions, however, we observed drastic slip-weakening behavior. The cause of this slip-weakening behavior is not yet fully understood, but FEM modeling suggests that thermal processes are not responsible for the slip weakening. We found that the critical nucleation length for the slip-weakening behavior is estimated to be ~10 km, which is consistent with the slip area estimated for VLFEs in the shallow Nankai Trough. As such a large critical nucleation length does not allow slip to accelerate by itself, the slip-weakening behavior at intermediate velocities could be a mechanism for slow earthquakes in shallow subduction zones.

Reference:

Hanaya Okuda, Takehiro Hirose, Asuka Yamaguchi (2023). Potential role of volcanic glass-smectite mixtures in slow earthquakes in shallow subduction zones: Insights from low- to high-velocity friction experiments. *Journal of Geophysical Research: Solid Earth*. 128, e2022JB026156. doi: 10.1029/2022JB026156

Frictional and mechanical properties of episodic tremor and slip zone: A brief review

Ken-ichi Hirauchi[1]

[1]Department of Geosciences, Faculty of Science, Shizuoka University

The zone of episodic tremor and slip (ETS) may mark a thermally-controlled transition in deformation behavior from unstable stick-slip to stable sliding. However, previous hydrothermal friction experiments on synthetic fault gouges conducted at ca. 10^{-5}–10^{-7} m s^{-1} have shown that the deep megathrust materials such as sediments (e.g., illite/muscovite + quartz) and hydrated mantle wedge (antigorite and talc) are mostly velocity strengthening at high temperatures (400–500 °C) relevant to the ETS zone, with exception of unaltered oceanic crust and mantle wedge (see compilation in Okazaki and Hamada, 2022, *Gekkan Chikyu*). Indeed, at Cascadia and Nankai, a spatial gap exists between the seismogenic and ETS zones, meaning that in the ETS zone (Gao and Wang, 2017, *Nature*), viscous deformation rather than frictional sliding predominates at the high temperatures and plate motion rates (ca. 10^{-9}–10^{-10} m s^{-1}), and inhibits the nucleation of any types of earthquakes. The only way to reconcile this discrepancy will be to take into account the presence of pore fluid pressures, which acts to reduce effective normal stress and thereby to promote brittle deformation rather than viscous creep.

In this presentation, I will suggest two possible scenarios for ETS generation along megathrust shear zones under high pore fluid pressure conditions: (1) unaltered mafic and/or ultramafic blocks act as velocity-weakening regions enclosed within a frictionally weak, velocity-strengthening matrix, and (2) a network of conjugate extensional (mode I) and extensional-shear (mode I–II) (i.e., fault-fracture meshes) failures develops. In scenario (1), a fault gouge zone(s) is formed dominantly along margins of the blocks, where strength contrast is high and stress amplification happens (Behr et al., 2021, *AGU Adv*.; Fagereng and Beall, 2021, *Phil*. *Trans*. *R*. *Soc*. *A*). In scenario (2), supra-lithostatic pore fluid pressure conditions are required. The development of fault-fracture meshes has been recognized in the shallow forearc mantle wedge (Hirauchi et al., 2021, *Earth Planet*. *Sci*. *Lett*.) and underthrust pelitic sediments (Ujiie et al., 2018, *Geophys*. *Res*. *Lett*.; Condit and French, 2022, *Geophys*. *Res*. *Lett*.), where temporal fluctuations in pore fluid pressure occur in association with cyclic fracturing and sealing (mineral precipitation) events, consistent with recent geophysical observations (e.g., Gosselin et al., 2020, *Sci*. *Adv*.).

Central shutdown and surrounding activation of aftershocks from megathrust earthquake stress transfer

Ross S. Stein[1] and Shinji Toda[2]

[1]Temblor, Inc., San Francisco, and Lecturer in Geophysics, Stanford University
[2]IRIDeS, Tohoku University, Sendai, Japan

Megathrust earthquakes release and transfer stress that has accumulated over hundreds of years, leading to large aftershocks that can be highly destructive. Understanding the spatiotemporal pattern of megathrust aftershocks is key to mitigating the seismic hazard. However, conflicting observations show aftershocks concentrated either along the rupture surface itself, along its periphery or well beyond it, with some arguing that they can persist for only few years and others contending they continue for decades.

Here we present aftershock data following the four largest megathrust earthquakes since 1960, focusing on the change in seismicity rate following the best-recorded 2011 Tohoku earthquake, which shows an initially high aftershock rate on the rupture surface that quickly shuts down, while a zone about six times larger forms a ring of enhanced seismicity around it. We find that the aftershock pattern of Tohoku and the three other megathrusts can be explained by rate-and-state Coulomb stress transfer.

We suggest that the shutdown in seismicity in the rupture zone persists for centuries, leaving seismicity gaps that can be used to identify prehistoric megathrust events. In contrast, the seismicity of the surrounding area decays over 4–6 decades, increasing the seismic hazard after a megathrust earthquake. This means that the coastal hazard generally rises, rather than falls, after a megathrust rupture, and that one can hunt for prehistoric megathrusts by searching for holes in current subduction zone seismicity.

(Reference: Toda and Stein, *Nature Geoscience*, 2022)

A simple observation of the 2011 M 9 Tohoku aftershocks reveals a temporal transition

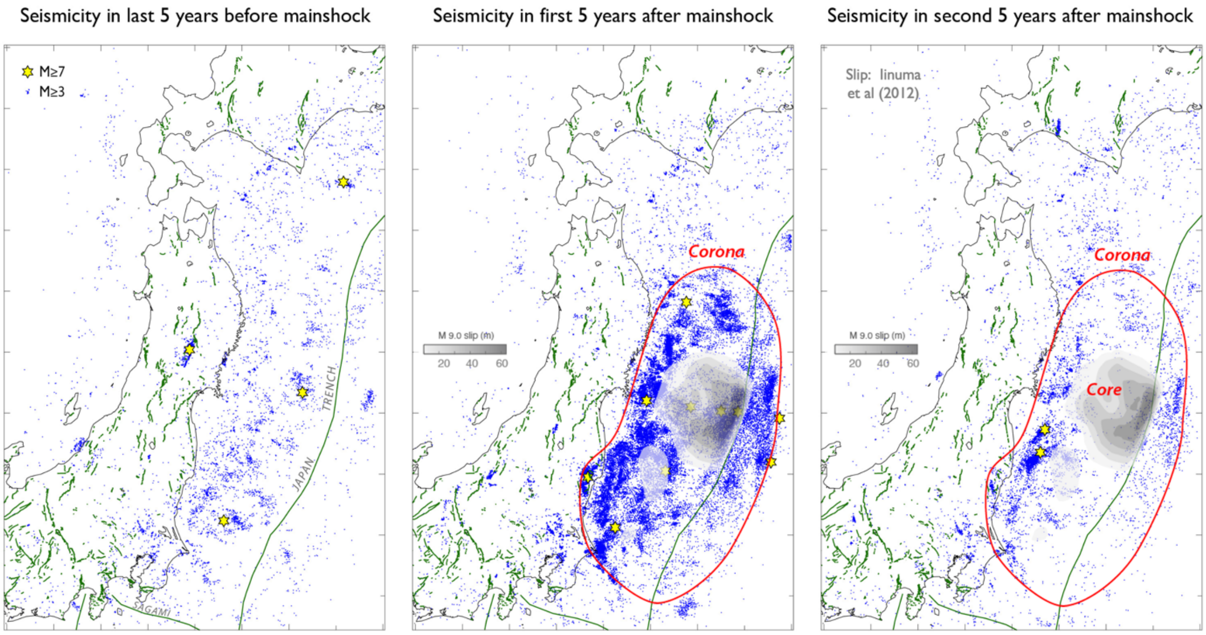

Lower dominant frequencies of fast earthquakes at the east of Izu peninsula

Ryo Kurihara

Hot springs research Institute of Kanagawa prefecture

In Japan, some types of slow earthquakes such as slow slip events, tremors, and very low-frequency earthquakes, were observed in many subduction zones including the Nankai Trough, Japan Trench (Tohoku region), and Ryukyu Trench. However, any slow earthquakes have not been observed in the Sagami Trough region, where the 1923 Great Kanto earthquakes occur. Sagami Trough locates near the Tokyo metropolitan area, therefore, the Kanto earthquake has the largest impact on Japan. For example, the 1923 Great Kanto earthquakes killed over 100,000 people. Therefore, it is important to understand plate tectonics and slow and fast earthquakes in the Sagami Trough.

We cannot investigate slow earthquakes in the Sagami Trough region because of non-observation. In this study, I focus on the fast earthquakes that occurred east of the Izu peninsula near the boundary of the Philippine Sea plate and the North American plate. In this area, although the Hakone volcano and Izu-east volcano groups locate and some swarms of volcanic earthquakes occur, however, the earthquakes also occur far from volcanoes. These earthquakes may occur at the plate boundary because some earthquakes have reverse-fault mechanisms (cf. Yukutake et al., 2012).

In this study, I calculated the Frequency Index for each earthquake based on the following equation,

FI= (spectrum of 8–16 Hz)/(spectrum of 1–2 Hz) ・・・(1).

As a result, I found that some east Izu earthquakes show low FI values, which means small dominant frequencies of the earthquakes. Although a large earthquake generally has a lower dominant frequency, however, a small earthquake also shows a low FI value in the area. In the east of the Izu peninsula area, earthquakes near the Izu east volcano groups do not have such low FI values, and earthquakes in the north Izu area have very low FI values. This result may suggest that fluids affect the occurrence of earthquakes. In addition, most earthquakes in this region occur in the earthquake swarms. Lower dominant frequency and swarm-like seismicity may show very small slow earthquakes which cannot be observed to occur in the background or such lower dominant frequency occur in substitute of slow earthquakes.

Revealing The Dynamics of the Feb 6th 2023 M7.8 Kahramanmaraş/Pazarcik Earthquake: Near-Field Records and Dynamic Rupture Modeling

Mohamed Abdelmeguid[1,] Chunhui Zhao[2], Esref Yalcinkaya[3], George Gazetas[4], Ahmed Elbanna[2,5] and Ares Rosakis[1]

[1]Graduate Aerospace Laboratories, California Institute of Technology, 1200 E. California Boulevard, Pasadena, 91125, CA, USA.

[2]Department of Civil and Environmental Engineering, University of Illinois at Urbana Champaign, 205 N. Mathews Avenue, Urbana, 61801, IL, USA.

[3]Department of Geophysical Engineering, Istanbul University-Cerrahpasa, 34320 Avcilar, Istanbul, Türkiye. [4]Department of Civil Engineering, National Technical University of Athens, 9, Iroon Polytechniou Str, Athens, Greece. [5]Beckman Institute of Advanced Science and Technology, University of Illinois at Urbana Champaign, 405 N. Mathews Avenue, Urbana, 61801, IL, USA.

The 2023 M7.8 Kahramanmaraş/Pazarcik earthquake was unfortunately larger and more destructive than what had been expected. Here we analyze near-field seismic records to constrain the underlying physics of this event and develope a dynamic rupture model that reconciles different conflicting inversion results. Our results reveal a spatially non-uniform propagation speed in this earthquake, with predominantly supershear speeds observed along the Narli fault and at the southwest (SW) end of the East Anatolian Fault (EAF). The locations of supershear are identified through unique near-fault ground motion signatures that vary with rupture propagation speeds. Within the ground motion records, we also observe field observational evidence showing the mechanism of sub-Rayleigh to supershear transition. Our numerical model highlights the important role of geometric complexity and varying frictional conditions in facilitating continued propagation and influencing rupture speed. Furthermore, in the absence of ground motion records in close proximity to the junction, we conduct a parametric study to constrain the conditions that allowed for the rupture to jump from the Narli fault to EAF and to generate the delayed backpropagating rupture towards the SW. Our findings have important implications for understanding earthquake hazard and guiding future response efforts and demonstrate the value of physics-based dynamic modeling fused with near-field data in enhancing our understanding of earthquake mechanisms and improving risk assessment.

Exploring aseismic slip beyond typical sizes and durations, and their potential link to earthquakes

Anne Socquet[1], Lou Marill[1], David Marsan[1], Mathilde Radiguet[1], Baptiste Rousset[2], Yuji Itoh[1,3]

[1]University of Grenoble Alpes, University Savoie Mont Blanc, CNRS, IRD, University of Gustave Eiffel, ISTerre, Grenoble, France, [2]Institut Terre et Environnement de Strasbourg, France, [3]ERI, Univ. Tokyo

The subduction along the Japan trench may host rare slow slip events, and are mostly suggested by slow earthquakes that occur with a lateral distribution showing a complementarity with the area ruptured by the Tohoku-Oki earthquake (e.g. Nishikawa et al., Science 2019). In addition, the precursory activity leading up to the Tohoku-Oki earthquake of 2011 has been suggested to feature both long- and short-term episodes of decoupling and suggests a particularly complex slow slip history. The analysis of the F3 solution of the Japanese GNSS network suggested that an accelerated slip occurred in the deeper part of the seismogenic zone during the 10 years preceding the earthquake (Heki & Mitsui, EPSL 2013; Mavrommatis et al., GRL 2014; Yokota & Koketsu, Nat. Com. 2015). During the two months preceding the earthquake, several anomalous geophysical signals have been reported (an extended foreshock crisis near the future hypocenter (Kato et al., Science 2012), a synchronized increase of intermediate-depth background seismicity (Bouchon et al., Nat Geosc. 2016), a signal in ocean-bottom pressure gauges and on-land strainmeter time series (Ito et al., Tectonoph. 2013), large scale gravity anomalies that suggest deep-seated slab deformation processes (Panet et al., Nat. Geosc. 2018 ; Wang & Burgmann, GRL 2019)), and large scale reversals of 4-8 millimetres in surface displacement called “wobbling” (Bedford et al., Nature 2020).

Motivated by these observations, we revisit here the slow slip history along the Japan trench and the Sagami through with an independent analysis of the GEONET GNSS data, including a full reprocessing of the raw data, a systematic analysis of the obtained time-series, with noise characterization and network filtering. We notably focus on: the large scale and long-term change of locking by assessing statistically the relevance of an acceleration term, the potential occurrence of slow slip events using a geodetic matched filter, and a benchmark analysis of the potential wobble by comparing with complementary processing approaches.

In agreement with previous studies, we find that the slip rate over the decade preceding Tohoku earthquake decelerates on the PAC-NAM boundary between 39-41°N and accelerates between 37 – 38° N with a maximum amplitude of 1.75mm/yr2 corresponding to an equivalent geodetic locking change of 0.3 over 14 years. More notably, our analysis reveals a novel and robust slip acceleration South of 36°N offshore Boso, which is a worrying sign of an on-going slow decoupling east of Tokyo. It is located noticeably far from the 2011 Tohoku earthquake rupture and is therefore unlikely connected to it. The slip acceleration inverted from the surface displacements is comparable to the changes observed in the seismicity rate.

Using our template matching method on GNSS data over 1997 – 2020, we find 12 slow slip events on the Philippine Sea plate, among which 8 are located on the known Boso slow slip event asperity and the 4 others are located offshore north-east relative to the Boso SSEs, at the transition with the Pacific plate. We find 9 SSEs on the Pacific plate, mainly on the northern section, offshore Iwate prefecture. A clear gap with no SSEs coincides with the main asperity that broke during the 2011 Tohoku earthquake. Most event locations correlate with low locking areas. We however do not find any clear temporal pattern apart from the regular occurrence of the largest Boso SSEs.

Finally, the revisit of GNSS time series preceding Tohoku do not support the relevance of a large-scale wobbling of the surface displacement, that is most likely an artefact due to common mode signals associated to space geodesy reference frame issues, and not a geophysical signal that should be interpreted as associated with the subduction.

Megathrust earthquake potential in Central Peru (Lima region) based on stress accumulation rates and the earthquake energy balance at the subduction interface

Nelson Pulido[1] , and Juan Carlos Villegas-Lanza[2]

[1]National Research Institute for Earth Science and Disaster Resilience, [2]Instituto Geofísico del Perú

The estimation of maximum magnitude and rupture scenarios for future megathrust earthquakes in subduction zones are typically based on the historical seismicity of a region. However, information in earthquakes catalogues for large earthquakes is usually incomplete compared to the inter-seismic cycles. In addition, there is a need to incorporate information on the physical processes that characterize large earthquake ruptures at the plate interface such as accumulation of stress and strain, and the fault resistance to rupture.

Recent studies in the Nankai-Tonankai subduction zone in Japan indicate that slip deficit areas do not directly reflect the local frictional strength characteristics controlling fault slip behavior at the plate interface. Therefore, the concepts of mechanical coupling (shear stress accumulation rate) and earthquake energy budget, have been proposed (Noda et al. 2021), to investigate the physical conditions for earthquake generation. Under this framework an earthquake rupture cannot occur unless the strain energy (half the product of average stress drop, slip and fault rupture area), overcomes the fault resistance to rupture (fracture energy). Their difference is defined as the residual energy (Eres). On the other hand, megathrust earthquakes rupture typically involve a strong dynamic weakening, likely as a result of large stress undershoot during fault rupture. In this study we incorporate the strong dynamic fault weakening effect into the energy balance method of Noda et al (2021), and apply it to investigate the earthquake potential of subduction megathrust earthquakes in Peru. To calculate fracture energy (G) we use the scaling law between average fault slip and G obtained for subduction interface earthquakes, using the NEIC global dataset of finite fault slip rupture models and the 2D finite width slip dynamic rupture model (Pulido 2023, in preparation).

We investigated earthquake potential of megathrust earthquakes along the Peruvian subduction zone based on the inter-seismic coupling model (ISC) (Villegas-Lanza et al. 2016). At the first order the slip deficit rate distribution shows that the Northern Peru segment displays a shallow and weak ISC, whereas that Central and Southern segments are highly coupled. We calculated the shear stress accumulation rate and total accumulated shear stress distributions at the Peruvian subduction margin, based on the slip deficit rate model, and inter- seismic periods since the last largest historical earthquakes for each individual segment. Our results indicate that Central Peru segment currently has the largest accumulation of shear stress along the Peruvian subduction margin. In addition, the subduction zone in Central Peru will fulfill the required condition for generating a ~Mw 8.9 earthquake, rupturing the entire segment, in at least 36 years (namely, when the strain energy accumulated at the plate interface will exceed fracture energy, Eres>0). This value possibly corresponds to the largest magnitude **(Mmax?)** that the Central Peru subduction segment could be able to mechanically resist. The large availability of ISC studies globally in recent years, combined with scaling laws of fault fracture energy at the plate interface, make our method suitable to estimate the earthquake potential of subductions zones worldwide.

Physics-Informed Neural Networks for fault slip monitoring: simulation, frictional parameter estimation, and prediction on slow slip events in a spring-slider system

Rikuto Fukushima[1], Masayuki Kano[2], and Kazuro Hirahara[3,4]

[1]Faculty of Science, Kyoto University, [2]Graduate School of Science, Tohoku University,
[3]RIKEN Center for Advanced Intelligence Project, [4] Kagawa University

The episodic transient fault slips called slow slip events (SSEs) have been observed in many subduction zones. These slips often occur in regions adjacent to the seismogenic zone during the interseismic period, making monitoring SSEs significant for understanding large earthquakes. Various fault slip behaviors, including SSEs and earthquakes, can be explained by the spatial heterogeneity of frictional properties on the fault. Therefore, estimating frictional properties from geodetic observations and physics-based models is crucial for fault slip monitoring. In this study, we propose a Physics-Informed Neural Network (PINN)-based new approach to simulate fault slip evolutions, estimate frictional parameters from observation data, and predict subsequent fault slips. PINNs, which integrate physical laws and observation data, represent the solution of physics-based differential equations. As a first step, we validate the effectiveness of the PINN-based approach using a simple single-degree-of-freedom spring-slider system to model SSEs. As a forward problem, we successfully reproduced the temporal evolution of SSEs using PINNs and indicated how we should choose the appropriate collocation points depending on the residuals of physics-based differential equations. As an inverse problem, we estimated the frictional parameters from synthetic observation data and demonstrated the ability to obtain accurate values regardless of the choice of first-guess values. Furthermore, we discussed the potential of the predictability of the subsequent fault slips using limited observation data, taking into account uncertainties. Our results indicate the significant potential of PINNs for fault slip monitoring.

Nucleation of Laboratory Earthquakes: Quantitative Analysis and Scalings

Alexandre Schubnel[1], Samson Marty[1], Harsha S. Bhat[1], Jérôme Aubry[1], Soumaya Latour[2], Stefan Nielsen[4], Eiichi Fukuyama[4] and Raùl Madariaga[1]

[1]Laboratoire de Géologie de l'ENS, Université PSL/ CNRS, France; [2]IRAP, Univ. Toulouse, France; [3]Univ. of Durham, UK; [4] NIED;

In this study we use the precursory acoustic emission (AE) activity during the nucleation of stick-slip instability as a proxy to investigate foreshock occurrence prior to natural earthquakes. We report on three stick-slip experiments performed on cylindrical samples of Indian metagabbro under upper crustal stress conditions (30–60 MPa). AEs were continuously recorded by eight calibrated acoustic sensors during the experiments. Seismological parameters (moment magnitude, corner frequency and stress-drop) of the detected AEs ($-8.8 \leq \mathbf{Mw} \leq -7$) follow the scaling law between moment magnitude and corner frequency that characterizes natural earthquakes. AE activity always increases toward failure and is driven by along fault slip velocity. The stacked AE foreshock sequences follow an inverse Omori type law, with a characteristic Omori time **c** inversely proportional to normal stress. AEs moment magnitudes increase toward failure, as manifested by a decrease in **b**-value from ~ 1 to ~ 0.5 at the end of the nucleation process. During nucleation, foreshocks migrate toward the mainshock epicenter location, and stabilize at a distance from the latter compatible with the predicted Rate-and-State nucleation size. Importantly, the nucleation characteristic timescale also scales inversely with applied normal stress and the expected nucleation size. Finally, we infer that foreshocks are the byproducts of the nucleation phase which is an almost fully aseismic process. Nevertheless, the seismic/ aseismic energy release ratio continuously increases during nucleation, highlighting that, the nucleation process starts as a fully aseismic process, and evolves toward a cascading process at the onset of dynamic rupture.

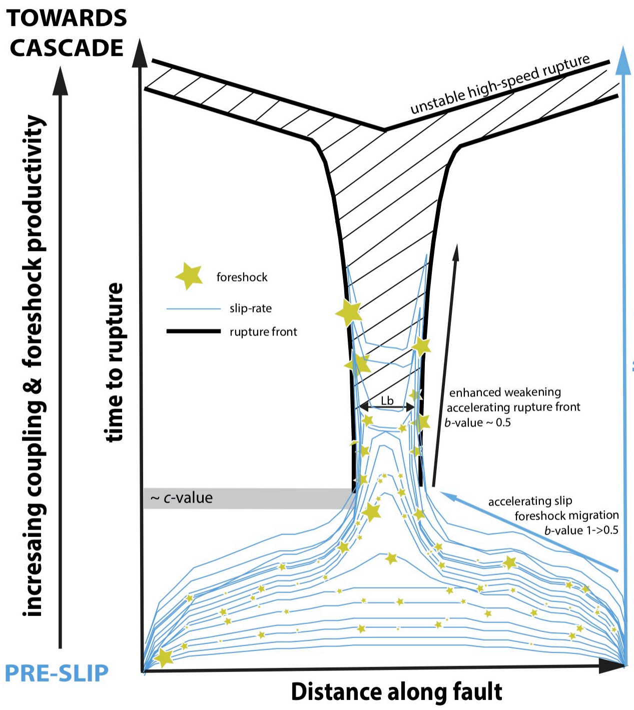

Schematics of nucleation phase dynamics. Slip and stress heterogeneities result in slip localization onto a patch of the fault, which is reflected by foreshock migration toward the epicenter. At t = c of the inverse Omori-law, we observe the transition from a frictional, "Dieterich like" (Dieterich, 1992), instability, to that of a fracture, "Ohnaka-like" (Ohnaka, 2003), process.

Physical mechanism of the temporal decrease of a Gutenberg-Richter b-value prior to a large earthquake

Yoshihiro Kaneko[1], Ryo Ito[1]

[1]Dept. Geophysics, Kyoto Univ.

Observations of seismicity prior to large earthquakes show that the slope of a Gutenberg-Richter magnitude-frequency relation, referred to as a *b*-value, often decreases with time leading to a large earthquake. For example, the temporal decrease of *b*-values in the hypocentral region of the 2011 Mw 9.0 Tohoku-Oki earthquake was observed prior to the mainshock, indicating the potential usefulness of *b*-values for earthquake forecasting. Yet, underlying physical processes associated with temporal changes of *b*-values remain unclear. Here we utilize continuum models of fully-dynamic earthquake cycles with fault frictional heterogeneities and aim to simulate the temporal variation of *b*-values. We first identify a parameter regime in which the model gives rise to an active and accelerating foreshock behavior prior to mainshocks. We then focus on the spatio-temporal pattern of the simulated foreshocks and analyze their statistics. We find that, like in observations, the *b*-value of simulated foreshocks decreases with time prior to a mainshock. In this model, increased shear stress in creeping (or rate-strengthening) patches resulting from numerous foreshocks in the neighboring rate-weakening patches makes these creeping patches more susceptible to future coseismic slip, increasing the likelihood of a large rupture and resulting in smaller *b*-values with time. This mechanism differs from a widely invoked idea that *b*-value reduction is caused by a rapid increase in shear stress that promotes micro-cracks growth over the mainshock source region. These results have important implications for the mechanism of foreshock generation and earthquake forecasting.

Rheology and structure of model smectite clay from coarse-grained molecular dynamics

Zhu-Yuan Lin[1], Takahiro Hatano[1]

[1]Osaka Univ.

The rheology and stability of fault zone is governed by the mechanical behavior of fault gouge. Smectites are commonly found in shallow fault gouges and are well known for their low frictional strength. Although smectite clay is well studied in experiments, rheology and the development of microscopic structure of clay platelets are still not well understood. The difficulty lies in how to describe the sheet-like shape and charge-carrying ability of smectites. In this study, clay platelets are simplified as rigid oblate ellipsoids interacting via the Gay-Berne potential. We investigate rheology of this model system using Coarse-Grained Molecular Dynamics (CGMD). The system exhibits velocity-strengthening behavior over a range of normal stresses from 1.68 to 56.18 MPa and a range of strain rates from 6.93×10^5 to 2.77×10^9 /s. The relationship between shear stress and strain rate follows the Herschel-Bulkley model with exponent (n) smaller than 1 (0.16~0.67). A yield stress at zero strain rate limit is found to increase linearly with normal stress. The friction coefficient decreases with increasing normal stress.

During shear, the shear stress exhibits an initial peak followed by a decrease to the residual value, similar to previous shear experiments. The volume fraction increases with normal stress and decreases with strain rate. We also examine the fabric of the system developed during shear. Particles tend to align into the same direction with orientational order parameter increased above 0.9 within the strain of 200 % . The orientational order parameter then slowly increases to near 1.0. The shear is found to be controlled by a localized shear zone at strain rates lower than 6.93×10^6 /s with nonlinear velocity profile. At higher strain rates, we estimate the structural order via a characteristic stacking size defined in the parallel radial distribution function (PaRDF). We find the the stacking size decreases during shear at normal stress of 5.62 MPa. The final stacking size at steady state decreases at higher strain rates.

The Effect of a Fluid Phase on Rheological Properties of a Sheared Granular System

Chengrui Chang[1], Kohei Ohno[1,2], Tetsuo Yamaguchi[1]

[1]Dept. Biomaterial Sciences, Univ. Tokyo

[2]Dept. Materials Science and Engineering, Tokyo Tech

Systems consisting of a solid and a fluid phase are common in nature, such as debris flows, landslides, faults, river deltas, and partially molten magmas. In these settings, the interstitial fluid can either partially or completely immerse particles and largely affect the dynamical behavior of particles (e.g., Higashi & Sumita, 2009; Ladd & Reber, 2020). In this study, we report our experiments on a two-phase granular system in a double-cylinder geometry. We use spherical glass beads as the solid phase and silicone oil as the fluid phase and vary the volume fraction of silicone oil from 0 to 100%. The torque is measured at a constant rotation rate and shear zone thickness is captured from the bottom using time-lapsed images. Consequently, we find an abnormal volume fraction dependence on the time-averaged torque, as shown in Figure 1: the average torque exhibits two maxima at small and intermediate volume fractions of silicone oil, and such drastic variations are associated with the segregation processes of glass beads.

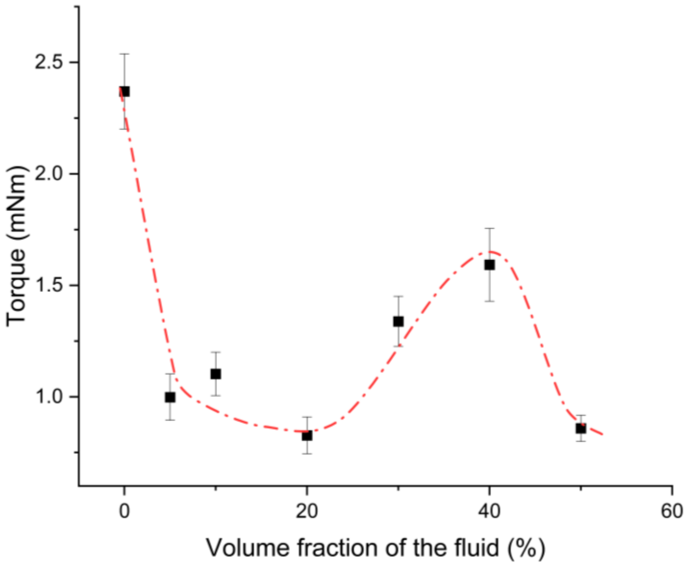

Figure 1. Dependence of average torque on volume fraction of silicone oil.

Reference

Ladd, C. R., & Reber, J. E. (2020). The Effect of a Liquid Phase on Force Distribution During Deformation in a Granular System. Journal of Geophysical Research: Solid Earth, 125(8). https://doi.org/10.1029/2020JB019771

Higashi, N., & Sumita, I. (2009). Experiments on granular rheology: Effects of particle size and fluid viscosity. Journal of Geophysical Research: Solid Earth, 114(B4). https://doi.org/10.1029/2008JB005999

Condition of transition between slow and fast earthquakes in terms of fluid pressure and porosity

Takehito Suzuki[1], and Hiroshi Matsukawa[1]

[1]Dept. Phys. Sci., AGU

Spring-block model taking into account the interaction among heat, fluid pressure, and porosity is considered to systematically treat the transition between slow and fast earthquakes. In particular, we analytically obtain the condition where the transition emerges. First, the energy difference of the system before and after the earthquake is written as $F(u_f)$, where u_f is the slip distance or each earthquake. The function $F(u_f)$ is given by

$$F(u_f) = \frac{1}{2} k_p\, u_f^2 + \mu_{\mathrm{stat}}(\sigma_n^0 + p_0)\, S\, u_f \\ -\mu_{\mathrm{slid}} \left[\frac{1}{\gamma} (\, \sigma_n^0 + p_0 - A)\, (1 - e^{-\gamma u_f}) + \frac{1}{\gamma'} A \left(1 - e^{-\gamma' u_f}\right) \right] S, \tag{1}$$

where the parameters are introduced in the presentation. Since the equation $F(u_f) = 0$ describes the energy conservation law, the slip satisfying $F(u_f) = 0$ is realized for the earthquakes. In actuality, slow earthquakes occur in the case where equation $F(u_f) = 0$ has three positive solutions and the smallest one is physically realized, whereas fast earthquakes occur in the case where the equation has a single positive solution. Therefore, we should obtain the condition where one of the solutions of the equation vanishes. We now consider three solutions of $dF(u_f)/du_f = 0$, and call them $u_1 < u_2 < u_3$. We consider the case where $F(u_1) < 0$ and $F(u_3) < 0$. Based on the boundary conditions $F(0) = 0$, $dF(u_f)/du_f|_{u_f=0} < 0$, and $\lim_{u_f \to \infty} F(u_f) = \infty$, we can conclude that the numbers of the real positive solutions of $F(u_f) = 0$ is one for $F(u_2) < 0$ and three for $F(u_2) > 0$. Actually, from the condition $dF(u_f)/du_f|_{u_f=u_2} = 0$, we have the relationship

$$e^{-\gamma' u_2} = \frac{k_p u_2}{\mu_{\mathrm{slid}} A S} + \frac{\mu_{\mathrm{stat}}(\sigma_n^0 + p_0)}{\mu_{\mathrm{slid}} A} - \frac{\sigma_n^0 + p_0 - A}{A} e^{-\gamma u_2}. \tag{2}$$

With this equation and the condition where the two of the solutions degenerate, $F(u_2) = 0$, we have the equation for u_f at the transition,

$$\frac{1}{2} k_p u_2^2 + \left(\mu_{\mathrm{stat}}(\sigma_n^0 + p_0)S + \frac{k_p}{\gamma'}\right) u_2 - \frac{\mu_{\mathrm{slid}}}{\gamma}(\sigma_n^0 + p_0 - A)S - \frac{\mu_{\mathrm{slid}}}{\gamma'} AS + \\ \frac{\mu_{\mathrm{stat}}}{\gamma'}(\sigma_n^0 + p_0)S + \mu_{\mathrm{slid}}(\sigma_n^0 + p_0 - A)S \left(\frac{1}{\gamma} - \frac{1}{\gamma'}\right) e^{-\gamma u_2} = 0. \tag{3}$$

If we can neglect $e^{-\gamma u_2}$, Eq. (3) is a quadratic equation for u_f. Solving the equation and substituting the solution into the equation $F(u_2) = 0$, we can analytically write the condition where the transition occurs. We also report the numerical results in the presentation, and discuss the validity of the assumption of neglecting $e^{-\gamma u_2}$.

Tremor activity in April 1988 revealed from analog seismograms of the Kanto-Tokai Observation Network

Takanori Matsuzawa[1], and Tetsuya Takeda[1]

[1]National Research Institute for Earth Science and Disaster Resilience

In the Nankai region, the past activity of tectonic tremor before 1990s is still not clear, due to the lack of continuous digital seismic data in this period. Tremor activities in the Kii region are successfully detected by the application of a recent machine learning technology to analog seismograms (Kaneko et al., 2023), although the location of tremor was not revealed. Kobayashi et al. (2006, Zisin) detected short-term slow slip events (SSEs) since 1984 using strainmeters in the Tokai region, although the location of SSEs before 1998 are not clear as only two strainmeters are available. National Research Institute for Earth Science and Disaster Resilience (NIED) operated the Kanto-Tokai Observation Network since late 1970, and has stored continuous analog seismograms on recording paper. In our previous study, we tried to develop a technique for digitizing the seismograms on the recording paper (e.g., Matsuzawa and Takeda, 2021, AGU), and tried to locate tremor reducing the effect of contaminated time mark information (Matsuzawa and Takeda, 2023, JpGU). In this study, we applied our digitization technique to the analog seismograms during a short-term SSE in April 1988.

In this study, traces of seismograms are automatically extracted from image files of the scanned analog seismogram. However, at this process, extracted traces are contaminated by other information (e.g., stamps of date, holes of paper, and stains of ink). In addition, seismic data are sometimes not correctly extracted, especially, due to the crossing of traces. Even a trace of a moderate-sized earthquake or test signal for seismometers crosses several neighboring traces. This means that more than several minutes data around the earthquake or signal cannot be used. In such case, the time label on the same sheet can be also affected. Thus, we manually removed the contaminated points from the extracted traces. Then, the time label is corrected, if it is clearly identified manually. We did not use the data with incorrect time label. As the length of each trace is 35s with an overwrap of 5s, we connect traces and obtained continuous data.

Obtained waveform data was bandpass-filtered between 2 and 8 Hz, and decimated to 50 samples/s. Then, we calculated smoothed envelope waveforms, and cross correlation function of the envelope waveforms for each minute using 2-minutes data. Using the time difference at the peak cross correlation value, we located the tremor source by the grid search technique, fixing the source depth at 30km. In the result of our tentative analysis, tremor epicenters seem to migrate in the north-east direction from April 27 to April 28, 1988 at the eastern Aichi and southern Nagano region, although estimated epicenters are largely scattered. Our study shows that past tremor activity can be revealed from the analog seismograms, while further improvement of digitization technique is still necessary.

Comparison of statistical seismicity models of low-frequency earthquakes (LFEs) and its implications for the mechanisms governing LFE activity

Tomoaki Nishikawa[1]

[1]DPRI, Kyoto Univ.

Slow earthquakes are a general term for various slow fault-slip events. In subduction zones, the relationship between slow earthquakes and megathrust earthquakes has been actively studied (e.g., Obara & Kato, 2016). Quantifying characteristics of slow earthquake activity and monitoring them are important because they may change before a megathrust earthquake (e.g., Matsuzawa et al., 2010; Luo & Liu, 2019).

Statistical seismicity models are useful for quantifying seismicity characteristics. For the activity of ordinary fast earthquakes, the epidemic-type aftershock-sequence (ETAS) model is widely used (e.g., Ogata, 1988). However, there is still no standard statistical model for slow earthquake activity. Statistical modeling of low-frequency earthquakes (LFEs), a type of slow earthquake, has begun recently. Lengliné et al. (2017) and Tan & Marsan (2020) proposed statistical models similar to the ETAS model (hereafter referred to as the L model), in which the LFE occurrence rate is expressed as the summation of a stationary background rate and the effect of each LFE inducing future LFEs. Ide & Nomura (2022) proposed a statistical model (hereafter referred to as the IN model) for tectonic tremors, a swarm of LFEs. Their model was based on an approach different from the L model; they described the probability distribution of interevent times using log-normal and Brownian passage time distributions. Furthermore, their model does not explicitly include the effect of event-to-event triggering.

Identifying the best statistical model for LFE activity is important for elucidating the mechanisms governing LFE activity. However, the existing statistical models have never been compared. Here, I applied the existing models to M 0.6 or larger LFEs in the Nankai Trough (Kato & Nakagawa, 2020) and examined their performance using Akaike's information criterion (Akaike 1974). As a result, I found the IN model often outperforms the L and ETAS models. This result indicates that the effect of LFE-to-LFE triggering is not significant. In other words, the cascade model (e.g., Ellsworth & Bulut, 2018), in which the rupture of one asperity leads to the rupture of the next asperity, cannot explain LFE activity. This is also evident from the fact that intense LFE bursts do not decay gradually but rather stop abruptly. My result places constraints on future physical modeling of LFE activity.

Deciphering the interplay between permeability and seismicity rate changes at Axial Seamount caused by dynamic stresses

Adnan Barkat[1], Yen Joe Tan[1], Guangyu Xu[2], Felix Waldhauser[3],

Maya Tolstoy[4], William S. D. Wilcock[4]

[1]Earth and Environmental Sciences Programme, The Chinese University of Hong Kong, China.

[2]Applied Physics Laboratory, University of Washington, Seattle, WA, USA.

[3]Lamont-Doherty Earth Observatory of Columbia University, Palisades, New York, USA.

[4]School of Oceanography, University of Washington, Seattle, Washington, USA.

Abstract

Our understanding of dynamic earthquake triggering in submarine environments is limited due to the lack of offshore observations. Here, we analyze the triggering susceptibility of a magmatically robust, seismically active submarine volcano (Axial Seamount), located at the intersection of the Juan de Fuca ridge and the Cobb hotspot in the northeast Pacific Ocean. Axial Seamount hosts a cabled network of geodetic and seismic instruments since late 2014. Axial Seamount last erupted in April 2015 and has continued to inflate since. We utilize a high-resolution micro-seismicity catalog to evaluate the triggering response from July 2015 to July 2022 based on seismicity rate change estimates for potential triggering sources. We report statistically significant episodes of dynamic earthquake triggering for ~18% of cases, including instances of both instant ($0 < t < 2\ hr$) and delayed ($2 < t < 24\ hr$) increases in local earthquake rate following the arrival of teleseismic waves. Initial results do not show any obvious dependence of triggering strength on the amplitude of the peak ground velocity. To evaluate the possible influence of permeability change on dynamic earthquake triggering, we compute the phase lag between vent-fluid temperature and tidal loading for the 5-day periods before and after the arrival of teleseismic waves. We report permeability changes for both triggering and non-triggering cases. Our findings provide useful insights into the physical mechanisms controlling the dynamic earthquake triggering at submarine volcanic environments.

Keywords: Volcanic inflation, Dynamic stresses, Permeability changes, Remote triggering.

Changes in very low frequency earthquake activity in the South Ryukyu Trench over 23 years

Mamoru Nakamura[1]

[1]Fac. Science, Univ. Ryukyus

Very low-frequency earthquakes (VLFEs) occur regularly in the southwestern Ryukyu Trench. The activity of VLFEs reflects the state of the interplate coupling or frictional conditions at the subducting plate interface. Therefore, I investigated the long-term VLFE activity and clarified the state of interplate slip.

First, VLFEs were detected using the F-Net and BATS broadband seismic waveform records. This detection was done using a template matching method, covering the period 2000-2022. 3-component waveforms were bandpass filtered at 0.02-0.05 Hz, and cross-correlations with the template earthquakes were calculated. For template earthquakes, I used regular thrust-type earthquakes and VLFEs. After removing JMA catalogs and teleseismic earthquakes, events with a cross-correlation greater than 0.6 were determined to be VLFEs. Based on the relationship between the magnitude and frequency distribution of VLFEs, a magnitude-completeness of 3.6 was used.

The obtained VLFEs were distributed along the trench axis at slab depths of 10-15 km. 123.0 E to 124.25 E, the VLFEs were concentrated at a depth of 15 km, and the VLFE activity in this region was very active. On the other hand, in 124.25-125.25 E, VLFEs are distributed at a slab depth of 10 km. VLFE activity was particularly active in 2000-2004 and 2015-2019; the 2000-2004 activation was most pronounced in 123.0-124.0 E. In 2015, activation was widespread from 123.0 to 125.0E.

In the southern Ryukyu Arc, crustal seismic activity and SSE rates increased from to 2002-2006 and after 2013 (Nakamura and Kinjo, 2018; Tu and Heki, 2017). This increase in activity was triggered by the 2002 afterslip and 2013 dyke intrusion in the Okinawa Trough. However, the timing of these two events does not coincide with the activation of VLFEs; in 2002, VLFEs were already active and became active again two years after the 2013 dyke intrusion; in 2015, an M6.4 earthquake occurred off the east coast of Taiwan, the timing of which coincided with the activation of VLFEs. However, the M6.4 earthquake caused a seismic stress change of less than 1 kPa in the area of the VLFEs, which was small enough to activate VLFE activity. Similarly, it is possible that VLFEs were active before 2002, and that they were activated by factors other than those responsible for activating crustal activity in the Ryukyu Arc. This suggets that a change in the interplate coupling or a long-term slow slip event occurred in the VLFE region.

Shallow fault-related folding and late Quaternary slip rate of the Osaka Bay Fault, western Japan

Mari Hamahashi[1], Hironori Otsuka[2], Yoshiaki Suzuki[3], Jun Arimoto[3], Tetsuo Matsuno[2], Nobukazu Seama[4,2], Yuzuru Yamamoto[4,2], Hiroko Sugioka[2,4], Stephen A. Bowden[5], Satoshi Shimizu[7,2], Hikaru Iwamaru[2,6], Mamoru Sano[2,6], Keita Suzuki[6], Katsuya Kaneko[4,2], Kazuo Nakahigashi[8,2], Yoshiyuki Tatsumi[2]

[1]Faculty of Global and Science Studies, Yamaguchi University, [2]Kobe Ocean-Bottom Exploration Center, Kobe University, [3]Geological Survey of Japan, National Institute of Advanced Industrial Science and Technology, [4]Department of Planetology, Graduate School of Science, Kobe University, [5]School of Geosciences, University of Aberdeen, [6]Nippon Marine Enterprises, Ltd., [7]Seisgadget Ltd., [8]School of Marine Resources and Environment, Tokyo University of Marine Science and Technology

The Osaka Bay is situated at a seismically active region north of the Median Tectonic Line and east of Awaji Island in western Japan, known as part of the Kinki Triangle and the Niigata-Kobe Tectonic Zone. Dense distribution of active faults and high geodetic strain rates characterize the region, posing a major seismic hazard potential to the coastal and metropolitan areas of the Kansai region. To investigate the shallow structure and recent deformation history of active faults in the Osaka Bay, we acquired 15 high-resolution seismic profiles using a Mini-GI airgun and a Boomer as active sources, together with multi-beam bathymetry data across the Osaka Bay Fault. Our seismic sections image a ~0.1–3.7 km-wide asymmetric anticline forelimb above the Osaka Bay Fault at shallow depths, coupled with a ~2.2 km-wide syncline to the west, and a broad, ~4.2 km-wide syncline in the footwall to the east. The synclinal axial surface at shallow depths measured in this study ranges 75–89°. We observe the vertical displacement of the Osaka Bay Fault increasing northwards along strike. The sediment thickness on the hanging wall, however, is variable, and modified by non-tectonic processes such as by tidal currents that affect the geometry of growth strata. The most recent deformation by the Osaka Bay Fault reaches near to the seafloor as active folding, with large vertical offsets of 8–14 m over the last ~11 ka, and 5–11 m over the last ~5 ka. In combination with previously reported borehole age data and deep seismic sections, the average uplift rate on the Osaka Bay Fault is estimated to be ~1.0–1.7 m/ka during the Latest Pleistocene to Holocene, and ~0.1–0.6 m/ka during the Middle- to Late Pleistocene. The inferred slip of the Osaka Bay Fault during the Holocene is likely to account for >5% of the regional geodetic strain accumulation within the Kinki Triangle. Further studies to evaluate the Holocene slip rates of regional faults are necessary to assess the seismic hazards and the internal strain budgets within the Niigata-Kobe Tectonic Zone.

New seismicity catalog and Site characterization from a regional array in Bangladesh: possible correlation of seismicity and seasonal monsoon

Syed Idros Bin Abdul Rahman[1, 2], Karen Lythgoe[2, 3], MD. Golam Muktadir[4, 5], Syed Humayun Akhter[5, 6], Judith Hubbard[2, 7] and Shengji Wei[2]

[1]Kyushu University, Graduate School of Science, Department of Earth and Planetary Sciences, [2]Earth Observatory of Singapore, Nanyang Technological University, Singapore, [3]University of Edinburgh, [4]Bangladesh University of Professionals, Bangladesh, [5]University of Dhaka, Department of Geology, Bangladesh, [6]Bangladesh Open University, Bangladesh, [7]Cornell University

Bangladesh, densely populated and located on the eastern fringe of the India-Asia collision zone, has a history marked by natural disasters such as earthquakes, cyclones, and floods, causing significant human and property losses. The eastern region experiences substantial seismic activity and rests over the Chittagong-Myanmar Fold and Thrust Belt—a geological structure resulting from the oblique subduction of the Indian Plate beneath the Burmese Plate. The Bengal Basin, situated on the descending plate, holds thick Cenozoic sedimentary layers, occasionally reaching depths of 20 kilometers. The subduction interface of this descending plate holds potential for generating major earthquakes exceeding 8.2 magnitude, posing considerable danger to the densely inhabited area.

However, uncertainties hinder seismic hazard assessment, including issues about slip distribution among frontal and interior faults within the fold and thrust belt, the influence of Bangladesh's thick sedimentary cover on earthquake shaking, and whether faults are locked and will eventually rupture at seismic speeds. Moreover, being located on one of the world's largest river deltas and near sea level, Bangladesh faces secondary risks like liquefaction and flooding from earthquake-triggered shaking.

In 2016, we deployed a network of 28 seismometers in Bangladesh's northeastern (Sylhet region) and southeastern (Chittagong region) parts. This network aims to continually monitor seismic activity and deepen our understanding of the underground geology. Operational for over six years, it has captured data from more than 3000 regional earthquakes and 170 tele-seismic events. This report presents ongoing findings from this initiative. We refined the earthquake catalog for 2016 to 2022 using meticulous methods, including manual identification of arrival times and a three-dimensional grid search technique. To better grasp the unique characteristics of seismic station sites, we employed the horizontal to vertical spectral ratio method to determine resonance frequency and amplitude. Significantly, only 32% of stations exhibited clear HVSR peaks, while others lacked discernible peaks or showed broader spectral features. This implies a low impedance contrast beneath these stations, likely due to thick sedimentary columns where seismic velocity gradually increases. Given Bangladesh's extensive sedimentary cover, reaching depths of 15 to 20 kilometers, the absence of distinct impedance contrast aligns with expectations, as the basement-sediment boundary lies too deep for effective resolution in HVSR measurements. Interestingly, the network registered reduced seismic activity during monsoon seasons, potentially due to heightened ambient noise levels or indicating a relationship between regional seismic activity and cyclic monsoon rainfall patterns.

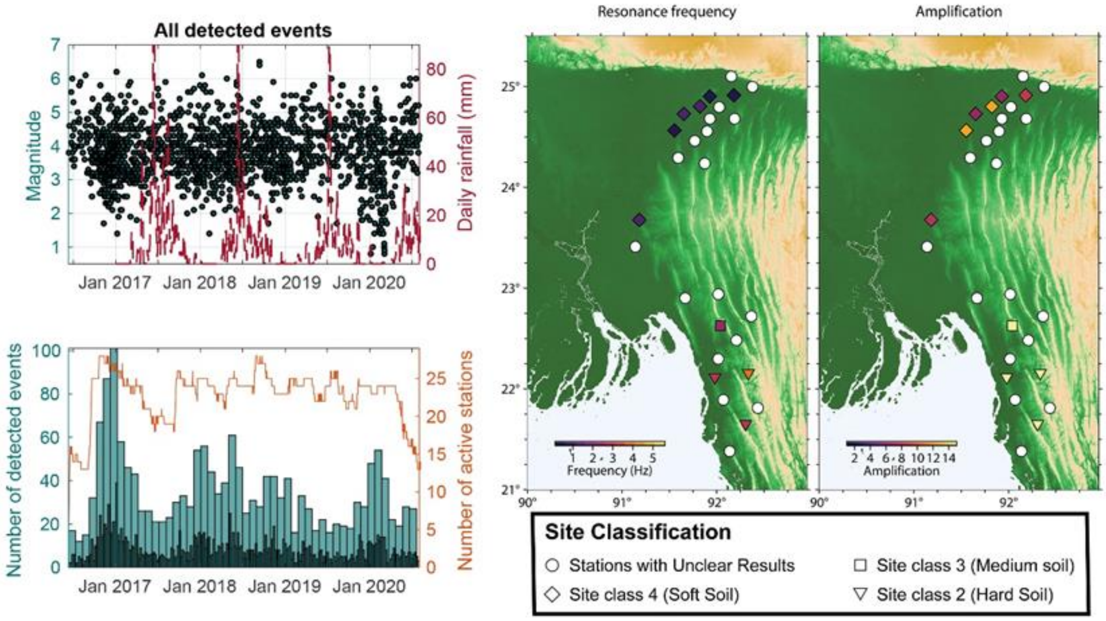
All detected events
Magnitude
Daily rainfall (mm)
Jan 2017 Jan 2018 Jan 2019 Jan 2020
Number of detected events
Number of active stations
Jan 2017 Jan 2018 Jan 2019 Jan 2020
Resonance frequency
Amplification
Frequency (Hz)
Amplification
Site Classification
Stations with Unclear Results
Site class 4 (Soft Soil)
Site class 3 (Medium soil)
Site class 2 (Hard Soil)

Shear strain energy change estimated by the current crustal deformation in Japan and spatial correlation with the crustal seismicity

Taku Ueda[1], and Takuya Nishimura[1]

[1]DPRI, Kyoto Univ.

Earthquakes are caused by the stress release in the earth's interior due to the relative plate motion. Therefore, it is considered that the strain rate estimated from geodetic data may correlate with seismicity assuming that the increase in strain corresponds to the stress accumulation in the seismogenic zone in the crust, and this relationship has been discussed in several areas in the world (e.g., Zeng et al., 2018; Stevens and Avouac, 2021; Kreemer and Young, 2022).
In Japan, however, there are azimuthal differences between the maximum contraction strain rate estimated by geodetic observations and the maximum compression stress estimated by seismological observations (Kosugi and Mitsui, 2022). Therefore, the increase in strain may not necessarily be consistent with stress accumulation. In this study, we compare the number of background events for the crustal seismicity in Japan with the shear strain energy change (Saito et al., 2018) which considers the background stress field and the current crustal deformation, instead of the strain rate (Ueda and Nishimura, 2023, JpGU).
For the strain rate estimation, we used GNSS displacement data archived at the Geospatial Information Authority of Japan (GSI), the Japan Coast Guard, Kyoto University, the International GNSS Service (IGS), and UNAVCO. The daily coordinates of GNSS stations from January 2006 to December 2009 were estimated using precise point positioning with ambiguity resolution implemented in the GipsyX Ver. 1.4 software package (Bertiger et al., 2020). We removed the common mode error and estimated secular velocities with seasonal components and significant step components using the DISSTANS python package (Köhne et al., 2023). We estimated the strain rate distribution using the basis function expansion proposed by Okazaki et al. (2021). We calculated the stress fluctuation using the estimated strain rate tensor assuming the state of plane stress and evaluated the spatial variations in shear strain energy change considering the background stress field estimated by Uchide et al. (2022).
We used the spatial variations in the number of background events ($M > 3.0$, 1980-2010, depth < 25km) estimated by Ueda and Nishimura (2023, JpGU). The study regions are in and around the four strain concentration zones: the Niigata Kobe Tectonic Zone (NKTZ), the Ou Backbone Range (OBR), the San-in shear zone (SSZ), and the Beppu-Shimabara graben (BSG).

As for NKTZ and OBR, the number of background events and shear strain energy change are weakly or moderately correlated (correlation coefficient = 0.1 ~ 0.5) and these correlations are statistically significant ($p < 0.05$). As for SSZ and BSG, we couldn't find a statistically significant correlation between the number of background events and shear strain energy change. These results are consistent with the results that the significant correlation between the number of background events and the strain rate in NKTZ and OBR, and the insignificant correlation between those values in SSZ and BSG (Ueda and Nishimura, 2023, JpGU). These results may suggest that the geodetically estimated strain rate includes the inelastic strain which is not released seismically, and there are azimuthal differences between the inelastic strain and the elastic strain.

Acknowledgements: The earthquake catalog was obtained from Japan Meteorological Agency (JMA). GNSS data was obtained from the Geospatial Information Authority of Japan (GSI), the Japan Coast Guard, the International GNSS Service (IGS), and UNAVCO. Dr. T. Okazaki provided the code for the estimation of strain rate distribution (Okazaki et al., 2021). This study was supported by JSPS KAKENHI Grant Numbers JP22KJ1770.

Mechanical plate coupling along the Sagami trough estimated from GNSS data and implication for the generation mechanism of great thrust-type earthquakes and slow slip events

Akemi Noda[1], and Tatsuhiko Saito[2]

[1]MRI, JMA, [2]NIED

In the Sagami trough subduction zone, central Japan, great thrust-type earthquakes (~M8) repeatedly occurred with recurrence times of several hundred years. The last two earthquakes were the 1703 Genroku Kanto earthquake (M_w 8.1-8.5) and the 1923 Taisho Kanto earthquake (M_w 8.0), which caused extensive damage to the Tokyo metropolitan area. The source models of these two earthquakes are similar, but there are differences. Although their source models share the fault rupture zone beneath the Miura peninsula, the source region of the 1703 event wraps around to the southeastern coast of the Boso Peninsula, and that of the 1923 event reaches the Izu-Mainland collision zone. Therefore, Sato et al. (2016) pointed out that there are three main rupture areas beneath the Miura peninsula, the Izu-Mainland collision zone and the southeastern coast of the Boso Peninsula. To understand the mechanisms that cause such complexity of great earthquakes consisting of the three main rupture areas, it is necessary to estimate the mechanical state of the plate interface along the Sagami trough.

We have developed a method to directly estimate stress accumulation rates at plate interfaces from geodetic data (Saito & Noda, 2022). In this study, this method is applied to GNSS displacement rate data in the Kanto region from March 1998 to February 2008 to estimate the stress accumulation rate in the Sagami trough subduction zone (Saito & Noda, 2023). Here, the data associated with the Boso slow slip events (SSEs) were removed before the analysis, so the estimated stress rate represents the state during the inter-SSE period. The estimated stress rate distribution has four peaks, which are isolated from each other. We recognize these stress accumulation areas as mechanically coupled areas. Three of them, named O, M, and A, are located in the source region of the past great earthquakes. Each peak corresponds to the three main rupture areas suggested by Sato et al. (2016), and the accumulated stress in these regions would cause the complexity of great earthquakes along the Sagami trough. In other words, these three stress accumulation regions can be the smallest units of fault segmentation, and the combination of the segmentation units produces a diversity of the sources. On the other hand, the remaining one of the mechanically coupled areas, named B, corresponds to the occurrence area of the Boso SSEs. We estimated the slip distribution when the stresses that accumulate during the inter-SSE period, assumed to be five years, at the stress accumulation region B are released. The resultant slip model is similar to that of the actual Boso SSEs. Therefore, the stress accumulation at the region B is considered to be released by SSEs.

Finally, using the estimated stress accumulation rate, we create rupture scenarios for great earthquakes along the Sagami trough with the method of Noda et al. (2021). We determine source regions by selecting a single mechanical coupling area from the candidate areas O, M, and A or a combination of these areas. A total of six scenarios are possible. The scenarios contain not only ones with similar source regions to the 1703 and 1923 events but also ones that we have not experienced in the past, such as the combination of all three mechanical coupling areas.

References:

Noda, A., *et al.* (2021). Energy-based scenarios for great thrust-type earthquakes in the Nankai trough subduction zone, southwest Japan, using an interseismic slip-deficit model. *Journal of Geophysical Research: Solid Earth*, **126**(5), e2020JB020417. https://doi.org/10.1029/2020JB020417

Saito, T., & Noda, A. (2022). Mechanically coupled areas on the plate interface in the Nankai trough, Japan and a possible seismic and aseismic rupture scenario for megathrust earthquakes. *Journal of Geophysical Research: Solid Earth*, **127**(8), e2022JB023992. https://doi.org/10.1029/2022JB023992

Saito, T., & Noda, A. (2023). Mechanically coupled areas on the plate interface in the Kanto region, central Japan, generating great earthquakes and slow slip events. *Bulletin of the Seismological Society of America*, accepted.

Sato, T. *et al.* (2016). The source model and recurrence interval of Genroku-type Kanto earthquakes estimated from paleo-shoreline data. *Earth, Planets and Space*, **68**, 17. https://doi.org/10.1186/s40623-016-0395-3

Detection of immediate aftershocks following the 2011 Tohoku Earthquake using a seismic array in the Kanto region

Takuro Imadera[1], Aitaro Kato[1], Shin'ichi Sakai[2]

[1]ERI, Univ. Tokyo, [2]Interfaculty Initiative in Information Studies, Univ. Tokyo

Due to intensive aftershocks following the 2011 Tohoku Earthquake, the wavefields generated by large events have reduced the detectability of medium- and small events, resulting in missing events in existing earthquake catalogs. Although there have been several attempts to recover the missing events [e.g., Lengliné et al., 2012; Hi-net catalog], it is still challenging to reveal the detailed space-time evolution of the immediate aftershocks because of a shutdown of seismic networks in the entire Tohoku region.

To enhance the detectability of the immediate aftershocks, we applied the matched-filter method to the continuous waveform (over a month duration from the mainshock) recorded by the MeSO-net, which is a seismic array installed in the Kanto region. As template events, we used waveforms of earthquakes ($M \geq 4.5$) listed in the JMA catalog events for about one year after the mainshock. The template and continuous waveforms were downsampled from 200 Hz to 25 Hz and applied a 1-8 Hz bandpass filter.

As a result, we detected about three times as many events as those listed in the JMA catalog for $M \geq 4.5$. Furthermore, we can identify smoother south-ward migration of the aftershock area than that of the previous studies [Lengliné et al., 2012; Hi-net catalog]. The migration of the aftershock front was approximately 5 km/h. This migration was interpreted to be driven by the afterslip of the mainshock or Mw7.7 aftershock off the coast of Ibaraki [Lengliné et al., 2012]. The migration of the aftershock front stopped near the contact zone between the Pacific Plate with the Philippine Sea Plate.

Development of a method for determining the epicenter of tectonic tremors using a deep learning decision basis method

Amane Sugii[1], Yoshihiro Hiramatsu[1], Takahiko Uchide[2], Kazutoshi Imanishi[2],

[1]Kanazawa Univ., [2]AIST

Slow slip events (SSEs) occur repeatedly at intervals of several months to several years at plate boundaries around the world. SSEs are accompanied by tectonic tremors in space and time. Tectonic tremors are suitable for monitoring of SSEs because they can be easily observed by seismometers. Several methods have been proposed for detecting tectonic tremors, such as an envelope cross-correlation method (Obara et al., 2002) and a semblance analysis (Neidell and Taner, 1971), which utilize the correlation of waveforms and their envelopes at multiple seismic stations. However, all these methods detect not only tremors but also noise and earthquakes as tremors. Another problem is the difficulty in locating tremors with high noise levels, preventing us from understanding the characteristics of tremors in detail. Misclassification between tremors and noise can be solved by using deep learning, which has made remarkable progress in recent years (e.g., Nakano et al., 2019). Using convolutional neural networks (CNN), a method for classifying spectrogram images between noise, tremors, and earthquakes has a discrimination accuracy of over 90 % for test data selected from a catalog.

CNN's decision-basis visualization images can enhance the accuracy of locating tremors because the decision-basis visualization image is a technique that visualizes the gazing part of an image when CNN classifies the image. Using this technique, it is possible to extract tectonic tremor with a low signal-to-noise ratio by reconstructing the waveform from the spectrogram by highlighting the gazing parts and removing the noise (e.g., Rouet-Leduc et al., 2019). This study aims to improve the accuracy of tremor source determination by developing a CNN that can classify noise, tremors, and earthquakes, and by constructing a new source determination method for tremors using a decision basis visualization method.

We used data from the array observation network of the National Institute of Advanced Industrial Science and Technology (AIST) located on the Kii Peninsula. The period is from April 2011 to December 2015. For training and evaluation of the CNN model, the period from April 2011 to March 2013 was classified as training, April 2013 to March 2014 as validation, and April 2014 to December 2015 as test data. Three-component velocity waveform data with a time length of one minute is used for the following analyses. To create the model, we visually classified a one-minute waveform into tremor, noise, and earthquake. For tremors, we selected events within a radius of 40 km from the central station of the array based on the tremor catalog (Imanishi et al., 2011). Earthquakes were selected from the JMA catalog of which an event was observed at more than one of the four Hi-net stations in the vicinity of the array. In addition, the noise was selected from periods in which tremors or earthquakes are not included in the catalogs. We applied a 2–10 Hz bandpass filter to the three component velocity waveforms and converted the filtered waveforms to spectrograms. The spectrograms are scaled from 0 to 1 by the minimum and maximum values of each component. The three spectrograms of an event are used as input to the model as a single piece of data. The trained CNN model consists of two convolutional layers and three all-coupled layers; the three component spectrograms are used as input to output three probabilities: noise, tremor, and earthquake. The model with the lowest loss in the validation data was used for the classification.

As a result of the training of the CNN model, an accuracy of more than 93 % was achieved in terms of both reproducibility and goodness-of-fit for a total of 9,000 test data for noise, tremors, and earthquakes. The highest fit rate for earthquakes was 98.2 %. More than 90% of the test data were correctly classified with a predicted probability of 90 % or higher for each event. We visually confirmed that the Score-CAM captured the P- and S-waves of an earthquake, the extinction of a tremor amplitude, and the sparse spectral distribution of noise. The application of the model to a 1-hour waveform showed that it was possible to extract tremors not listed in the tremor catalog.

We located the epicenters of tremors classified by the CNN model. We used Score-CAM (Wang et al., 2019) as the decision basis visualization method. The generated Score-CAM was averaged over the stations and binarized using the threshold value of 0.8. The waveform was reconstructed from the binarized Score-CAM and the spectrogram of the NS component for a semblance analysis. The waveform reconstruction using the Score-CAM provided a filtered waveform around the highest amplitude in a 1-minute waveform. The procedure for locating tremors is as follows. Grids were placed horizontally at 2 km intervals in the analysis area, and the depth of each grid was fixed at 5 km shallower than the Moho surface of the Philippine Sea slab (Shiomi et al., 2008). We used the slowness of the optimum ray path between a grid and the central station of the array for a semblance analysis (Nakamoto et al., 2021). The waveforms were aligned based on the slowness assigned to each grid and the height correction of each station was applied (Nakamoto et al., 2021). The semblance analysis shows that the maximum semblance value of a 1-hour waveform with Score-CAM was 0.1 higher than that without Score-CAM. The tremors with a semblance value of 0.4 or higher show a similar source location. On the other hand, locating is difficult for tremors with small amplitudes.

Extraction of deep tectonic tremor waveforms using deep learning: Application to Hi-net stations in the Shikoku region

Yuya Jinde[1], Amane Sugii[1], Yoshihiro Hiramatsu[1]

[1] Kanazawa Univ.

Tectonic tremors (hereinafter referred to as tremors) are observed in subduction zones around the world. The Nankai subduction zone in southwestern Japan is one of the most active tremor regions in the world. In the Nankai subduction zone, deep tremors occur within a belt-like zone at the downdip edge of the seismogenic zone and are distributed nearly continuously over a length of 600 km (Obara, 2002). Deep tremors are often accompanied by short-term slow-slip events (S-SSEs) and very-low-frequency earthquakes (VLFEs), which are referred to as ETS. ETS can induce the occurrence of megathrust events by inducing stress concentrations in the focal area (Obara and Kato, 2016). Therefore, understanding the nature of tremor activity is important.

Tremors are weak vibration phenomena with dominant frequencies ranging from 1 to 10 Hz and durations from several minutes to several hours and are characterized by the difficulty of detecting their phases. Therefore, it is difficult to apply ordinary earthquake detection methods to tremors, and envelope correlation methods (Obara, 2002) or hybrid methods that consider amplitude information in addition to envelope time differences (Maeda and Obara, 2009) are often used for automatic detection of tremors. However, these methods sometimes detect regular earthquakes and noise as tremors, requiring visual inspection. To solve this problem, previous studies have used deep learning to classify seismic waveforms (Nakano et al., 2019; Takahashi et al., 2021). These studies applied convolutional neural networks (CNN) as models and spectrograms formed from seismic waveform records as input data and reported that they could discriminate noise, tremor, and earthquake events with high accuracy based on the results of applying the CNN to test data. According to the results of previous studies, the application of deep learning seems to be suitable for realizing a more objective and unified analysis of tremor activity. However, systematic extraction of tremor waveforms over a wide area using deep learning and analysis using the extracted tremors have not yet been established. Therefore, in this study, we aim to establish a deep learning-based tremor analysis method, extracting tremors using a CNN and tentatively determining the tremor duration time, which is a basic indicator of the tremor size, from the extracted tremors.

The area of this study is the Shikoku region and the period is one year from January 1, 2016, to December 31, 2016. After applying a 2–30 Hz bandpass filter to a 1-minute seismic waveform recording, the spectrograms were generated under the following conditions: a 5-second time window, 80% overlap, and maximum and minimum normalization. We used the three components of the spectrograms as input data. The CNN model consists of two convolutional layers, two pooling layers, and three fully connected layers, with the output layers outputting noise, tremor, and earthquake probability values, respectively. The model was trained using 41,400 spectrograms, and when applied to test data consisting of 13,800 spectrograms, a 98.0 % accuracy was recorded. Tremors were extracted for each of the three sub-regions of the eastern Shikoku, the central Shikoku, and the western Shikoku, using 13 stations in the eastern region, 9 in the central region, and 18 in the western region. In this study, a tremor was defined as an event that was identified as a tremor at three or more stations and lasted at least two minutes. We obtained 4078 events in the eastern area, 4081 events in the central area, and 7215 events in the western area, with the longest event lasting 391 minutes. The cumulative time of events showed a step-like increase, which was synchronized with the onset of S-SSE. These results indicate that our method can appropriately capture the onset of tremor events. In addition, the tremor extraction using the CNN model can extract tremor waveforms during periods of high tremor activity, which are often undetected by the conventional method based on waveform correlation. Further investigation and studies are needed to determine the source location of tremors detected by the CNN model.

<Acknowledgments>
We used waveform data recorded by Hi-net and the tremor catalog created by a hybrid method (Maeda and Obara, 2009), and a hybrid clustering method (Obara et al., 2010). We also used the arrival time data and the unified earthquake catalog of JMA to create our earthquake catalog.

Current situation of onshore broadband seismic observation for slow earthquakes in Japan and worldwide, 2023

Akiko Takeo

[1]ERI, Univ. Tokyo,

The broadband characteristics of slow earthquakes have been pronounced since the discovery of very low frequency earthquakes (VLFEs) at a period range of around 20–50 s in Nankai, Ryukyu, Costa Rica, and Tohoku subduction zones. The VLFEs are now considered to be occurring at the interface between subducting oceanic plate and overlying continental plate. The activity can be divided into shallow and deep VLFEs based on whether they are occurring in the area shallower or deeper than the seismogenic zones.

Most of previous VLFE works use permanent broadband stations except for the work on deep VLFEs by Nanakaido-NECESSArray (Takeo et al. 2010) and shallow VLFEs by temporal deployment of broadband ocean bottom seismometers (Sugioka et al. 2012) in the Nankai, deep VLFEs by US Transportable Array (Ghosh et al. 2015) in the Cascadia, and shallow VLFEs by the TUCAN experiment (Baba et al. 2021) in the Costa Rica subduction zones. The data qualities of these temporal stations, especially for the onshore deployment, are usually limited by atmospheric disturbances and human activities.

In this presentation, I simply review onshore observation for broadband slow earthquakes in Japan including a campaign observation in 2008 (Takeo et al., 2010), 6 semi-permanent deployment from 2015 to 2017, and 14 deployment from 2019 to 2020 (Takeo et al., in prep.). I also briefly discuss the current situation of broadband seismic observation in other plate boundaries, and the current preparation for the next observation in Japan.

Controlled Shear Stress Experiments for Spontaneous Generation of Slow Earthquakes using a Rotating Shear Apparatus

Yohei Hamada[1], Takehiro Hirose[1], Wataru Tanikawa[1], Wakahiro Suzuki[2]

[1]JAMSTEC, X-star, [2]Marine Works Japan

Earthquake faults reside in a critical state of either slipping or remaining stationary. At this juncture, fluctuations in fluid pressure within the fault zone are considered contributory to diverse earthquakes transitioning from gradual to rapid. Although the traditional "slip displacement - rate control" approach has examined seismic origination, it fails to replicate the natural process of slip inception and acceleration. Our study thus employed a rotating friction apparatus, offering torque and fluid pressure control, to experimentally induce spontaneous fault slip.

Initially, a basic experiment employed a specimen (standard SiO2) to assess frictional dynamics under constant, low velocity. The torque was incrementally raised (0.3 N-m/s) at a normal stress of 5 MPa. Slip initiation transpired upon reaching a torque of 200 N-m (equivalent to a shear stress of 4 MPa and friction coefficient of 0.8), followed by a progressive acceleration to 170 microns/sec, demonstrating an acceleration rate of 20 micron/s/s. We conducted an additional experiment involving incremental elevation of fluid pressure subsequent to preset values of axial pressure and torque. This yielded comparable acceleration patterns. Notably, both experiments reached a terminal velocity of 170 microns/sec, with no escalation to the centimeter-per-second range, a predetermined threshold. While these findings may simulate the initial stages of a slow earthquake, it remains plausible that the observed outcomes stem from potential experimental anomalies, particularly uncontrolled torque leading to its decrease upon slip commencement. Our presentation will encompass these experimental outcomes alongside their interpretations, encompassing torque-controlled experiments and the genesis of slow earthquakes.

Evaluating uncertainties in CMT inversion to estimate non-double couple components of earthquakes

Suguru Yabe[1], Kazutoshi Imanishi[1], Shunsuke Takemura[2]

[1]Geological Survey of Japan, AIST, [2]ERI, Univ. Tokyo

It has been pointed out by many researchers since slow earthquakes was discovered that high-pressure pore fluid plays an important role in slow earthquakes. Geophysical evidence includes high tidal sensitivity of tectonic tremors (Shelly et al., 2007) and high V_p/V_s ratio estimated at source regions of slow earthquakes (Shelly et al., 2006). Crack seal quartz veins observed in subduction mélange also suggest that high-pressure pore fluid opened the cracks in slow earthquake source region (Ujiie et al., 2018). Non-double couple components in the centroid moment tensors (CMTs) could be one of clues to constrain the amount of fluid contribution in slow earthquake source process. Non-double couple components in CMTs are usually found at earthquakes in volcanic regions (Shuler et al., 2013) or complex strike-slip fault systems (Stierle et al., 2014), which are generally attributed to cosesimic crustal deformation with dilation or contraction. However, non-double couple components in CMTs are difficult to estimate accurately because imperfect knowledge on seismic structure can cause artificial non-double couple components in CMTs (Wang and Zhan, 2020). Therefore, evaluating accuracy of CMT estimation is an important task to confirm existence of non-double couple components in CMTs.
In this study, we evaluate uncertainties in CMT estimation in the southwest Japan using synthetic datasets. The target event was the earthquake occurred on 2021/12/03 09:28 (JST) beneath Kii Peninsula. We used the hypocentral location and focal mechanism listed in F-net catalog. First, by using OpenSWPC (Maeda et al. 2017), we prepared target waveforms using the Japan Integrated Velocity Structure Model (JIVSM; Koketsu et al., 2012) as a background three-dimensional velocity structure. We made 100 patterns of exponential-type random perturbations with wavelength of 10 km and amplitude strength of 5% and embedded to the JIVSM. Then, resultant 100 patterns of target waveforms were inverted for CMT using Green's function based on one-dimensional seismic structure of F-net, which were calculated with a wavenumber integration algorithm (Hermann et al., 2013).
Geological Survey of Japan, AIST has constructed borehole strain observatories in the southwest Japan. Strain observation data at those stations are usually used for monitoring slow slip events, though they can be used to monitor seismic waves as well. Therefore, we also developed the CMT inversion method, which integrated different types of ground motion data (translation, strain, and rotation). Using the synthetic data calculated above, we also evaluated the benefits of using different types of ground motion data in CMT inversion.

Numerical experiments using a friction law both for rapid and slow sliding with radiation damping effect

Takane Hori[1], and Hideo Aochi[2]

[1]JAMSTEC, [2]BRGM

To realize various fault slip behavior as regular and slow earthquakes, we assume a simple friction law. In the friction law, the frictional strength decreases due to fault slip and recovers with time. These two processes along the fault, slip-weakening and healing are the intrinsic ones to model regular and slow earthquake sequences. Here, an evolution equation of the frictional strength proposed by Nielsen et al. (2000) is used. In this equation, there are two frictional parameters, d_c and t_c, which represent a characteristic displacement for slip-weakening and a characteristic time for healing, respectively. The balance of these two parameters controls how frictional strength evolves depending on the fault slip history. To examine fault slip behavior with the evolution equation, a single degree of freedom elastic system, composed of a block and a spring with constant loading is introduced. The block starts to slip following the strength evolution equation when the shear stress acting on the contact surface of the block reaches the strength. On the other hand, the block is in stationary contact if the shear stress is less than the strength. Note that this is a classical constitutive law without direct effect in a rate- and state-dependent friction law (Nakatani, 2001). To examine the slip behavior depending on the above system, we modified a simulation code used in Aochi and Matsu'ura (2002), which introduces more complex evolution equation of fault strength. Some preliminary results show that both intermittent rapid and slow sliding with can be demonstrated depending on the two frictional parameters. These slip behaviors are similar with regular and slow earthquakes. In this presentation, we specifically investigate how radiation damping effect affects the slow sliding behavior.

Numerical simulation with a multiscale circular patch model in the northern segment along the Japan Trench (IV)

Ryoko Nakata[1], Takane Hori[2], Hideo Aochi[3,4], Satoshi Ide[1]

[1]Dept. EPS, Univ. Tokyo, [2]JAMSTEC, [3]BRGM, France, [4]ENS-CNRS PSL, France

Earthquakes of various magnitudes have occurred in the subduction zones. The magnitude range of fast earthquakes is generally continuous in seismically active areas such as along the Japan Trench. To reproduce some of them, we performed numerical simulations of earthquake generation cycles, approximating M ~ 9 and M ~ 7 interplate earthquakes along the Japan Trench as rectangular and circular patches, respectively (Nakata et al., 2016; 2023). However, these are only some of the historical earthquakes that have occurred in the area.

In this study, to understand the continuous distribution of magnitudes and their physical processes of earthquake cycles by a simple model, we performed quasi-dynamic simulations of earthquake cycles using a multiscale circular patch model (Ide & Aochi, 2005; Aochi & Ide, 2009; Ide & Aochi, 2013) off Sanriku along the Japan Trench. The multiscale patch model was used by Ide & Aochi (2013) to document the complex dynamic rupture process of the 2011 Tohoku-Oki earthquake. To determine the spatial heterogeneity of seismic events, historical earthquakes with Mj = 6.5 to 8.0 were divided into three groups. The slip weakening distance *Dc* was set to be constant within each group and proportional to the patch radius.

We extracted earthquakes in the northern segment of the Japan Trench from the list used in Ide & Aochi (2013). The largest is the 1896 Meiji-Sanriku earthquake with M = 8. This event belongs to group 1. The second group includes six earthquakes with Mj = 7.1 to 7.6. The third group contains nine earthquakes with Mj = 6.6 to 7.2. In addition to the three groups, we used the historical earthquakes with Mj = 5.6 to 6.5 from the JMA catalog since 1923 as a fourth group. Our simulation is based on the rate- and state-dependent friction law, which represents the process of stress accumulation and release at the plate interface. The equations, initial conditions, basic parameters, and discretization of the plate geometry were the same as those used in our previous studies (Nakata et al. 2016; 2021; 2023). In our simulation, the characteristic slip distance *L* corresponds to *Dc*. We assumed *L* to be constant within each group and proportional to the patch radius. We assumed that *A*-*B* is uniform regardless of the magnitude of the earthquake.

When all the events are used to determine the spatial heterogeneity of *L* as it is, group 4 patches covered a large area and group 2 and 3 patches were almost invisible as the frictional heterogeneity. As a result, the slip area of large to moderate earthquakes was larger than that of group 1, 2 and 3 patches. Then, the number of group 4 patches was reduced from 362 to 28 by grouping them according to their distances. As a result, large to moderate earthquakes sometimes ruptured simultaneously with closely spaced and partially overlapping patches, showing the complex earthquake cycles with a wide range of magnitudes. Isolated patches ruptured with nearly constant recurrence intervals. On the other hand, when multiple patches are close together, the recurrence interval of earthquakes at the smallest patch is not constant, but tends to be shorter after large to moderate nearby earthquakes. We show the difference between one- to four-scale patch models in terms of properties such as slip distribution, rupture initiation and propagation, magnitude-frequency distribution, and recurrence interval. Our results suggest that a hierarchical structure is fundamentally important for simulating not only the dynamic rupture process, but also earthquake cycles.

Runaway slip in fault rock analog

Miki Takahashi[1]

[1]Geological Survey of Japan, AIST

It is considered that a runaway slip on the fault yielding a large-scale earthquake occurs in the brittle-ductile transition (BDT) zone. However, how the ductile deformation, considered as the deformation with stable behavior, plays a role for an onset of runaway slip in BDT zone has been rarely discussed. Understanding of slip acceleration process of ductile deforming fault would be necessary to understand the earthquake nucleation process in BDT zone. Moreover, shear experiments to monitor the evolution of slip velocity (*V*) under a boundary condition which constrained imposed shear stress (τ_{imp}) have been insufficiently conducted in the first place. Here, I would like to report results of the shear experiments giving step increases in τ_{imp} on fault rock analog, brine-saturated, 80:20 (wt. %) mixture of halite and muscovite gouge, at room-temperature and 5 MPa in the normal stress. I used a rotary shear apparatus set at GSJ, AIST. In this presentation, additionally, I would also like to show a result of examination of the microphysical model to explain our experiments.

Frictional properties of that fault rock analog have been well investigated [e.g., Niemeijer and Spiers, 2007, JGR; Takahashi et al., 2017, G-cubed]. The fault rock analog have showed *V*-strengthening at < 1 μm/s driven by pressure-solution and precipitation creep of brine-saturated halite and *V*-weakening at > 1 μm/s caused by shear induced dilation, respectively. At around 1 μm/s, thus, the shear strength became maximum (τ_{max}), which value was ~3.8 MPa. Moreover, at < 20 μm/sec, steady-state shear strength of the fault rock analog was 1.0~1.5 MPa and showed a less dependence on *V*.

For cases of $\tau_{imp} < \tau_{max}$, well-reproducible *V*-strengthening relationship was comparable with those found in previous studies that limited *V* to be < 1 μm/s. Once τ_{imp} exceeded τ_{max}, meaning *V* exceeded 1 μm/sec, I observed an acceleration of the slip followed by dynamic weakening (runaway slip). That dynamic weakening appeared at around 20 μm/sec. It was notable that the fault rock analog remained the shear stress constant at τ_{max} for a several hours before the appearance of the dynamic weakening, even though the steady-state shear strength should be significantly decreased. Additionally, I observed that a localized shear zone with a several tens of micrometer thick cut a zone of S-C' mylonitic structure which has been formed pervasively under lower τ_{imp} conditions.

According to those results, I conclude there were two key velocities, 1 μm/s and 20 μm/s, to characterize a process of the dynamic weakening of the fault rock analog that has been deforming in stable creep regime. I think that several hours delay prior to an occurrence of the dynamic weakening would be caused by an abnormally high value of the direct effect (>0.1) when *V* was less than 1 μm/sec [Takahashi et al., 2017]; the fault rock analog could obtain strength temporary by slip acceleration as long as the direct effect had a value. However, as known by Takahashi et al., [2017], the direct effect became almost negligible and the steady-state strength became much low if *V* exceeded 20 μm/sec, inducing the dynamic weakening. Additionally, a process of shear localization after τ_{imp} excessed τ_{max} could be of the ductile failure. To measure these key velocities relevant to the process of the ductile failure in nature would be very important to understand the earthquake nucleation process in BDT zone.

Geological constraint on fluid pressure ratio during mélange formation in a shallow ductile-to-brittle transition zone along a subduction plate interface

Takahiro Hosokawa[1], Yoshitaka Hashimoto[1], Hiroki Inui[1], Kazuki Honda[1]

[1]Kochi University

Fluids play key roles in deformation and mass transfer along subduction plate interface. In particular, fluid pressure along décollement has a significant effect on slip behaviors in subduction zone. There are, however, few examples of quantitative constraints on fluid pressure ratios along décollement, except for these in the shallow portions of subduction zone. Therefore, the purpose of this study is to constrain fluid pressure ratio around a shallow transition zone during mélange formation in an exhumed accretionary complex, the Yokonami mélange, the Cretaceous Shimanto Belt, SW Japan.

The study area is the Yokonami mélange, which is bounded by the Goshikinohama fault from a coherent unit in the north. The Yokonami mélange is composed mainly of sandstone and black shale, with minor amounts of tuffs, red shales, limestones, cherts, and basalts. Fluid inclusion microthermometry for shear veins revealed fluid temperature and pressure of about 175-225 °C and about 143-215 MPa. In this study, we focus on extension veins in the Yokonami mélange and, classified the veins into two. One is observed only in the mélange blocks (Type 1 vein) and the other is found in the matrix surrounding the blocks (Type 2 vein).

We used mixed Bingham statistics to estimate the paleo stress state for Type 1 veins and Type 2 veins. The latter was used for the examination of block rotations by the consistency in their paleo stresses. In addition, we estimated temperatures and pressures of fluid for Type 1 veins using fluid inclusion microthermometry.

The results of stress analysis indicated that the mélange blocks were not rotated, and Type 1 veins was formed under a normal fault stress regime. Temperatures and pressures of Type 1 veins are obtained about 175-203.5 °C of and about 171.2-217.9 MPa.

Our result and a previous study show that temperature conditions for Type 1 veins and shear veins are overlapping, suggesting the coexistence of ductile and brittle deformations. Thus, the Yokonami mélange located in the shallow ductile-brittle transition zone.
We constrained the rock tensile strength and the formation depth to be about 11.7 MPa and about 7.9 km, using the rock failure theory and the fluid pressure variations. Furthermore, we calculated fluid pressure ratio and maximum differential stress to be about 0.83-1.05 and about 46.8 MPa. Our study indicates a high fluid pressure ratio and the mechanical weakness in the footwall below the décollement at the shallow ductile-to-brittle transition zone.

Comparison between the porosity of gravels of submarine landslide deposit and that of accretionary prism sediment in the off-Kumano Nankai Trough

Rina Fukuchi[1], Yang Zhao [2], Kazuya Shiraishi[3], Mari Hamahashi[4], Masashi Murayama [5], Juichiro Ashi[2], and Asuka Yamaguchi[2]

[1] Naruto Univ. of Education, [2] AORI, Univ. Tokyo, [3] JAMSTEC, [4] Yamaguchi Univ., [5] Kochi Univ.

The relationship between the variety of developmental process of accretionary prisms due to subduction of topographic high such as seamounts and seismic activity, including slow earthquakes, has been widely discussed and become clear (e.g. Cloos and Shreve, 1996; Scholz and Small, 1997; Wang and Bilek, 2014, Sun et al., 2020). For instance, the friction at the plate boundary fault plane in addition to seafloor irregularities contributes to the structural development of the accretionary prism margin based an analogue model experiment (Okuma et al., 2022). However, field data to elucidate their causes, developmental processes, and spatio-temporal variation are scarce. On the western side of International Ocean Drilling Program (IODP) drill sites (C0006, C0007 and C0024) off-Kumano, a submarine landslide topography (~10 km^2 size) is identified (Moore et al., 2009) and it is considered to be caused by the subduction of any topographic high.
To investigate the nature of the submarine landslide and the effect of seamount subduction offshore Kumano, KS-22-3 cruise was carried out in March 2022 by the R/V Shinsei Maru and a piston core sample was retrieved from surface sediments. The piston core sample was collected down to 2.8 m below the seafloor (mbsf). The piston core sample was nondestructively measured and lithologically described, and gravels of sedimentary rock harder than the matrix were identified from 1.4 m mbsf. Porosity of the sampled gravels were measured and compared with porosity of the IODP sites to clarify the origin of the gravels. The measured porosity of the gravels showed 48-58%, with similar values at several depths of the IODP sites, such as 1-77 mbsf and 450-600 mbsf at site C0006, between 3-34 mbsf and 74-84 mbsf at site C0007, and at depths between 4-113 mbsf at site C0024. At the drill site C0011, the values of porosity are equivalent to approximately 250 mbsf within the Shikoku Basin sediments above the incoming oceanic basement. Based on the distribution of porosity, the gravels with low porosity are considered to have been uplifted and exposed by thrust faulting of the frontal prism. Furthermore, because seismic reflection profiles at the sampling site show subsurface structure with deformation and slope collapse of the accretionary prism above the trench-ward side of a significant topographic high, it is probable that the landslide was caused by the effect of the subducted topographic high, which was added to the uplift caused by the thrust faulting during accretionary structure development. The excessive uplift due to the subduction of the topographic high might trigger the seafloor landslides at least from about 100 mbsf at the paleo-frontal prism sediments, which was inferred at the IODP sites comparing with the porosity of the sampled gravels of sedimentary rock.

Cloos, M. and Shreve, R.L. (1996), Geology, doi:10.1130/0091-7613(1996)024<0107:SZTATS>2.3.CO;2
Moore et al. (2009) Proc. IODP Vol. 314. No. 315/316, doi:10.2204/iodp.proc.314315316.102.2009.
Okuma et al. (2022). Tectonophysics, doi:10.1016/j.tecto.2022.229644
Scholz and Small, (1997) ,Geology, doi: 10.1130/0091-7613(1997)025<0487:TEOSSO>2.3.CO;2
Sun et al. (2020), Nat. Geosci., doi: 10.1038/s41561-020-0542-0
Yamaguchi et al., 2020 ; IODP Expedition 358 C0024, doi: 10.14379/iodp.proc.358.104.2020

Exothermic events in the fossil seismogenic fault yielded as the secondary magnetization; Cretaceous accretionary complex, Shimanto Belt

Taizo Uchida[1], Yoshitaka Hashimoto[1], Yuhji Yamamoto[2] and Tadahiro Hatakeyama[3]

[1]Univ. Kochi, [2]MaCRI, Univ. Kochi, [3]Okayama Univ. of Science

Various slips of faults along subduction plate interfaces have been reported by geophysical observations (e.g., Obara and Kato, 2016). Geologically, frictional heating generated by a seismic slip has been employed to evaluate the slip rate (e.g., Rice, 2006). Although magnetic properties have been also used for temperature constraints (e.g., Mishima et al., 2006), remanent magnetization which may record a seismic event is less discussed. We hence compared magnetic properties and remanence between fault rocks and host rocks to detect exothermic events in a fossil plate boundary fault.

The study area is mélange and coherent units in the northern Cretaceous accretionary complex, Shimanto Belt. The paleomaximum temperature were estimated ~250 °C and ~200 °C at mélange (Ohmori et al., 1997) and coherent units (Sakaguchi, 1999), respectively. A few meters thick fault zone with cataclastic shear zones are observed within the mélange unit. The samples were collected from cataclasite in the fault zone, host rocks from mélange and coherent units.

Thin section observations, SEM-EDS analyses, and rock magnetic experiments all indicate consistently that pyrite and magnetite are included in all lithology and pyrrhotite is existed only in cataclasite. The occurrence of magnetite in cataclasite is, however, displaying framboidal crystal. The occurrence implies that the magnetite in cataclasite was replaced from framboidal pyrite. Magnetite in host rock has euhedral shape. Therefore, although magnetite is observed both in cataclasite and host rocks, their origins could be different.

The remanence is comprised of multiple components for all lithologies. In case of cataclasite, three demagnetized components were identified, 1) viscous acquired at current setting, 2) medium–temperature at 300–360 ℃ and –coercivity demagnetized at about 20 mT component (medium temperature (MT) component) and 3) characteristic remanent magnetization (ChRM). The second one is observed only in cataclasite. Other lithologies have only two components: viscous and ChRM.

MT component is carried by monoclinic pyrrhotite and magnetite. The unblocking temperature of MT component, 300 to 360 ℃, is higher than the paleomaximum temperature of host rock and lower than Curie temperature (T_c) of magnetite (~580 ℃), suggesting thermoremanent magnetization of monoclinic pyrrhotite (Tc= 320 ℃) or thermoviscous remanent magnetization of magnetite. The direction of MT component does not consist with the direction of other lithologies' remanence. Therefore, MT component could be acquired due to exothermic events localized in cataclasite.

Along-strike segmentation of tremor and its relationship with the hydraulic structure of the subduction zone

Gaspard Farge[1,2], Claude Jaupart[2], Nikolai Shapiro[3]

[1] Dept. Earth and Planetary Science, UC Santa Cruz, [2] Université Paris-Cité, Institut de physique du globe de Paris, CNRS, [3] Institut de Sciences de la Terre, Université Grenoble-Alpes, CNRS

Along the strike of subduction zones, tectonic tremor activity is segmented on a geologic scale, indicating local variations of the tremor-generating process. We study how strong temporal clustering and long-term recurrence of tremor activity can emerge from the synchronization of elementary tremor sources, as they interact through fluid pressure transients.

We model a permeable fault zone channeling the upward flow of deep metamorphic fluids, in which seismic tremor emissions are associated with rapid openings of low-permeability valves in the fault. Valve openings trigger fast pressure transients that allow tremor sources to interact and therefore synchronize. In such a system, tremor activity is thus shaped by unsteady fluid circulation. Using numerical simulations of fluid flow for a large number of different valve populations, we show that the synchronized, collective activity of sources generates episodic activity, and that along-strike variations of fluid flux and fluid transport properties can lead to the segmentation of tremor activity. Strong tremor bursts that coherently activate wide parts of the fault and recur with a long period are associated with patches densely populated with valves and characterized by below-average permeability. Long-term tremor episodicity emerges from the synchronous activity of valves in such patches and is responsible for fluid-pressure cycling at the subduction scale. In the tremor zone of Shikoku (Japan), the most temporally clustered segment coincides with a downgoing seamount chain, suggesting that the segmentation of the fault zone permeability, and hence of tremor activity, could be inherited from the topography of the subducting oceanic plate.

Although the model we developed is a simplified description of fluid circulation and seismic source processes, it provides a framework for understanding how hydraulic stress in the subduction zone is accumulated and released, and for discussing how spatial variations of this dynamic could shape the activity of slow-earthquake phenomena in subduction zones.

Temporal variation of the physical property of the plate boundary in the Nankai subduction zone

Takashi Tonegawa[1], Eiichiro Araki[1], Yuya Machida[1]

[1]JAMSTEC

We use ambient noise records obtained by a vertical array at C0002 site in the Kumano basin of the Nankai subduction zone (Kimura et al. 2019,SSJ). The vertical array contains a geophone deployed at the seafloor (4.5 Hz short period sensor) and a borehole broadband sensor at a depth of 900 m from the seafloor. If reflections from deep interfaces, e.g., plate boundary, are detected persistently using the vertical array, we can monitor the physical properties of plate boundary with the amplitudes and phases of the reflections.

The analyzed period is from 2015 to the beginning of 2021. We used the two horizontal components, and rotated them with an increment of 1º. To retrieve S reflections for every polarization direction from below, we employed the normalized cross correlation using ambient noise records for every polarization direction at the seafloor and borehole, in which the reference site was the seafloor. The bandpass filter is 0.5–2.5 Hz.

Our results show S reflections from the megasplay fault and the top of the subducting oceanic crust. The arrival time of the S reflection for a polarization direction of N70ºE was faster, indicating that the direction is the fast polarization direction. We also investigated the temporal variation of the amplitudes of the S reflections, and obtained scattered amplitudes of the S reflections from megasplay fault at the timing for relatively large slow earthquake activities. Moreover, we observe a long-term variation of the S reflection amplitudes.

Acknowledgement

We thank T. Kimura for deploying the geophone at the seafloor at C0002 site. This work was supported by JSPS KAKENHI Grant No. 21H05202 in Scientific Research on Transformative Research Areas “Science of Slow-to-Fast earthquakes”.

Evaluation of the dip angle of the Median Tectonic Line active fault system by quasi-dynamic earthquake sequence simulation

Kazunori Muramatsu[1], Ryosuke Ando[1], So Ozawa[2]

[1]Department of Earth and Planetary Science, the University of Tokyo, [2]Department of Geophysics, Stanford University

The Median Tectonic Line Active Fault System (MTLAFS, Ikeda et al., 2009) is a 400km long group of active faults in Western Japan. The fault traces of the MTLAFS are sub-parallel to the MBMTL(Miyawaki & Sakaguchi, 2021). Right-lateral strike-slip faulting is dominant along the MTLAFS (e.g. Satake et al., 1999; Goto, 2018). There is a debate about the dip angle of the MTLAFS: one perspective proposes a vertical, high-angle fault plane, supported by studies of the high-angle fault plane at shallow depths such as trenching surveys (Okada & Tsutsumi, 1997), structural geology studies (Kubota & Takeshita, 2008), seismic reflection studies (Miyawaki & Sakaguchi, 2021), and slip tendency (Uchide et al., 2022). The other perspective argues for the shallow merging of the MTLAFS with the MBMTL and suggests that faulting occurs on the north-dipping fault plane, which is supported by various studies: the distribution of hypocenters with $2 \leq Mj \leq 6.5$ (Sato et al., 2015), slip partitioning in a moderately dipping strike-slip fault plane (Sato et al., 2015), and GPS traverse surveys and inversion analysis (Tabei et al., 2002). To discuss which of the vertical and the north-dipping planes more closely follows the recent fault activity of the MTLAFS, based on the tectonic loading and the mechanical failure conditions, and the frictional strength, we apply quasi-dynamic earthquake sequence simulation to the MTLAFS with a 3D non-planar vertical or north-dipping fault model. We employ the quasi-dynamic boundary element method developed in a package called HBI(Ozawa et al., 2023), which is highly efficient for parallel computation using the Lattice H-matrices (Ida, 2018). The slip direction is constrained by the spatial pattern of the stress field (Uchide et al., 2022) and the shear stress rate is constrained by the GNSS measurements (Nishimura, 2022). These models are validated to assess which dip angle is appropriate for the activity of the MTLAFS by comparison with paleoseismic and geological observations, which are independent of the seismological and geodetic observations used to determine the loading parameters.

The mean recurrence interval and horizontal displacement rate are consistent with those obtained from paleoseismic surveys within the same order of magnitude in both the north-dipping and vertical models. The mean vertical displacement rate for the north-dipping model is between -3 m/kyr and 3 m/kyr, which is a much larger range than between -1 m/kyr and 1 m/kyr in Segment 6 and Segment 4 to Segment 2. In contrast, the mean vertical displacement rate for the vertical model is between -2 m/kyr and 1 m/kyr, which is consistent with the paleoseismic surveys. The vertical displacement is known to be a southerly uplift on the side west of the Sakaime Pass in Segment 6 and a northerly uplift on the side to the east (Goto, 2018). The simulation results for the vertical model of the vertical displacement rate also transition from uplift on the southern side to uplift on the northern side. However, the north-dipping model does not show this transition at Sakaime Pass, but instead shows consistent uplift on the southern side between Segment 7 and Segment 5. The simulation results of the vertical model are more consistent with the observed activity of the Median Tectonic Line Active Fault System (MTLAFS).

The role of afterslip in the stress interaction between repeating earthquakes and microseismicity in Parkfield

Chingchieh Su[1], Kate Huihsuan Chen[1], Kaj Johnson[2], Roland Burgmann[3], Robert Nadeau[4]

[1]Dept. of Earth Sciences, National Taiwan Normal University
[2]Dept. of Earth and Atmospheric Sciences, Indiana University Bloomington, Indiana, U.S.A.
[3]Dept. of Earth and Planetary Science, UC Berkeley, California, U.S.A.
[4]Berkeley Seismological Lab., UC Berkeley, California, U.S.A.

Earthquake can be triggered by small stress changes from local to distant earthquakes, seasonal forcing, and human activities. While the calculated magnitude and sign of stress change greatly varies with the assumption of source stress drop, receiver fault geometry, and consideration of aseismic slip, the near-field stress triggering can be easily misinterpreted. With a large number of repetitive occurrence times, small repeating earthquakes provides a unique opportunity to examine and model the extent to which fault interaction in the form of static stress changes and transient postseismic fault creep produces the observed aperiodicity in the occurrence of these events. Using the 655 repeating earthquakes (repeater) and M≥ 1 4499 earthquakes during the period of 1984 – 2004 (before M6 Parkfield event), the significant triggering between small earthquakes were previously documented as the increased rate of events producing(incurring) higher stress changes during the days preceding(following) a repeater. However, how to describe the stress in the vicinity of earthquakes has been a challenge especially that (1) the negative static shear stresses could be mistakenly resolved on the closely-located receiver and (2) the role of afterslip induced very small earthquakes on the stress interactions could be largely underestimated. In this study, we propose the stress model that properly represents the relative three-dimensional location of the events and determine the instantaneous static stress fields associated with each event as well as the time-dependent contributions from afterslip. We hope to provide a better interpretation of the short-term triggering between the closely-spaced small earthquakes on the creeping strands of the SAF.

Extension of Aseismic Slip Propagation Theory to Slow Earthquake Migration

Keisuke Ariyoshi[1]

[1]JAMSTEC

Natural faults host various types of migrating slow earthquake phenomena, with migration speeds much lower than seismic wave speeds and different moment-duration scaling from regular earthquakes. To advance the obtained quantitative understanding of the migration process and long duration of slow earthquakes, I study a chain reaction model in a population of brittle asperities based on a rate- and state-dependent friction on a 3-D subduction plate boundary. Simulation results show that the migration speed is quantitatively related to frictional properties by an analytical relation derived here. By assuming that local pore water in front of the migration drives rapid tremor reversal and is so local as to hold a constant stress drop, the application of the analytical solution to observational results suggests that (i) the temporal changes of observed migration speeds for the rapid tremor reversal could be explained by about 70% reduction of the effective normal stress; (ii) effective normal stress for the deeper extension of the seismogenic segment in the western part of Shikoku is about 1.5 times greater than that in the central part. Applying rupture time delay between slow earthquake asperities for a duration longer than regular earthquake, I also conclude that (iii) the characteristic slip distance of rate-and-state friction for low-frequency earthquakes is roughly between 30 μm and 30 mm; (iv) the stress and strength drops of very low-frequency earthquakes is much smaller than 1 MPa.

Reference:

Ariyoshi, K. (2022). Extension of aseismic slip propagation theory to slow earthquake migration. *Journal of Geophysical Research: Solid Earth*, 127, e2021JB023800. https://doi.org/10.1029/2021JB023800

3D viscoelastic earthquake sequence simulation of subduction zone with inland faults

Ryoya Matsushima[1], So Ozawa [2], Ryosuke Ando[1]

[1]Graduate School of Science, University of Tokyo, [2]Stanford University

Introduction

Stress changes and crustal deformation around subduction zones are influenced by many factors such as plate subduction, plate-boundary earthquakes, and viscoelastic relaxation of the asthenosphere. For example, after the 2011 off the Pacific coast of Tohoku earthquake, the long-wavelength component of the strain rate in northeastern Japan turned from contraction to elongation, while the short-wavelength component of the strain rate continued to contract after the earthquake (Meneses-Gutierrez and Sagiya, 2016). In Addition, despite stress drops caused by subduction zone earthquakes, tectonic stresses accumulate on inland active faults, resulting in reverse fault earthquakes.

However, the mechanism of the interaction between plate subduction, plate-boundary earthquakes, viscoelastic relaxation of the asthenosphere, and inland active fault earthquakes has not yet been modeled in the framework of earthquake sequence simulation. In this study, we propose a new method to solve the problem by preparing surfaces representing faults and surfaces representing the lithosphere-asthenosphere boundaries (LABs) in an elastic medium, and by providing appropriate boundary conditions for each.

Methods

A vertical transform fault was placed, and a surface imitating LAB was placed at the depth of 60km in elastic half-space to verify this method using the analytical solution derived by Savage and Prescott, 1978 which modeled seismic fault slip and resulting after-slip due to bulk viscoelasticity. The LAB was subjected to viscous resistance ($\tau = \eta\dot{\varepsilon}$) as a stress boundary condition.

Then, the time evolution of the LAB displacement due to fault slip was calculated using a simulation code that was a rewrite of hbi (Ozawa et al. 2023) to handle viscous resistance, and the displacement of the ground surface due to LAB displacement was calculated to compare with the analytical solution.

Next, to model plate-boundary earthquakes, viscoelastic relaxation of the asthenosphere, and stress accumulation on inland faults, we prepared surfaces corresponding to the upper oceanic plate, lower oceanic plate, lower continental plate, and inland faults. The LABs of the upper and lower oceanic plates were subjected to displacement boundary conditions, and simulations were performed.

Results

We performed simulations under the same conditions as the analytical solution and compared the ground surface displacements. We found good agreement between this method and the analytical solution near the fault and within the relaxation time. The simulations of a subduction zone model showed that plate-boundary earthquakes occurred with recurrence intervals of several hundred years. In addition, normal fault earthquakes occurred cyclically on the inland faults. The recurrence interval of the inland earthquakes was about 10 times that of plate-boundary earthquakes.

Repeated viscoelastic fracturing under shear as an analog of slow to fast earthquakes

Yuki Shinohara, Hiroki Maeda, Yutaka Sumino

Dept. Applied Physics., Tokyo University Science

Seismic activities in subduction zones are related to their viscoelastic nature [1]. In the shallow area where fast earthquakes occur, rocks behave as elastic solids, which show brittle fracture as a source of seismicity. In the deeper region, rocks deform as ductile materials and seismic activities disappear. In the intermediate area between the two regions, rocks undergo brittle-ductile transition, where slow earthquakes are observed.

To explain such a relation between rock's rheology and seismic activities, laboratory experiments imitating subduction zones with using analog material of rocks were performed in the previous study [2]. In their experiment, shear strain is applied to a gel which can be regarded as a Maxwell fluid with a single relaxation time, then observed its deformation and slip behavior. Another study using the gel is an injection experiment in which low-viscous fluid is injected into a Hele-Shaw cell filled with viscoelastic gel [3]. When the injection rate is high, viscoelastic fracturing is observed, while viscous fingering is observed due to Saffman-Taylor instability when the injection rate is low [4].

In this study, we tried to create an analog experimental system that viscoelastic fracturing is observed by applying shear strain to the gel. In particular, we focused on the condition under which viscoelastic fracturing was repeatedly observed to have statistical data.

We used a sample made of oil in water droplets microemulsion connected by telechelic polymers as a viscoelastic fluid [5]. The fluid behaves as a Maxwell fluid, characterized by a single relaxation time τ. A Maxwell fluid behaves as a viscous fluid at a long time scale (larger than τ), and as an elastic solid at a short time scale (shorter than τ). This transition is described with Weissenberg number, $Wi = \dot{\gamma}\tau$: the sample shows viscous behavior when $Wi < 1$, while the sample shows elastic when $Wi > 1$. In addition, the sample shows brittle fracture when external shear was kept with the condition $Wi > 1$. Fig.1 shows the result of viscoelastic measurements where the relaxation time was obtained as $\tau = 0.017$ s.

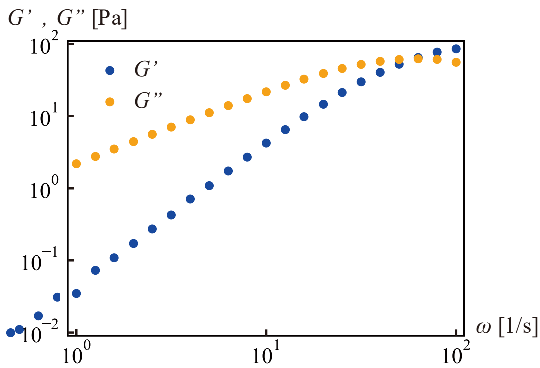

Fig. 1 Dynamic viscoelastic measurement of G' and G"

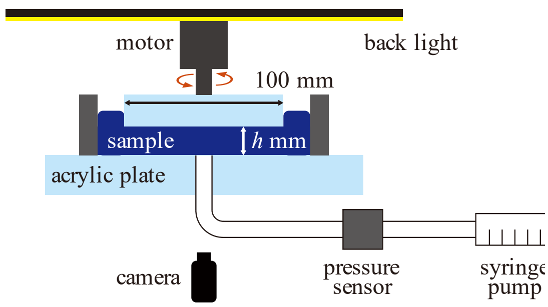

Fig. 2 Experimental setup

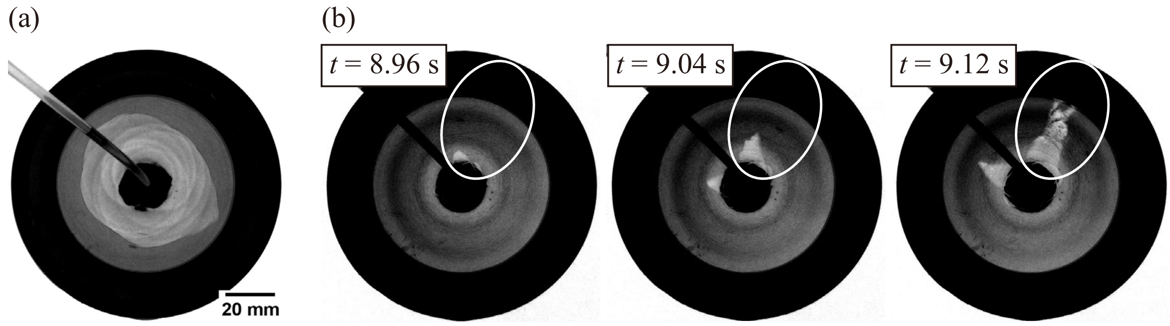

Fig. 3 Snapshots of air injection for (a) ω = 50 rpm, (b) ω =75 rpm.

The experimental system was composed of two parallel plates whose gap was h = 0.5 mm (Fig.2). The upper plate was connected to the motor to rotate while the lower one was fixed. Also, a syringe pump is connected to the lower plate. After introducing the sample between the plates, we rotated the upper plates with a constant angular velocity ω. In this setup, the sample was sheared with the shear rate $\dot{\gamma} = R\omega/h$, where R is the radial distance from the center of the rotating plate. Thus, Wi depends on both ω and R. In this experiment, we fixed the angular velocity of the parallel plate. We then injected air at a fixed loading rate of 50 mL/min with a syringe pomp from the center of the fixed bottom plate. This air injection rate was insufficient to create a viscoelastic fracture without external shear. We measured the injected air pressure while the dynamics of fracture formation were recorded with the video camera.

Fig. 3 shows typical results for (a) the viscous behavior of the sample, (b) viscoelastic fracturing. In the case of Fig. 3(a) with ω = 50 rpm, the sample behaves like viscous fluid because Wi does not exceed 1 for R < 50 mm. Therefore, air spreads isotopically. However, the sample showed fracture formation by air, indicated by white circles in Fig. 3(b), where Wi exceeds 1 at the central part. Interestingly, we could observe crack propagation repeatedly because a crack was sealed by the sample, which also shows the nature of the viscous liquid. Fig. 4 shows the injected air pressure P in repeated viscoelastic fracturing. When crack propagation occurs, pressure decreases steeply, while pressure gradually increases when a crack is sealed.

[1] K. Obara and A. Kato, Science 353, 253-257(2016).
[2] A. Namiki et al., J. Geophys. Res. 119, 3169-3181(2014).
[3] E. Lemaire et al., Phys. Rev. Lett. 67, 2009-2012(1991).
[4] G. M. Homsy, Annu. Rev. Fluid Mech. 19, 271-311(1987).
[5] M. Filali et al., J. Phys. Chem. B 103, 7293-7301(1999).

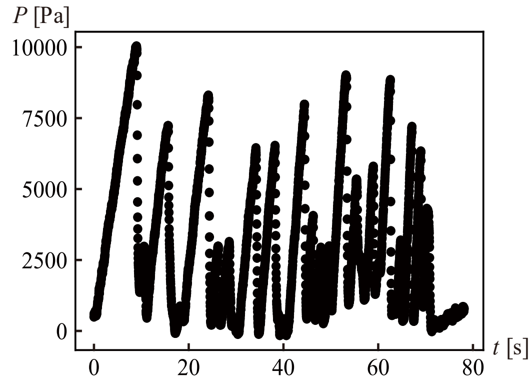

Fig. 4 Temporal change in injected air pressure

Model for heterogeneous faults with randomly distributed frictional parameters

Ryo Mizushima[1], Takahiro Hatano[1]

[1]Osaka Univ.

Previous rock experiments have shown that slow earthquakes in subduction zones occur at the depths where the frictional properties of rocks switch from stable to unstable. However, natural faults are far larger than the laboratory scale and have spatial heterogeneity of frictional properties not seen in the laboratory scale. Therefore, to understand the actual slow and fast earthquake dynamics, it is necessary to consider how heterogeneity affects the behavior of the fault slippage.

From a theoretical point of view, there have been some studies considering the heterogeneity of frictional properties (Skarbek et.al. 2012, Yabe and Ide 2017, 2018). In these studies, periodically aligned velocity-weakening and velocity-strengthening regions are considered on a 1D fault, and it is shown that slow earthquakes are realized depending on the weakening strength etc. However, the setup of periodic heterogeneity is artificial. Moreover, since there are numerous factors that cause inhomogeneity in fault and that direct observation of fault surfaces is almost impossible, it is difficult to dealing with the heterogeneity deterministically.

Therefore, in the present study, we examine how probabilistically distributed frictional properties affects fault slippage. As in other studies, we solve a quasi-dynamic one-dimensional elastic fault model using the boundary integral equation method (BIEM). For the friction law, we use the rate-state-dependent friction law with the aging law. Regarding the heterogeneity of friction properties, we control the range of variation in the friction parameter values (b-a) and the percentage of velocity-weakening regions.

As a result, it is shown that the model realizes a slip behavior of transition from stable slip to unstable slip as the ratio of velocity weakening region increases. Especially, in some parameter regions, slow slips like oscillations are also observed. Regarding the spatial distribution of slip, it is found that the larger variation of the friction parameters leads to localization of the slip region. This fact may suggest that the variety of the slow and fast earthquakes along the dip direction is related to the degree of variation of the friction parameters.

Finally, to estimate the effective critical nucleation length of the heterogeneous fault, a velocity step test is carried out on this model. That is, the loading rate applied to the fault is increased or decreased instantaneously, and the following relaxation behavior is observed. Then, from the behavior, the characteristic slip length (Dc) of the fault scale is estimated. As a result, it is observed that the Dc changes remarkably depending on the heterogeneity degree. This point will be discussed more in detail at the presentation.

Systematic Changes in Quartz Precipitation on Granite Surfaces Revealed by Hydrothermal Experiments

Edward L. Vinis[1], Jumpei Sugioka[1], Atsushi Okamoto[1]

[1]Graduate School of Environmental Studies, Tohoku Univ.

Fractures and faults act as the dominant fluid pathways in the crust. Faults are often sealed by silica precipitation (quartz veins), which is thought to have significant influences on fluid pressure, permeability, and strength [1]. The silica precipitation is usually modeled by the overgrowth of quartz on the pre-existing grains, but under high supersaturation in response to seismic rupture, silica precipitation via metastable phases and nucleation are possible. Specifically, in high temperature regions of the crust such as those with geothermal activity, silica precipitation preferentially occurs from the change in density of H_2O going from a liquid to a supercritical fluid [2, 3]. However, due to the variability in silica precipitation, our knowledge of its effects on fracture porosity is still limited, which prevents our understanding of how permeability and strength recover during quartz precipitation.

We conducted a series of flow-through experiments to precipitate silica on granite surfaces. In these experiments, high-Si solutions flowed through the vessel as temperature changed from sub- to supercritical. Twenty granite blocks (2.5 mm x 2.5 mm x 10 mm) were placed in a vertical flow path as temperature increased from 350°C to 430°C while at a constant 25 MPa. Si rich solutions (Si = 228-283 mg/kg (H2O), Al = 2.5-5 mg/kg (H2O)) were used to promote precipitation and flowed over the surface of the granite samples for 48 hours. Multiple experiments were performed under the same conditions but with a slight variation of input solutions to allow for trace elemental analyses. Samples were analyzed using X-Ray Computed Tomography (X-Ray CT), X-Ray Fluorescence (XRF), Scanning Electron Microscope Energy Dispersive Spectroscopy (SEM-EDS), optical microscopy, Scanning Electron Microscope Cathodoluminescence (SEM-CL), Electron Probe Microanalyzer (EPMA), and solution chemistry was analyzing using Inductively Coupled Plasma Atomic Emission Spectroscopy (ICP-AES).

In all experiments, systematic changes were found along the length of the flow path. Early flow-path granite samples experienced quartz dissolution as conditions remained sub-critical. Right before the mid-point of the flow path, a sudden transition from dissolution to precipitation occurred as conditions reached supercritical, first with the appearance of amorphous silica while Si solution concentrations were highest. Then, we saw a brief window of cristobalite precipitation with euhedral quartz nucleating inside the formations. Around the mid-point of the flow path, we saw the peak mass of precipitation occur mostly in the form of homogenous quartz nucleation with heterogeneous syntaxial quartz overgrowing existing quartz grains on the granite surface. After the peak precipitation, Si saturation in solution decreased significantly, homogenous nucleation waned, and heterogenous growths made up an increasing proportion of the remaining precipitation. These masses steadily declined to near-nothing by the downstream end of the flow path. The systematic ordering of minerals was similar to what was seen in previous research [4], supporting the role of Si concentration in a stepwise formation of minerals from metastable to stable quartz. Initial SEM-CL analyses indicate that trace Al and K concentrations may have a positive correlation with CL intensity while other trace elements remain independent. Impurities in solution are likely playing a role in the direct nucleation of quartz, preventing formation of opal. These results tell us that (1) sealing and pressure build up may occur from homogeneous quartz nucleation, (2) quartz/silica vein formation has a predictable ordering of minerals based on Si saturation levels, and (3) we can expect crustal strengthening in the narrow region where homogeneous nucleation is highest, while flow paths may form shortly thereafter from heterogeneous growth textures.

References:

[1] Cox, S. F. (2016). Economic Geology, 111(3), 559-587.
[2] Okamoto, A., & Sekine, K. (2011). Journal of Structural Geology, 33(12), 1764-1775.
[3] Saishu, H., Okamoto, A., & Tsuchiya, N. (2014). Terra Nova, 26(4), 253-259.
[4] Okamoto, A., Saishu, H., Hirano, N., & Tsuchiya, N. (2010). Geochimica et Cosmochimica Acta, 74(13), 3692-3706.

Seismic imaging for seamount subduction at Hyuga-Nada using active and passive OBS data

Rie Nakata[1,2], Kimi Mochizuki[1], Nori Nakata[2,3], Masa Kinoshita[1], Yoshitaka Hashimoto[4], Yohei Hamada[5], Yasuyuki Nakamura[5], Seiichi Miura[5], Ryuta Arai[5]

[1]ERI, Univ. Tokyo, [2]LBNL, [3]MIT, [4]Kochi Univ., [5]JAMSTEC

Subducting seamounts are becoming a critically important controlling factor for slow earthquake occurrences through modulating structural, rheological and geomechanical properties. Determining these properties on, over and in the area surrounding seamounts provide essential insights into the effects of such a topographic relief. At Hyuga-Nada, the Kyushu-Palau Ridge (KPR), a remnant of the Izu-Bonin Arc, is subducting and separates the Ryukyu trench and the Nankai Trough. A rich distribution of tremors and very low frequency earthquakes has been observed around a currently subducting seamount. We use a dense Ocean Bottom Seismograph survey performed in 2020 to estimate both P-wave and S-wave velocity structures. The short-period OBSs recorded continuously over a month. Extracting waves excited by air-gun shots allows us to estimate P-wave velocities by traveltime tomography and full waveform inversion. Low P-wave velocity zones are indicated in the vicinity of topographic highs of the subducting seamount. In turn, ambient noise data provide S-wave velocity distribution by using interferometry techniques. We extract multiple modes of Scholte waves propagating between 0.5 to 1.0 km/s and then estimate the velocity model down to 500 m from the seabed. By integrating P- and S-wave velocities from the OBS survey with previously obtained seismic reflection images, we infer the links between the structural features such as faults and structures and the slow-earthquake distribution.

New insight of low frequency earthquakes (LFEs) in continuous ocean bottom seismometers at the Guerrero Seismic Gap, Mexico

Yanhan Chen[1], Yoshihiro Ito[1], Masanao Shinohara[2], Victor M Cruz-Atienza[3], Yusuke Yamashita[1], Raymundo Omar Plata Martinez[4], Emmanuel Soliman Garcia[1], Shukei Ohyanagi[1], Ketzallina Flores[1]

[1]Disaster Prevention Research Institute, Kyoto University, [2]Earthquake Research Institute, The University of Tokyo, [3]Universidad Nacional Autónoma de México, Instituto de Geofísica, Mexico, [4]Japan Agency for Marine-Earth Science and Technology (JAMSTEC), Research Institute for Marine Geodynamics

Over the past few years, there have been numerous reports of slow earthquake activity occurring near the Guerrero Gap in the Mexican subduction zone. Additionally, several significant earthquakes have been triggered by slow earthquakes. However, no major earthquakes have occurred in the northwest of Guerrero seismic gap. According to a seismic cycle, slow and fast earthquakes possibly exhibit periodicity. Since November 2017, an Ocean Bottom Seismometers (OBS) array was deployed in the western part of the Guerrero Gap to enhance observations. Tectonic tremors have been observed based on the OBS array, but low-frequency earthquakes (LFEs) have not been detected yet.

We use a modified envelope correlation technique (Mizuno and Ide, 2019) to detect and locate tectonic tremors. Then we visually inspect the waveforms and spectrogram to finalize the tremor catalog. We apply the frequency band between 2 and 8Hz. Over 300 tectonic tremors were found. We analysis the spatio-temporal distribution to cluster the tremor sources.

For the LFEs detection, we select the LFE templates visually from the tremors catalog we detected. After inspecting the LFE templates, we use the matched filter technique (Peng and Zhao, 2009) to detect LFEs with 12 templates. The bandpass is the same as tremor processing. About 140 LFEs are generated from the one year's OBS data, we then inspect and pick phase arrivals using the WIN system (Urabe and Tsukada 1992) and use hypoMH (Hirata and Matsu'ura M 1987) for hypocenter determination. Waveform stacking is used to enhance the signal-to-noise ratio, confirming the LFEs. The spectrum analysis is also conducted to compare tremors, and regular earthquakes.

The study of shallow tremors and LFEs has significantly contributed to monitoring slow earthquake in the Guerrero seismic gap. Achieving a completeness of regional slow earthquakes will also help us gain a better understanding of mechanisms from slow to fast earthquakes.

Identification of Possible Tsunami Earthquakes along the Mexican Subduction Zone

Ketzallina Flores[1], Yoshihiro Ito [1]

[1]DPRI, Kyoto Univ.

Tsunami earthquakes generate large tsunamis but only moderate ground motion, when compared to the ground motion from ordinary earthquake with the same magnitude (e.g. Geersen, 2019). These earthquakes share many seismological characteristics, such as a long source duration component of high-frequency energy, and rupture near the trench. Despite their seismological similarity, there is, however, no commonly accepted model for the structural or morphological conditions on or around source areas, which are conducive to tsunami earthquakes with no strong ground motion.
On April 18th, 2002, an earthquake with M_W 6.7 occurred about 55 km from the coast of Guerrero, Mexico. The hypocenter of the earthquake was located near the trench of the northwest Guerrero seismic gap. Despite being relatively small in magnitude, the earthquake has all the characteristics of a tsunami earthquake.

Okal and Borrero (2011) conducted a detailed seismological study of the large Colima, Mexico earthquake. The mainshock occurred on June 3rd, 1932, followed by aftershocks on June 18th and 22nd of the same year. The aftershock on June 22nd generated a more devastating tsunami than that of the mainshock, despite having much smaller seismic magnitudes. Okal and Borrero (2011) suggests that this aftershock had the characteristics of a tsunami earthquake.
Newman and Okal (1998) demonstrated that the scaled energy (E_S/M_0) is a powerful discriminant for tsunami earthquakes. Tsunami earthquakes typically have the scaled energy from $7x10^{-7}$ to $3x10^{-6}$ (Venkataraman and Kanamori, 2004). For instance, the scaled energy were calculated as $1.5x10^{-6}$, $0.6x10^{-6}$ and $2.6x10^{-6}$ for the tsunami earthquakes of Nicaragua (2 September 1992, M_W 7.6), Java (2 June 1994, M_W 7.8), and Peru (21 February 1996, M_W 7.5), respectively (Venkataraman, 2002).

In this work, we calculate scaled energy of events occurred in the Mexican subduction zone. With this information, we analyze the differences in the scaled energy of some events and their implications. We utilize the scaled energy to identify Mexican tsunami earthquakes. By examining and comparing their scaled energy, we aim to gain insights into the seismological characteristics of tsunami earthquakes in this region.

Deformation mechanisms and rheology of mélange shear zones associated with seamount subduction

Madison Frank[1]*, Kohtaro Ujiie[1], Ginta Motohashi[1], Takayoshi Nagaya[2]

[1]Grad. S. Science & Tech., Univ. Tsukuba, [2]Grad. S. EPS, Tokyo Gakugei Univ.

Exhumed subduction mélanges are expected to provide critical information on the lithology, fluid conditions, and deformation mechanisms related to slow slip events or aseismic creep along a megathrust. Slow earthquakes are frequently observed where seamounts are subducting, but mélanges formed in association with seamount subduction have rarely been examined. The Chichibu accretionary complex in Amami-Oshima, Ryukyu Arc, contains shear zones composed of mudstone-dominated mélange (MDM) and basalt-limestone mélange (BLM), showing a shear sense consistent with megathrust shear. MDM is characterized by lenses of sandstone, siliceous mudstone, and rare massive basalt in an illitic matrix. BLM is marked by lenses of micritic limestone and basalt blocks in a chloritic matrix, which originated from the mixing of limestone and basalt at the foot of seamount. Peak temperature of MDM from Raman carbonaceous material geothermometers is ~285 °C. Deformation microstructures indicate that shear deformation in MDM was accommodated by dislocation creep of quartz and combined quartz pressure solution and frictional sliding of illite, whereas dominant deformation mechanisms in BLM indicate diffusion creep of very fine-grained calcite and frictional sliding of chlorite. To estimate the range of strain rates responsible for megathrust shear, we constructed rheological models of mélange shear zones taking deformation mechanisms of the MDM and BLM and experimentally derived constitutive laws for quartz, combined quartz + illite, calcite, and chlorite into consideration. For the MDM, our model predicts that dislocation creep of quartz and combined quartz pressure solution and frictional sliding of illite can occur at strain rates between ~10^{-15} to 10^{-12} s^{-1} over fluid pressures ranging from hydrostatic to near-lithostatic. For the BLM, frictional sliding of chlorite and diffusion creep of calcite can occur at strain rates of ~10^{-13} to 10^{-10} s^{-1} between hydrostatic to near-lithostatic fluid pressure, two orders of magnitude faster than the MDM. Our models indicate that the BLM recorded faster slip events with respect to the MDM. If the mélange shear zones are 100 m thick, BLM could accommodate slow slip rates while MDM could accommodate aseismic creep rates.

Tidal sensitivity of tectonic tremors in Hikurangi subduction zones

Ruyu Yan[1,2], Satoshi Ide[1]

[1]Dept. EPS, Univ. Tokyo, [2]APM, CAS

Investigating the slow earthquakes occurring within subduction zones in relation to periodic stress fluctuations can significantly enhance our comprehension of the seismic cycle, the seismogenic process, and the state of stress. Notably, tremor initiation exhibits distinct sensitivity to tidal forces throughout the subduction zone, including regions such as Cascadia, Nankai, and others. Recent studies have identified exponential relationships between tremor rate and tidal stress (Ide, 2014; Yabe, 2015). Within the vicinity of the Hikurangi subduction zone, situated beneath New Zealand's North Island, a range of faulting phenomena, such as slow slip events (SSEs), tremors, and earthquake swarms, have been observed. This study examines the response of tectonic tremors under the fluctuation of the tide in the Hikurangi subduction zones and specifically investigates the relation between the tremor rate and the amplitude of tidal stress. The observed tidal sensitivity is expected to reflect the inherent heterogeneity of the plate interface and understand the physical mechanisms of slow earthquakes.

The tectonic tremors in New Zealand utilized in this study were obtained from Romanet and Ide (2019). Based on the location (latitude, longitude, and depth) and the time, we can calculate the tidal stress tensor including solid earth tide and ocean loading using a code developed by Yabe et al. (2014). For the ocean loading, we adopted the ocean model TPXO 7.2 Atlas (Egbert and Erofeeva, 2002) which proved the best fit with the tide-gauge data in this area (Gladkikh, 2011). Assuming that slow earthquakes transpire along the plate interface, strike and dip are calculated by the interpolate plate models, and the rake angle is obtained based on the relative motion of the plates. Subsequently, the tidal normal and shear stress were calculated on the plate interface for 10 years from 2005. The approach employed to investigate the relationship between tremor rate and tidal stress amplitude adheres to the method outlined in Yabe (2015).

Firstly, we use Schuster's test to investigate the correlation between tremors and normal/shear tidal stress using the plate's focal mechanism, which represents a threshold of $p < 5\%$ to judge a significant correlation. It also can provide a tidal angle where most events occurred. Schuster's test revealed that p values are found to be less than 5% in the Manawatu, Turnagain ($p = 1.61\%$) and Puysegur ($p = 3.58\%$) for shear/normal stress. And the p value is more than 5% in the Marlborough which means that there is no correlation between tremor and tidal stress. Then, we use the maximum likelihood method to estimate α-value, which represents tidal sensitivity. Our preliminary results shows that $\alpha = -0.49 \pm 0.31$ kPa^{-1} with a 95% confidence interval in the Manawatu for the normal stress and $\alpha = -0.47 \pm 0.27$ kPa^{-1} for the shear stress in the Puysegur.

Keywords: Earth tide, Hikurangi subduction zone, Tidal sensitivity, slow earthquakes

Development of UAV technology to realize high-frequency GNSS-A observation: experimental verification

Yusuke Yokota[1], Masata Kaneda[2], Takenori Hashimoto[2], Shusaku Yamaura[2], Kenji Kouno[1], Yoshiaki Hirakawa[4]

[1]IIS, Univ. Tokyo, [2]SELAB, Co., Ltd., [3]Yokohama National Univ.

GNSS-A is a technology that realizes steady seafloor geodetic observation. It has already been shown that the current vessel observations lack accuracy and frequency, and do not have sufficient detection capability (Yokota et al., 2021, PEPS). Observation methods using second-generation sea-surface platforms such as a wave-glider and a buoy have been proposed and studied (Tadokoro et al., 2020, FES; Iinuma et al., 2021, FES; Sakic et al., 2021, FES; Brooks et al., 2023, Sci Adv), but there is a problem with their ability to maintain a sea surface in areas with strong tidal currents. Therefore, we are now developing the flying boat type UAV as a third-generation platform to underwater and seafloor observations and the GNSS-A method using it.

SELAB's flying boat type sea-surface landing UAV HAMADORI can take off and land only on the surface of the water, and its application to transportation, fisheries, and others … is already underway. This paper describes the experimental verification of GNSS-A technology by a float plane type UAV.

In 2022, we proceeded with the development of the seafloor geodetic observation device inside the fuselage. GNSS, acoustic sonar, IMS, development of PCs for operation, and water tank tests. After that, in November 2022, we conducted an actual test of seafloor geodetic observation in Sagami Bay. We described a detail situation at this test in Yokota et al. (2023, Sci Rep). Figure show the observation by the UAV under development.

For a detail SSE monitoring, the GNSS-A sites in the Nankai Trough region should be frequently observed (about every 1 month ~ week). Then, we set new two sites off the Kii channel and Kumano-nada region. These sites will be observed using UAV and vessels in the collaboration research project with the Hydrographic and Oceanographic department, Japan Coast Guard.

Acknowledgement:
This study is supported by ERI JURP 2022-Y-KOBO25 in Earthquake Research Institute, the University of Tokyo, by the University of Tokyo Excellent Young Researcher project, by SECOM science and technology foundation, and by JSPS KAKENHI Grant Number JP21H05200 in Grant-in-Aid for Transformative Research Areas (A) "Science of Slow-to-Fast Earthquakes."

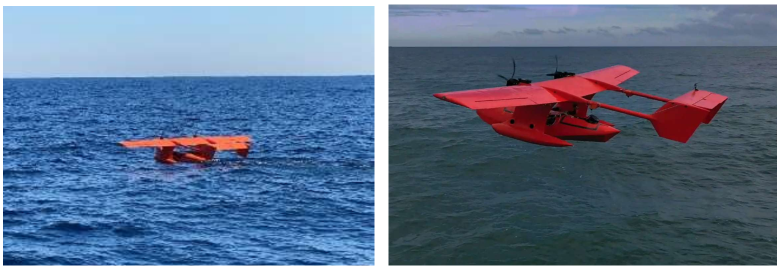

Figure. Photographs of the UAV HAMADORI6000 prototype model used in this study during observation (Yokota et al., 2023, Sci Rep).

Spatiotemporal evaluations for configuration of a sensor network to detect slow slip events from the seafloor deformation signal in the Hikurangi subduction zone

Tomohiro Inoue[1], Yoshihiro Ito[2]

[1]Institute of Industrial Science, the University of Tokyo, [2]DPRI, Kyoto University

In recent decades, ocean bottom pressure gauges (OBP) have been deployed worldwide to measure seafloor crustal deformation resulting from tectonic events, such as slow slip events (SSEs) and axial seamount activities. However, despite their extensive use, suitable techniques have not been firmly established for detecting SSEs from OBP data. The primary objective of this study is to develop a robust method for isolating nontidal components and optimizing the OBP sensor network configuration to enhance the signal of SSEs in the shallow portion of the Hikurangi subduction zone offshore New Zealand.

To evaluate the effectiveness of SSE detection methods, we assess the detectability of short-term SSEs using various approaches to eliminate nontidal components on the OBP data in the Hikurangi subduction zone. Specifically, we explored five distinct methods:

1) Utilizing no-preprocessing, solely detiding the dataset.
2) Subtracting an ocean model from landward sites.
3) Subtracting data of sites on the seaward slope of the trench from those on the landward slope.
4) Calculating the difference between the select paired sites with similar depth.
5) Calculating the difference between all the paired sites.

Our finding reveals that the approach of computing the difference between all the paired sites yielded the highest capability for detecting SSEs, as demonstrated by both synthetic and observed OBP time series data. Notably, this outcome underscores the effectiveness of utilizing the time series difference across all the paired OBP sites, particularly for capturing the signals from small-scale SSEs (~Mw 6), especially in proximity to the trench.

Subsequent to these findings, we proposed an OBP and GNSS network configuration designed to maximize SSE detectability. This configuration is based on the most efficacious pre-processing method identified in this study. Furthermore, we explore the correlation between potential OBP network setups and their corresponding detectability, utilizing synthetic time series data for both OBP and GNSS measurements.

In summary, our study contributes to the advancement of SSE detection methods by presenting a robust approach to process OBP data and configure the sensor network for optimal SSE detectability. This study enhances our understanding of SSEs within the context of the Hikurangi subduction zone and provides valuable insights into their potential implications.

Adjoint tomography of an accretionary wedge and shallow slow-slip regions in the North Island of New Zealand

Shun Adachi[1], Bryant Chow[2], Yoshihiro Kaneko[1], Yasunori Sawaki[1,7], Kimihiro Mochizuki[3], YusukeYamashita[4], Tomoaki Yamada[3], Martha K Savage[5], Emily Warren-Smith[6], Katie Jacobs[6]

[1]Graduate School of Science, Kyoto University, [2]University of Alaska Fairbanks, [3]Earthquake Research Institute, University of Tokyo, [4]Disaster Prevention Research Institute, Kyoto University, [5]Victoria University of Wellington, [6]GNS Science, [7]Now at Geological Survey of Japan, National Institute of Advanced Industrial Science and Technology

The Hikurangi subduction zone in the North Island of New Zealand hosts repeating slow-slip events, a thick accretionary wedge, subducted seamounts, and a fully-locked plate interface that is capable of generating megathrust earthquakes. Recently, Chow et al. (2022a,b) undertook the first application of earthquake-based adjoint tomography to the Hikurangi subduction zone and imaged two sections of high-velocity anomaly below the East Coast of the North Island, which have been interpreted as previously unidentified, deeply subducted seamounts. The presence of these seamounts is supported by independent evidence including seafloor bathymetry data and the presence of nearby geophysical anomalies. Deep seamounts are also linked with spatial variations in slip behavior observed along the Hikurangi subduction margin. In this tomographic study, we extend the domain of Chow et al. (2022a,b) 400 km to the northeast to cover the 2017-2018 IODP (International Ocean Discovery Program) drill sites (Barnes et al., 2020), the source region of the 2021 M7.3 East Cape earthquake (Okuwaki et al., 2021), offshore seamounts identified by active source seismics (Bell et al., 2010) and a thick low-velocity wedge in the northern margin (Kaneko et al., 2019). Using 60 geographically well-distributed events recorded by 101 permanent or temporary broadband seismic stations, including 9 OBSs (Ocean Bottom Seismometers), we perform iterative model updates using spectral element and adjoint simulations with L-BFGS optimization algorithm (Liu & Nocedal, 1989) to fit waveforms with periods ranging from 6 to 30 s. The final model improves the data fit and introduces P and S wave velocity changes of up to ±15% with respect to the initial 3D model. Sedimentary wedges in the final model are characterized by low seismic velocities (Vs of ~2500 m/s) extending down to ~15 km depth in the northeastern North Island. In addition, the final model shows a prominent (~30 km), previously unidentified high-velocity anomaly underneath the Raukumara basin at ~20 km depth. The updated velocity model, which covers Auckland and southern Kermadec, will contribute toward interpretations of tectonic evolution, the assessment of ground motion from a possible megathrust earthquake and accurate inversion of slow slip events at Hikurangi (e.g., William and Wallace, 2018).

b values dependency on olivine grain size in phase transformation faulting: Implication for deep-focus earthquakes

Sando Sawa[1], Nobuyoshi Miyajima[2], Julien Gasc[3], Alexandre Schubnel[3], Marie Baïsset[4], and Jun Muto[1]

[1]Dept. ES, Tohoku Univ., [2]BGI, Germany, [3]ENS, Paris, [4]ISTEP, Sorbonne Univ.

Deep-focus earthquakes occur at 300-600 km depth. The phase transformation faulting mechanism is presumed as the mechanism for deep-focus earthquakes by the geophysical observation (Zhan et al., 2014) and deformation experiments (Green & Burnley, 1989; Schubnel et al., 2013, Gasc et al., 2022). The phase transformation faulting mechanism occurs due to the phase transformation from olivine to denser spinel phases (wadsleyite and ringwoodite). The geophysical observation suggested that the fault rupture geometry controlled *b* values in the Gutengberg-Richter (G-R) law for the phase transformation faulting, and *b* values are 0.5 in warm slabs and 1.0 in cold slabs (Zhan, 2017). However, *b* values can also be affected by the rock properties, such as structural heterogeneity (Mogi, 1962). In particular, the grain size has the strong possibility of controlling *b* values because the grain size changes the rate of phase transformation affecting the occurrence of faulting (Cahn, 1956; Burnley et al., 1991). Therefore, we conducted deformation experiments of germanate olivine, an analog silicate olivine material, with various grain sizes to reveal the effect of grain size on the difference in *b* value during the phase transformation faulting. We used a Griggs-type solid-confining media deformation apparatus at Tohoku University and a Green-type deformation apparatus at École Normale Supérieure, Paris. The confining pressure, temperature, and strain rate are 1.2~1.5 GPa, 700~992 °C, and 4.2×10^{-5}~2.0×10^{-4} s^{-1}, respectively. The deformation experiments at ENS Paris equipped calibrated S-wave transducers that can detect the magnitudes of acoustic emissions (AE) generated during the phase transformation faulting. As a result, both fine-grained and coarse-grained aggregates deformed at higher than 800 °C showed strain weakening. AE activities started after the peak stress in the fine-grained aggregates, while AE activities started before the peak stress in the coarse-grained aggregates. The *b* values in the fine-grained aggregates ($b = 0.63 \pm 0.083$ at $T = 875$ °C, $b = 1.49\pm0.24$ at $T = 992$ °C) are smaller than those in the coarse-grained aggregates ($b = 1.49\pm0.041$ at $T = 875$ °C, $b = 3.56\pm3.08$ at $T = 992$ °C) although the standard error is large for b value of coarse-grained aggregates at $T = 992$ °C due to a small number of AE event. The calibrated AE measurements indicate that the phase transformation faulting follows the scaling law among seismic moment, corner frequency, and stress drop of natural shallow and deep-focus earthquakes. Natural deep-focus earthquakes have large stress drops (~10^3 MPa). Similarly, the phase transformation faulting in the experiments also has large stress drops (1-10^4 MPa). The microstructural observation using a scanning electron microscope (SEM) and a transmission electron microscope (TEM) revealed that the phase transformation occurred at the olivine grain boundaries in the fine-grained aggregates, while it occurred within olivine grains in the coarse-grained aggregates. The different mechanisms for the phase transformation can possibly control the *b* values for the phase transformation faulting responsible for the deep-focus earthquakes.

[References]

Zhan et al. (2014), *EPSL*, *385*, 89-96.
Green & Burnley (1989), *Nature*, *341* (6244), 733-737.
Schubnel et al. (2013), *Science*, 341, 1377-1380.
Gasc et al. (2022), *Geology*, 50(9), 1018-1022.
Zhan et al. (2014), *EPSL*, *385*, 89-96.
Zhan (2017), *EPSL*, *461*, 1-7.
Mogi (1962), *Bull. Earthquake Res. Inst.*, 40, 125-173.
Cahn (1956), *Acta Metallurgica*, *4*, 449-459.
Burnley et al. (1991), *JGR*, *96*, 425-443

Illuminating low-viscosity zone beneath Quaternary volcanoes by numerical simulation of postseismic deformation of the 2011 Tohoku-oki earthquake

Sambuddha Dhar[1], Youichiro Takada[2], Jun Muto[1]

[1]Department of Earth Science, Tohoku University, Japan
[2]Department of Earth and Planetary Sciences, Hokkaido University, Japan

The nationwide geodetic network across northeastern (NE) Japan recorded heterogeneous crustal deformation following the 2011 Tohoku-oki earthquake (Ozawa et al., 2012 JGR). Although the postseismic horizontal motion is wholesale eastward, the vertical motion is more complex, with subsidence near the volcanic front and uplift at the forearc (Freed et al., 2017 EPSL). The decade-long efforts for modeling these crustal deformations highlight the prevalence of heterogeneous rheology beneath NE Japan (Dhar et al., 2023 PEPS). In particular, the low-viscosity zone (LVZ) related to Quaternary volcanoes adds small-scale subsidence that continues several years after the earthquake (Muto et al., 2016 GRL). The InSAR analysis also revealed local elliptical subsidence during the coseismic period (Takada & Fukushima, 2013 Nat. Geosci.). Yet, the structure of these LVZs is not fully understood.

Here, we resolve the three-dimensional structure of LVZ beneath five Quaternary volcanoes (Mt. Akitakoma, Mt. Kurikoma, Mt. Zhao, Mt. Azuma, and Mt. Nasu), above which significant small-scale coseismic subsidence occurred (Takada & Fukushima, 2013). We used two years (2012–2014) postseismic GNSS data observed at GEONET stations to calculate the strain rate field around NE Japan. First, we applied a moving average filter (Meneses-Gutierrez & Sagiya, 2016 EPSL) to the post-seismic displacement field to remove the long-wavelength deformation. The filtered displacement field, which strongly reflects the short wave-length heterogeneities, is then used to calculate strain rate field by the method of Shen et al. (1996 JGR). To explain thus obtained strain rates, we constructed numerical models including LVZs represented by a series of cuboids where each cuboid reproduces a distributed viscoelastic deformation in response to the coseismic stress perturbation (Barbot et al., 2017 BSSA; Moore et al., 2017 Science). We calculated the spatiotemporal evolution of post-seismic surface strain rates considering the power-law Burgers rheology (Muto et al., 2019 Sci. Adv.; Dhar et al., 2022 GJI). With this model, we explored the dimension, shape, locations, and effective viscosity of LVZs beneath the volcanoes. The residuals between observed and modeled strain rates guide us to the optimal LVZ models.

The observed strain rate field indicates small-scale contraction in the proximity of the volcanoes except Mt. Zhao. We explained the observed short-wavelength strain rates by the LVZ model across the five volcanoes. Our LVZ model reveals the three-dimensional shape of viscous bodies beneath the volcanoes (average 40–60 km along the arc, 60–80 km normal to the arc, up to 40 km depth), which causes strain rate concentration due to the localized viscoelastic relaxation shortly after the 2011 Tohoku–oki earthquake. The location of these LVZ coincides with the areas with Late Cenozoic calderas (Yoshida, 2001 Sci. Rep., Tohoku Univ.) and high heat flow (Matsumoto et al., 2022 EPS). These LVZs take a narrower shape in the shallower crust (~10 km), while having a wider (~100 km) and deeper root (up to 40 km depth) in the lower crust/upper mantle. Such a characteristic shape of the LVZ is consistent with the reports from seismic tomography (Okada et al., 2014 EPS), magnetotelluric surveys (Ogawa et al., 2014 EPS), and a 2-D large-scale numerical simulation (Muto et al., 2016). In addition to the transient deformation, our modeled LVZ can also illuminate different rheological behavior of Quaternary volcanoes during interseismic (Miura et al., 2004 EPS) and coseismic (Takada & Fukushima, 2013) periods. Resolving the LVZ related to arc volcanism contributes to precisely explain the surface deformation due to viscoelastic relaxation and may provide additional constrains in understanding interplate coupling. Moreover, as LVZ significantly influences postseismic crustal uplift, our study may help understand the long-term crustal evolution over the megathrust earthquake cycles.

Seismological observation by distributed acoustic sensing using automatic phase picking method around the Tsugaru Strait, northeastern Japan

Satoru Baba[1], Eiichiro Araki[1], Takashi Yokobiki[1], Kei Kawamata[2], Keisuke Uchiyama[2], and Takuji Yoshizuka[2]

[1]JAMSTEC, [2]Electric Power Development Co.,Ltd.

Since megathrust earthquakes have their source areas often in offshore regions, seismological observation in offshore regions is important. However, detection capability and the resolution of locations of offshore earthquakes are low due to the small number of offshore permanent seismic stations. Recently, distributed acoustic sensing (DAS) measurement, which uses an optic fiber cable as a high-density strain rate sensor, has been widely used for seismological observations. DAS measurement using submarine fiber-optic cable has the potential for seismological observation in offshore regions at a high resolution. To evaluate the detectability of earthquakes by DAS measurement, locate earthquakes near the cable, and derive the empirical relationship between magnitude and DAS S-wave strain rate amplitude, we conducted DAS measurement from October 2022 to February 2023 and from June 2023 using a fiber-optic cable around the Tsugaru Strait.

In the observation from October 2022 to February 2023, 1101 events were observed. Earthquakes with magnitudes smaller than 1 and small earthquakes that are not listed in the earthquake catalog by Japan Meteorological Agency (JMA) were observed. It indicates the high seismic detection capability of DAS measurement near the cable. We located earthquakes in the Tsugaru Strait by manually picking the arrivals of P- and S-waves and using a hypocenter location program, hypomh (Hirata and Matsu'ura, 1987). The hypocenters of events near the cable were located near those of the JMA catalog at km resolution; therefore, DAS data has the potential to locate earthquakes near the cable. We derived an equation related to the maximum S-wave strain rate amplitude, hypocentral distance, and magnitude of earthquakes. By using the derived equation, the magnitude of an earthquake can be estimated by using DAS data. As the hypocentral distance increases by one order, S-wave strain rate amplitude decreases by approximately 1.8 orders. We compared the S-wave amplitudes of the DAS strain rate and acceleration amplitude of permanent inland stations near both ends of the cable. The relationship between these two amplitudes can be comparable to the apparent S-wave velocity of ~710 m/s in the sediment.

In the DAS observation from June 2023, earthquake detection capability is better than the observation from October 2022 to February 2023, probably because waves and winds in the summer around the Tsugaru Strait are quieter than in the winter. In this observation, to aim a real-time automatic seismological observation, we conduct automatic P- and S-phases picking by a deep-neural-network-based method, PhaseNet (Zhu and Beroza, 2018) and locate earthquakes based on these picking using hypomh (Hirata and Matsu'ura, 1987). When training the PhaseNet, we used waveforms of earthquakes recorded in the DAS observation from October 2022 to February 2023. To locate earthquakes at a higher resolution, we will validate the accuracy of picks.

Kilometre-scale ductile fractures instigated by deformation-induced nanocavities

Thomas Yeo[1,2], Norio Shigematsu[1], Simon Wallis[2], Tatsuya Sumita[1], Chunjie Zhang[3], Takuma Katori[4], and Ayumu Miyakawa[1]

[1]GSJ, AIST, [2]GSS, Univ Tokyo, [3]ERI, Univ. Tokyo, [4]Fossa Magna Museum.

Ductile fracture is a well-known phenomenon in metallurgy, where the nucleation, growth and coalescence of cavities result in fracturing during ductile deformation. A comparable process in rocks is potentially linked to observed tectonic tremors in crustal faults such as the San Andreas fault. However, there are only limited reports on this phenomenon in rocks. In this study, the relationship between cavity density, strain and fracturing in mylonites was examined to identify if ductile fracturing was an active process in the area. Additionally, we examined the scale of the associated structures to determine they have potential to be detected using geophysical observations.

This study was performed on Ryoke granitic-mylonites located in the hanging wall side of the Median Tectonic Line (MTL). These mylonites underwent heterogeneous ductile shearing and the associated deformation is interpreted as fossilised deformation from the base of the brittle-ductile transition zone. Microstructures of fractures and cavities were characterised using optical and scanning electron microscopy (SEM). The quartz recrystallised fraction, serving as a strain proxy, was measured using electron backscattered diffraction (EBSD). The continuity of the geological structure was evaluated by construction of a high-accuracy digital outcrop model (DOM).

Our data demonstrate that nano-sized cavities increase with increasing strain and evolve into ductile fractures when the area cavity density approaches ~7.5%. The DOMs enable the identification of ductile fractures with a minimum length of ~1200 m along the strike and a thickness of ~100 m in the MTL. Microstructures of cataclasite fragments within ductile fractures suggest deformation with a relatively slow slip rate. Therefore, the presence of this km-scale ductile fracture has the potential to host tremor.

Interlocking asperities revealed inside the focal zones of Bungo-Channel slow slip events and massive earthquakes along the Nankai Trough, Japan

Daisuke Sato[1], Takane Hori[1], Yukitoshi Fukahata[2]

[1] Japan Agency for Marine-Earth Science and Technology,

[2] Disaster Prevention Research Institute, Kyoto University

The Nankai subduction zone in Japan is a rich source of rupture events. Paleoseismic studies clarify repeating Mw>8 earthquake events, while recent studies have detected a range of slow earthquakes. Their relationship is still under debate (Kato & Obara, 2016).

Since both slow and fast earthquakes are strain-releasing phenomena, interseismic strain accumulation tells us the property of the upcoming failures. Many researchers have attempted to constrain the interseismic slip deficit rate by utilizing the framework of the slip inversion, but the associated frictional property is poorly constrained. In this study, we construct a simple method to invert frictional interlocking zones, so-called asperities in physics-based modeling, directly from interseismic geodetic data. We apply it to actual data to address the frictional property along the Nankai subduction zone, Japan.

We start from one universal nature of frictional motions, known as the principle of complementarity (Smaï & Aochi, 2017), which states either slip or traction is almost constant at frictional boundaries. A binary phase is then defined to express stick and slip at each point along the plate boundary. The stick phase represents interlocking asperity, while the slip phase represents the stable creeping zone in an interseismic period. Thus, keeping high generality without presuming specific friction laws, the estimation of interlocking asperity reduces to the inversion on the stick-slip model studied earlier (e.g., Burgmann+2005).

In the application, we analyze on-shore GNSS data of GEONET and off-shore GNSS-Acoustic data obtained by Yokota et al. (2016). First, from the ordinary slip deficit inversion using Green's functions for the three-dimensional elastic structure of the Nankai subduction zone (Hori et al., 2021), we find three elliptic slip deficit zones near the focal zones of the 1944 To-Nankai and 1946 Nankai Mw>8 earthquakes and the 2018-2019 Bungo-Channel long-term slow-slip event (L-SSE). We then conduct the stick-slip inversion to find the associated interlocking asperity centroids, where we optimize the centers and radii of those centroids. The results indicate that around 100km-wide interlocking zones result in twice larger slip deficit zones. In terms of the estimated asperity location, we confirm clear separability between the three interlocking asperities for the two earthquakes and one slow slip event. Meanwhile, we also find overlaps between the estimated slip deficit zones corresponding to the 1946 Nankai Mw>8 earthquakes and 2018-2019 Bungo-Channel L-SSE. These suggest that the frictional asperities of large slow and fast earthquakes are partitioned by the stably creeping zone along the Nankai subduction zone, but these asperities are close enough to interact and trigger each other by the stress transfer.

Periodic swarm of shallow earthquake and tremor near the Japan Trench, Off Fukushima

Shukei Ohyanagi[1], Kazuaki Ohta[2], Yoshihiro Ito[3], and Ryota Hino[4],

[1]Graduate School of Science, Kyoto Univ., [2]NIED, [3]DPRI, Kyoto Univ., [4]Tohoku Univ.

In recent years, interaction of slow and fast earthquakes; particularly influence to large earthquakes has caught peoples' attention. Several large earthquakes are reported to be preceded by Slow Slip Events [e.g. 2011 Tohoku-Oki: Kato et al., 2012; Ito et al., 2013; 2014 Iquique: Ruiz et al., 2014; 2017 Guerrero: Cruz-Atienza et al., 2021]. However, such observations are still limited. Most of the slow earthquake sequences do not accompany notable large earthquakes. In order to investigate the slow-to-fast interaction from observational perspective, it may be more efficient to focus on relation of microseismicity and slow earthquake activities since their synchronizations are potentially occurring more frequently. In Off Kii Peninsula of the Nankai subduction zone, Yamamoto et al. (2022) reported shallow SSEs in the Nankai subduction zone frequently accompany earthquake swarms. Similar synchronous activity also occurs in the Japan Trench subduction zone. Obana et al. (2020) reported bursts of shallow tremor often synchronized with earthquake activity in the Off Fukushima section, where is the southern proximity of the coseismic slip region of the 2011 Tohoku-Oki Earthquake [Iinuma et al., 2012; Kubota et al., 2023]. However, their observation was made by short-term (4 months) Ocean-Bottom Seismometer (OBS) observation. Because of the limited observational period, it was not clear how frequent such synchronous activity of slow and fast seismicity is occurring in the Off Fukushima.

Here, we compare the long-term (7 years; 2016 - 2023) catalog of tectonic tremor and ordinary fast earthquakes to investigate how frequent such synchronization is occurring. To construct both catalogs, we used OBS recordings of S-net (Aoi et al., 2020). We picked 8 S-net OBSs located around a known slow earthquake source region of Off Fukushima (Nishikawa et al., 2019; 2022; Matsuzawa et al., 2015; Ohta et al., 2019). Tectonic tremors are detected and located using a modified envelope correlation method (Mizuno and Ide, 2019). Fast earthquakes are detected by the Earthquake Transformer (Mousavi et al., 2020), which is a deep learning-based module to detect a fast earthquake from a continuous waveform. Detected earthquakes are phase-associated by the REAL (Zha et al., 2019) and located by hypomh (Hirata and Matsu'ura, 1987) with a local 1D velocity model.

Based on the constructed catalog, we identified at least 5 earthquake swarms synchronous to tremor bursts. Those swarms are occurred at up-dip of the tremor source region after the tremor bursts. While the tremor bursts itself recur every ~ 3 months, the earthquake swarms synchronous with the tremor bursts occur almost every ~ 1 year. This result indicates that even though tremor burst does not always accompany seismicity activation, episodic synchronization of slow and fast earthquakes taking place in the shallow part of the Japan Trench subduction zone.

Effects of site amplification and high-frequency seismic wave propagation on seismic energy estimation for shallow tremors

Shunsuke Takemura[1], Kentaro Emoto[2], and Suguru Yabe[6]

[1]ERI, UTokyo, [2]Kyushu Univ., [3]AIST

The seismic energies of shallow tremors have been estimated in various studies to understand the physical properties of shallow slow earthquakes (e.g., Yabe et al., 2019, 2021). High-frequency seismic waves at ocean bottom seismometers (OBSs) are typically complex because of propagation path and site amplification. Regular earthquakes have often been used to correct site amplification in OBS data. Due to the lack of interplate earthquakes in shallow tremor regions, vertical incident waves from intraslab earthquakes are typically used in estimations of site amplifications. After site corrections, the seismic energies of shallow tremors are estimated by assuming a homogeneous medium. However, due to shallower source depths, high-frequency seismic waves from shallow tremor sources are effectively trapped within the oceanic sediments. Consequently, envelope broadening and amplification due to path effects occur (Takemura et al., 2020, 2023). To achieve more accurate seismic energy estimations,

We synthesized high-frequency seismograms for tremor and intraslab earthquakes using a wavenumber integration algorithm (Hermann et al., 2013). DONET 1D (Nakano et al., 2013) and empirical relationships of other physical parameters (Brocher 2005, 2008) were assumed. The DONET 1D model includes a 5.43 km-thick sedimentary layer and a 2.64 km-thick water layer. The minimum S-wave velocity in the solid column is 0.61 km/s. The source depths of a shallow tremor and an intraslab earthquake are 8.3 and 40 km, respectively. These depths are typical values along Nankai Trough. We also synthesized waveforms using the model where low-velocity layers were replaced as physical parameters of crust (Vs = 3.27 km/s) to evaluate the effects of a thick sedimentary layer.

For an intraslab earthquake, synthetic seismograms using both models exhibited pulsive S waves, and maximum amplitudes of DONET 1D were 1.5 times amplified compared to those without a sedimentary layer. By using intraslab earthquakes, a major cause of 5~20 times amplifications estimated by Yabe et al. (2019) can be considered as thin lower velocity (Vs < 0.6 km/s) sediments just below DONET stations. On the other hand, for a shallow tremor case, envelope shapes of DONET 1D were significantly elongated, and amplitudes were 2~5 times amplified. These elongation and amplification are caused by gentle-incident and trapping of S wave energy within the thick sedimentary layer. The effects of both propagation path and site amplifications should be incorporated to precisely estimate the seismic energies of shallow tremors.

Preparation for an estimation of seismic structures around slow earthquake areas in the Nankai subduction zone using receiver functions in multi-frequency bands

Akifumi Takayama[1], Yasunori Sawaki[2], Yihuan Ruan[1] and Yoshihiro Ito[3]
[1]Kyoto University, Graduate School of Science, Kyoto, Japan, [2]National Institute of Advanced Industrial Science and Technology (AIST), Geological Survey of Japan, Tsukuba, Japan,
[3]Kyoto University, Disaster Prevention Research Institute, Kyoto, Japan

Seismic heterogeneity around a subducted slab often reflects the source environment of deep slow earthquakes (e.g., Kodaira et al., 2004; Kato et al., 2010). A subducted seamount is one of the factors that yield heterogeneity, and previous studies showed subducted seamounts might control shallow slow earthquakes (e.g., Sun et al., 2020). In contrast, the influence of subducting seamounts at the deeper portion along the Nankai trough is not fully clarified. Particularly, little is known about the effects of subducting seamounts on the occurrence of slow earthquakes and related physical models. In addition, there are few previous studies on the influence of seismic structural variation between high and low activity of slow earthquakes with subducting seamounts at the deeper potion of subduction zones.

Our final goal of this study is to understand detailed seismic structures that affect the occurrence of slow earthquakes at deeper portion of the Nankai subduction zone, using the receiver function (RF). Specifically, we focus on understanding the difference between seismic structures accompanying both high and low activity of slow earthquakes. The RF analysis is useful in detecting shear-wave velocity discontinuities through the extraction of converted waves (e.g. Langston, 1979). Here, we apply the multi-band RF analysis (Sawaki et al., 2021) that uses a wider frequency bandwidth of seismic waves than conventional methods. The multi-band RF analysis can obtain detailed seismic structural images by combining RFs at both the low and high frequency sides.

As an initial step in this study, we compare observed RFs with synthetic ones in the western Shikoku, where subducted seamounts might control the deep slow earthquake source distribution (Ide, 2010). One of the synthetic RFs is based on the ray-theoretical seismograms for incident plane wave with dipping interfaces (Raysum, Frederiksen and Bostock, 2000). The other is calculated from the finite difference method, considering a three-dimensional heterogeneous structure (OpenSWPC, Maeda et al., 2017). We also discuss detectability of inclined seismic wave velocity discontinuities, anisotropy and three-dimensional heterogeneous structures with comparing observed and synthetic RFs.

Analysis of slow-to-fast earthquakes using strain and rotational observations

Kazutoshi Imanishi[1] and Suguru Yabe[1]

[1]Geological Survey of Japan, AIST

Nearly 20 years have passed since the discovery of slow earthquakes, which have different characteristics from ordinary tectonic earthquakes. The mechanism of slow earthquakes is an essential problem in seismology and has long been understood in terms of shear rupture at a plate boundary, primarily on the basis of seismic waveform analysis. However, slow earthquakes, which exhibit complex behavior, are unlikely to be explained by such a simple process. Now that numerous new findings have been accumulated, it is worth reconsidering the interpretation of "slow earthquakes = shear rupture".

In this study, we are developing a method for estimating the moment tensor of earthquakes using strain and rotational components as new observables, and aim to estimate the non-double-couple component of earthquakes with high accuracy. For the strain components, we can utilize data from borehole strainmeters deployed by the Geological Survey of Japan, AIST, in southwestern Japan. For the observation of rotational components, we have started temporary array observations using 4 broadband seismometers at Nii-Oshima in Niihama City, Ehime Prefecture (Fig. 1). In this array, we have already obtained good records, including two M4-class earthquakes around the Bungo Channel. In the presentation on the day, we will show the inferred rotations and strains of the ground beneath the array and discuss the impact of incorporating new observables on the accuracy of moment tensor solution.

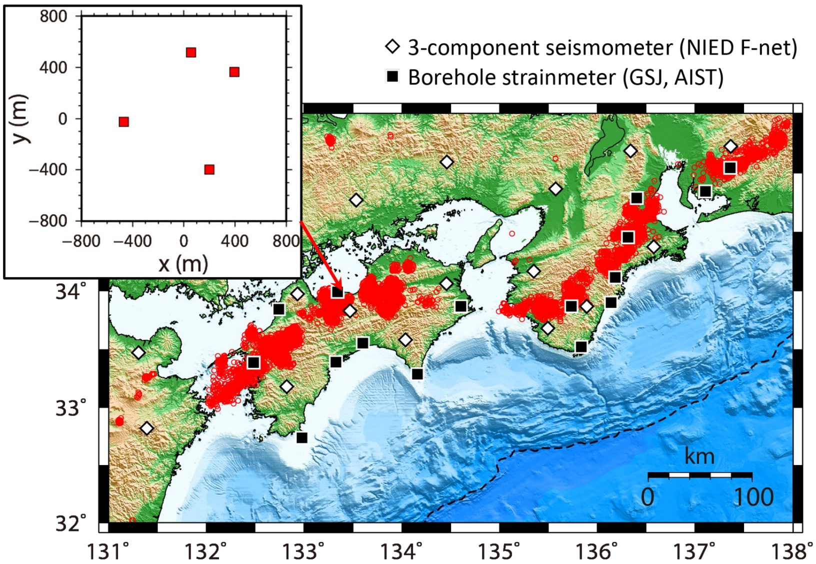

Figure 1. Map of the studied area and station distribution. The inset shows the configuration of the seismic array at Nii-Oshima in Niihama City, Ehime Prefecture. Red circles represent deep low-frequency earthquakes reported by the Japan Meteorological Agency.

Slow and fast seismic activity in the southeastern Guerrero seismic gap from 2022 to 2023

Kentaro Kuniyoshi[1], Yoshihiro Ito[2], Shukei Ohyanagi[1], Raymundo Plata-Martinez[3], Ketzalina Flores[1], Yanhan Chen[1], Emmanuel Soliman M. Garcia[2], Victor M.Cruz-Atienza[4],

[1]Graduate School of Science, Kyoto Univ., [2]DPRI, Kyoto Univ., [3]JAMSTEC, [4]Instituto de Geofísica, Universidad Nacional Autónoma de México

Slow earthquakes have the potential to trigger huge earthquakes. Monitoring slow earthquakes activity may help us reach forecasts of huge earthquakes. Accurately determining the source of tremors plays an important role in comprehending the spatial features hosting slow earthquakes by comparing them with other spatial information, such as seismic velocity and gravitational structure.

Along the Pacific coast Mexico, large earthquakes frequently occur due to the subduction of the Cocos Plate beneath the North American Plate. However, there exists a seismic gap offshore Gurrero (GGAP). Based on records observed by ocean bottom seismometers (OBSs) in the northwestern part of the GGAP from 2017 to 2018, Plata-Martinez et al., (2021) demonstrated the spatial pattern of fast and slow earthquakes, comparing residual gravity and bathymetry data in northwestern part of the GGAP.

In this study, we determine hypocenters of tremor and fast earthquake in the southeastern part of GGAP from March 2022 to March 2023. To detect fast earthquakes, the travel times of P-waves and S-waves are picked by using Earthquake Transformer (Mousavi et al., 2020) from the continuous OBS records at each station. Then, we calculate hypocenters with assuming a horizontal-layered velocity structure using Hypomh (Hirata and Matu'ura, 1987). We used a modified envelope correlation method (Mizuno and Ide, 2019) to detect and locate tremor sources.

Identification of Eruptive Activity Anomalies at Mt. Aso Based on the Gradient Boosting Method of Multimodal Observation Data from Seismographs and GPS

Minoeu Ideno[1], Takeshi Tsuji[1]

[1]Univ. Tokyo

Identifying complex anomalies from multimodal data such as seismograms and GPS is important for predicting volcanic eruptions as well as characterizing fast and slow earthquakes. Here, we propose to use a machine learning method, gradient boosting trees (GBDT), to evaluate anomalies in observed data; GBDT is a machine learning method that optimizes model predictions and enables fast feature engineering. In this study, we focus on the multimodal data acquired at Mt Aso.

First, to create the training model, we used GPS and seismometer data before and after the October 2016 eruption of Mt. Aso. Four parameters (seismic wave velocity, scattering characteristics, amplitude of volcanic tremor, and baseline length) were calculated from those data. Features were extracted from those time-series data and modeled by GBDT for quantitative prediction of the height of the volcanic plume. The results demonstrate that the combination of historical volcanic plume data and amplitude of 6 seismometer data can provide accurate predictions.

Machine learning predicts earthquakes in the continuum model of a rate-and -state fault with frictional heterogeneities

Reiju Norisugi[1], Yoshihiro Kaneko[1], Bertrand Rouet-Leduc[2]

[1]Department of Geophysics, Kyoto Univ., [2]DPRI, Kyoto Univ.,

Machine learning has been used to study the predictability of laboratory earthquakes. For example, Rouet-Leduc et al. (2017) showed that using continuous acoustic signals emitted by a laboratory fault, machine learning can predict the time remaining before a larger slip event (i.e., the mainshock). However, the question remains whether or not this approach can be applied in a tectonic setting where one may have to rely on sparse earthquake catalogs, and where important timescales vary by orders of magnitude. In this study, we apply machine learning to a synthetic seismicity catalog generated by the continuum model of a rate-and-state fault with frictional heterogeneities. The synthetic catalog contains foreshocks, mainshocks and aftershocks that nucleate in a similar way, making it difficult to assess which output parameters contain key information for the mainshock predictability. We develop a network representation of the earthquake catalog to train a machine-learning model. We find that the trained model can predict the time remaining before the mainshock with great accuracy, from the scale of decades, long before the upcoming earthquake, down to the scale of hours to minutes, right before the mainshock. Important features that arise from the machine learning model are seismic moment and recurrence time averaged over a certain foreshock network size. We also find that the network representation of the catalog enables incorporating features at various time scales, allowing to accurately predict the timing of mainshocks throughout the earthquake cycle and at all timescales, a limitation of the initial 2017 study. These results offer clues as to why machine learning can predict laboratory earthquakes and how the developed approach could be applied to a more complex setting (e.g., real earthquake catalogs) where multiple timescales are at play.

Seismic source spectral properties of dynamic rupture with a self-similar, self-healing slip pulse

Yuto Kano[1], Yoshihiro Kaneko[2], Peter M Shearer[3]

[1]Kyoto University, [2]Kyoto University, [3]University of California San Diego

Large earthquakes commonly exhibit pulse-like rupture modes, but stress drops of small earthquakes are often estimated from far-field body-wave spectra using measurements of seismic moment, corner frequency, and a theoretical model of rupture in a crack-like mode. Assuming earthquakes are self-similar, with scale-independent stress drop and scaled energy, a majority of small earthquakes likely exhibit a pulse-like rupture. In this study, we develop a fundamental model of earthquake rupture with a self-similar, self-healing slip pulse. We examine the resulting spectral properties, estimated stress drops and scaled energy, and compare them to those derived from self-similar, crack-like rupture models. The source spectra of pulse-like rupture models show classical double corners, each corresponding to the overall size of the rupture and growing slip-pulse width, respectively. The spherical averages of P- and S-wave corner frequencies increase the rupture speed and are higher than those of their crack-like rupture counterparts, as expected. The variability of estimated stress drops due to differences in the rupture speed and source geometry is larger in the pulse-like rupture models than that in the crack-like rupture models. The dependence of radiation efficiency on the overall rupture speed in the pulse-like rupture models is more consistent with observations than in the crack-like rupture models. These results suggest that if small earthquakes are indeed mostly pulse-like ruptures, the large variability of estimated stress drops often seen in observational studies may come from variability in source characteristics almost independent of the actual stress drops.

Direct investigations of the fracture flow with asperity contact, and its relationship to the geophysical properties

Kazuki Sawayama[1] and Jiei So[1]

[1]BGRL, Dept. Science, Kyoto Univ.

Crustal permeability anisotropy could be a possible cause of the occurrence of the slow earthquake and its spatiotemporal variations. Recent observations have revealed microtremors that cannot be explained by mineral dehydration, and it has been interpreted that permeability differences at plate boundaries increase fluid pressure. Considering the heterogeneous asperity distribution in seismogenic zones, the asperity contact may influence such permeability differences. Many experimental studies have shown that the permeability in the weakly contacted discontinuity (i.e., faulted rock) is highly stress dependent, whereas the permeability in the strongly contacted fracture becomes almost constant. Since slow earthquakes are sensitive to changes in ambient stress, the small changes in stress can trigger the change in such a contact state, causing drastic changes in permeability. Although in-situ permeability measurements are not available, geophysical properties (e.g., electrical resistivity, seismic velocity and amplitude) have the potential to estimate crustal permeability differences. In fact, recent observations have detected changes in electrical resistivity and seismic velocity due to changes in crustal stress, which may be related to permeability. This study investigates how the magnitude of the permeability change is induced by the asperity contact state based on numerical simulations of the digital rock. To propose a model for estimating crustal permeability changes from observed geophysical properties, we also investigated the changes in electrical and elastic properties at elevated asperity contact ratio of different fracture models.

We produced three-dimensional printed rocks with synthesized fault planes. The fault roughness was generated based on fractional Brownian motion and measured surfaces of natural rock fractures. The size of the fault model is 60×60 mm with a 0.1 mm square grid. Laboratory experiments and numerical simulations were performed on the same fault model: 3D printed material for experiments and the digital model for simulations. In the experiment, we performed flow measurements, resistivity measurements, and elastic wave array measurements during uniaxial compression tests up to ~70 MPa. Flow measurements were conducted with a syringe pump (ISCO, 260X) and an electric balance. Resistivity was measured with an LCR meter (ZM 2376) at frequencies between 1 mHz and 5.5 MHz. For impedance measurements, the four-electrode method with Kelvin connection was used, where the electrodes were made of Ag-AgCl. The velocity measurements were based on the pulse transmission method. In our system, the input trigger of a pulse was generated by a function generator (WF1974), and the transmitted wave was recorded by an oscilloscope (DLM5034). We used Olympus ultrasonic transducers (V103-RM for P-wave velocity measurements and V153-RM for S-wave velocity measurements) as a pair of transmitter and receiver transducers. Based on their resonant frequency, the input pulse was set to 1 MHz frequency and 10 V amplitude. To improve the signal-to-noise ratio, the transmitted waveforms were amplified by a preamplifier (NF9913) and stacked 256 times. We used Akaike's information criterion (AIC) to select the first arrival time of P-wave and S-wave. Based on the first arrival time and the distance between the transmitter and receiver transducers, we calculated the spatial distribution of P-wave and S-wave velocities. The numerical simulations were based on the boundary element method (half-space based dry contact model) for the elastic-fully plastic deformation, and the finite volume method (local cubic law) for the fluid and electrical flows.

As a result, the changes in permeability and resistivity are well correlated with the evolution of the asperity contact. The local fluid flow and electric current show similar tendencies (Figure). On the other hand, the P-wave velocity and the Vp/Vs ratio are less dependent on the flow paths and are more sensitive to the local asperity contacts. These results may indicate that the electrical resistivity is sensitive to the fluid flow, while the velocities are related to the asperity contacts or other mechanical properties.

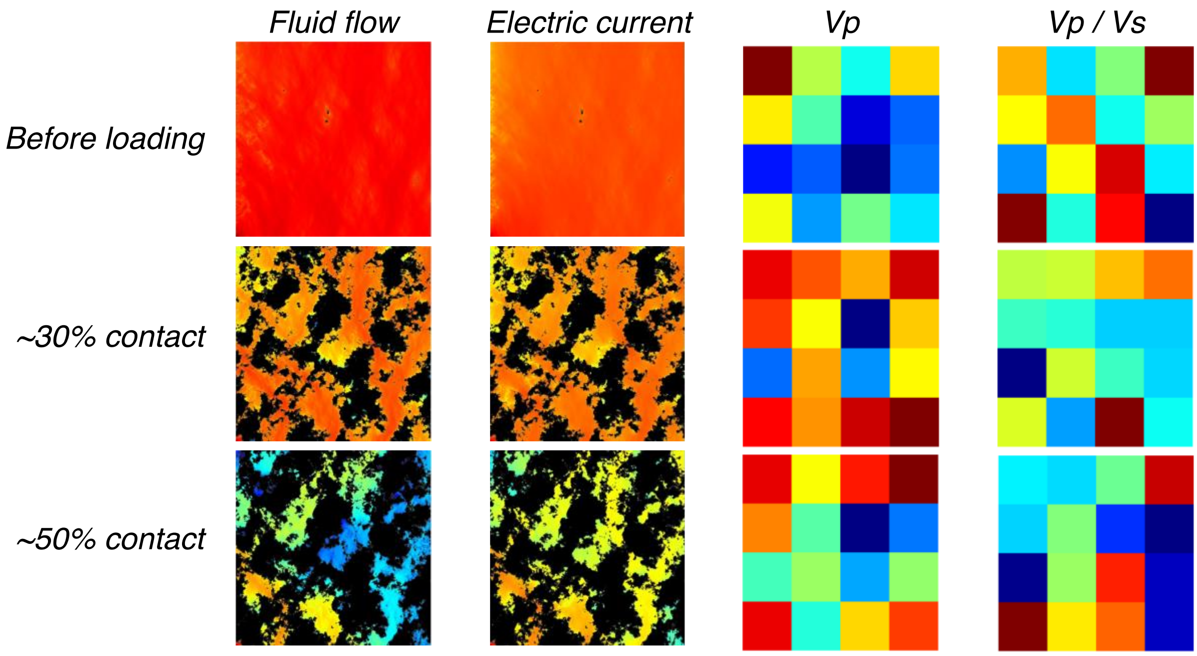

Figure: Images showing local fluid flow, electric current, P-wave velocity and Vp/Vs ratio with asperity contact ratio. The red color represents higher values, whereas the blue color represents lower values.

Waveform-based methods for the analysis of Distributed Acoustic Sensing (DAS) data

Francesco Grigoli[1], Juan Porras[1], Davide Pecci[1], Gian Maria Bocchini[2], Sonja Gaviano[1], Giacomo Rapagnani[1] and Chiara Cocorullo[3]

[1]Department of Earth Sciences, University of Pisa, Italy
[1]Department of Earth Sciences, University of Bochum, Germany
[3]Seismix, Palermo, Italy

In the last few years, the number of Distributed Acoustic Sensing (DAS) installations deployed around the world has grown exponentially and will continue to grow in the next years, producing larger and larger seismological datasets. DAS interrogators can transform fiber-optic cables into dense arrays of seismometers that sample seismic wavefields with a very high spatial density (inter-channel spacing of the order of a few meters) for several kilometers. The use of the already-installed telecommunication optical fiber-network infrastructure makes the DAS system particularly suitable for the seismic monitoring of logistically challenging scenarios such as volcanoes or offshore areas. In a typical setting, DAS datasets are collected with a sampling frequency of 1 kHz or higher and a spatial sampling between 1 and 10 m. Unfortunately, standard seismological techniques are not capable of exploiting this high temporal and spatial sampling and have to deal with different limitations reducing their performance. Since these approaches are not designed to exploit the characteristics of the DAS data, classical pick-based methods are often ineffective in processing this kind of data. In this work, we propose a waveform-based detection and location method that fully exploits the characteristics of the DAS data. This approach detects and locates seismic events by looking at waveform coherence along hyperbolas while changing the curvature and position of the vertex. The method returns a time series of coherence values. An event is detected (and consequently located) if the coherence values become higher than a fixed threshold. This workflow has the great advantage that it runs in near-real time and allows to increase the number of detected events if compared with classical approaches. We successfully validated our workflow both with synthetic and real datasets related to a fiber deployed in a borehole well at the FORGE Geothermal Project, Utah (US).

Fine-scale hypocenter migration of earthquake swarms beneath the northeastern Noto Peninsula, Japan

Kodai Sagae[1], Yuta Amezawa[1], Takahiko Uchide[1]

[1] Geological Survey of Japan, AIST

Earthquake swarms are spatiotemporally clustered activity without a clear mainshock. Hypocenter migration is one of the characteristics of swarms. The propagation distance at the swarm front is proportional to the square root of time, suggesting a diffusive behavior possibly due to the pore pressure diffusion (Shapiro et al., 1997). Significant variations in migration speed have been reported (0.1 km/day at the swarm front; 10 km/day in the swarm interior) (e.g., De Barros et al., 2020). An investigation both in the front and interior is key to understanding the physics controlling the swarm.

Earthquake swarms beneath the northeastern Noto Peninsula, Japan, have continued since 2018. The hypocenter distribution was spatially grouped into four clusters (S, W, N, and NE), with active areas starting from the S cluster and shifting in the order of the W, N, and NE clusters. At the swarm front, diffusive hypocenter migrations with diffusivities of ~ 0.1 m^2/s were observed in all but the S cluster (Amezawa et al., 2023). In this study, we investigated the spatiotemporal characteristics of the hypocenter migrations in detail to quantify the seismic activity of the swarm interior.

We objectively extracted hypocenter migration (3-D migration) in two steps. First, epicenter migration (2-D migration) was extracted using a space-time Hough transform (Sagae et al., 2023). Second, linear regression with depth and time was performed for earthquakes belonging to the 2-D migration. The 3-D migration was determined by adding information on the temporal change in depth to the 2-D migration.

In most clusters, the spatial characteristics of the hypocenter migrations showed that the median duration and the migration speed were longer than six days and slower than 0.1 km/day, respectively. On the other hand, in the S-cluster at depths >15 km, the median duration and the median migration speed were shorter than one day and higher than 2.0 km/day, respectively. The rapid hypocenter migrations in the S cluster at depths >15 km occurred intermittently and propagated upward along a ring-like hypocenter distribution. In addition, their diffusivity exceeded 10 m^2/s based on a relation between migration speed and duration. The rapid hypocenter migrations suggest that rapid and intermittent changes in pore pressure occurred along the ring-like hypocenter distribution.

This research was supported by JSPS KAKENHI Grant Number JP21H05205 in Grant-in-Aid for Transformative Research Areas (A) “Science of Slow-to-Fast Earthquakes”.

Tsunamigenic faulting events in submarine calderas: Observations and physics

Osamu Sandanbata[1]

[1]ERI, Univ. Tokyo

Tsunamis are generated not only by large earthquakes but also by submarine volcanic activity beneath/near the ocean. In recent collaborative research, we have shown the recurrence of atypical earthquake and tsunamis due to intra-caldera faulting events in submarine calderas. This presentation provides a comprehensive overview of the key findings from our recent research on the volcanic earthquakes and tsunamis.

At Sumisu caldera in the Izu-Bornin Arc, south of Japan, non-double-couple earthquakes with seismic magnitudes of M_w<6 unusually caused tsunamis with a maximum wave height of about a meter every decade. To explore the mechanism of the peculiar volcanic earthquakes and tsunamis, we conducted analyses of tsunami and long-period seismic waveform data of the earthquake in 2015 to find a source model that explains both datasets. The model showed *trapdoor faulting*, involving large intra-caldera fault slip of >5 m and deformation of its sill-like magma chamber, took place in the submarine calderas (**Figure**). The mechanism also proved applicable to similar seismic and tsunami events at a submarine caldera near Curtis Island, north of New Zealand.

We then investigated the physics of trapdoor faulting in calderas. Focusing on another series of similar events near a submarine caldera near Kita-Ioto Island, south of Japan, we develop a mechanical model of trapdoor faulting that links the pre-seismic magma pressure beneath the volcano, as a driving force, to the size of the earthquake and tsunami. By comparing the model prediction with the tsunami data, we inferred that magma overpressure of ~10 MPa drove the faulting event and suggested that the faulting much influences the magmatic system.

These discoveries of trapdoor faulting in submarine calderas revealed that the faulting phenomenon is more common than we had expected. Since faulting in calderas is closely interacted with their magmatic system, better knowledge of intra-caldera faulting behaviors in volcanic environments are important for understanding the caldera volcanism, including how volcanos inflate and lead to eruption.

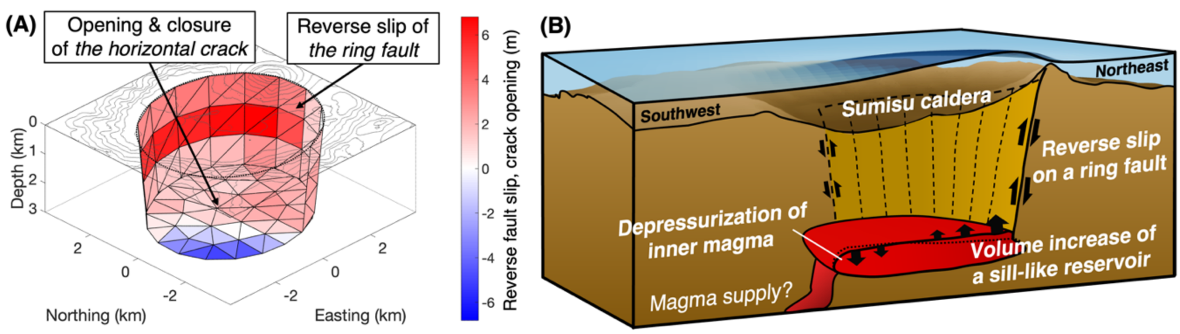

Figure. (**A**) Source model of the 2015 earthquake at Sumisu caldera. Colors represent reverse slip (red) on a ring fault, and vertical opening (red) and closing (blue) of a horizontal crack. (**B**) Schematic illustration of trapdoor faulting that caused tsunamis.

Towards adjoint tomography of the Nankai and Kyushu subduction zones

Samriddhi Prakash Mishra[1], Yoshihiro Kaneko[1], Bryant Chow[2], Shun Adachi[1], Yusuke Yamashita[3], and Masanao Shinohara[4]

[1]Graduate School of Science, Kyoto University, [2]University of Alaska- Fairbanks, Alaska, USA, [3]DPRI, Kyoto Univ., [4]ERI, Univ. Tokyo

The Nankai-Kyushu subduction system is a complex seismotectonic region marked by an abrupt transition in the inter-plate coupling, with a fully coupled megathrust in the northeast. In this study, we utilize an earthquake-based, full-waveform inversion technique termed adjoint tomography, to develop an accurate and high-resolution shear-wave velocity model in the megathrust regions and reveal the crustal structure responsible for the origin of the inter-plate coupling transition. Adjoint tomography has been previously applied to regional, continental, and global scales, with a proven track record of high probing applicability in subduction regions elsewhere in the world (e.g., Chow et al., 2022). Our target region includes ~150 permanent receivers as well as ~20 temporary OBS stations in the Hyuga-nada region. We first conduct a series of 2-D synthetic inversion tests for a SH-wave problem (e.g., Tape et al., 2007) of the target region using a recently developed automated tool (Chow et al., 2020; Modrak et al., 2018) to address the resolvability of small scale heterogeneities given the source-receiver coverage. We demonstrate that this technique in conjunction with the existing dataset has a potential to resolve crustal structure in fine detail and construct an accurate shear-wave velocity model in this region. We present our ongoing efforts towards imaging and understanding the crustal structure of the Nankai and Kyushu subduction zones and its link to the spatial variation in the megathrust locking behavior.

Scaling Microseismic Cloud Shape during Hydraulic Stimulation using In-situ Stress and Permeability

Yusuke Mukuhira[1], Meihua Yang[1,2], Takuya Ishibashi[3], Kyosuke Okamoto[3], Hirokazu Moriya[4], Yusuke Kumano[5], Hiroshi Asanuma[3], Serge A. Shapiro[6], Justin L. Rubinstein[7], Takatoshi Ito[1], Kangnan Yan[1,2], Yinhui Zuo[2]

[1]IFS, Tohoku Univ., [2]State Key Laboratory of Oil and Gas Reservoir Geology and Exploitation, Chengdu Univ. of Tech., [3]FREA, AIST, [4]School of Eng., Tohoku Univ., [5]JAPEX Co., Ltd., [6]Freie Universität Berlin, [7]USGS

Reliable prediction of the microseismic cloud shape, which serves as an indicator of the stimulated rock volume, is crucial for designing effective energy extraction systems. During hydraulic stimulation of geothermal reservoirs, the microseismic (MS) cloud is expected to expand in the direction of the maximum principal stress. However, observations of microseismic cloud growth don't always follow this expectation based on empirical findings, and the underlying mechanisms of microseismic cloud growth are not well understood. In this study, we investigate microseismic cloud growth by analyzing data from a hydraulic stimulation project in Basel, Switzerland, and examine its correlation with measured in-situ stress. By employing principal component analysis (PCA), we analyze the macroscopic characteristics of microseismic cloud growth in both two- and three-dimensional space. Our findings reveal that the microseismic cloud not only extends in the direction of maximum principal stress but also expands along the intermediate principal stress direction. Interestingly, the orientation of minimal microseismic cloud growth remains stable and aligns closely with the direction of minimum principal stress. PCA analysis provides the lengths of MS cloud along each principal component axes, so that we can evaluate the macroscopic shape of MS cloud by calculating the ratio of those lengths. When comparing microseismic cloud dimension aspect ratios with in-situ stress magnitude ratios, we observe a good agreement. To make the bridge of physical meaning between the in-situ stress and MS cloud shape, we also compute the permeability tensor from MS hypocenter distribution, independently. The permeability tensor also exhibits a strong correlation, both in terms of direction and magnitude, with the growth of the microseismic cloud. From the geomechanical point of view, the permeability is function of in-situ stress. Our study highlights the important role of in-situ stress in controlling the permeability of existing fractures within the reservoir fracture system. As a result, microseismic cloud growth can be roughly scaled using in-situ stress as a preliminary approximation, particularly when there is sufficient variability in the orientation of existing faults.

New Single-station Detection Method for Seismic Slow Earthquakes

Koki Masuda, Satoshi Ide

Department of Earth and Planetary Science, The University of Tokyo

Slow-earthquake signals are generally smaller than or comparable to noise levels at almost all seismological frequencies. Comprehensive detection of these events requires continuous waveforms from many stations, but such data are not always available, even in regions with high slow-earthquake activity. We therefore need a simple and stable detection method that is also applicable to regions with sparse seismic observation networks to truly advance our understanding of slow earthquakes.

In this study, we utilize the proportionality between the seismic energy rate and seismic moment rate of slow earthquakes to develop a slow-earthquake detection method using broadband waveforms from a single station. From a broadband seismogram recorded at a single station, we measure seismic energy rate as the squared-velocity waveform in 2-8 Hz and, and seismic moment rate as the displacement waveform in 0.02-0.05 Hz. Then we calculate the correlation coefficient between the seismic energy rate and seismic moment rate, every 10 s in a time window of 300 s, and take a moving average of 10000 s. We regard the timing when this value exceeds a certain threshold is "detection".

We apply this method to the stations in Japan and the Mexican subduction zone (Mauda and Ide, submitted). From the result of Japan, we confirm the new method only detects events when the tectonic tremors occur near the station, which suggests that the false-positive rate is low. Then, the results of the Guerrero and Oaxaca regions in the Mexican subduction zone are largely consistent with a previous research (Husker et al., 2019), and that of the Jalisco region in the Mexican subduction zone is the first seismological report of long-term slow-earthquake activity in this region. Furthermore, we also report a preliminary result of applying this method to stations around the world in this presentation.

Stress and temperature estimation for Sanbagawa metamorphic rocks in Kanto Mountains: A possibility of occurrence of deep slow earthquakes

Seiya Maehara[1], Simon Wallis[1]

[1]Univ. Tokyo

The down-dip limit of the seismogenic zone corresponds to the depth of the brittle-to-ductile transition zone, and in warm subduction zones such as Nankai of SW Japan, this transition zone is main location for deep slow earthquakes including episodic tremor and slip (ETS). Despite advances in geophysical modeling and geodetic studies, the geological structures corresponding to the transition zone are still unclear. In this study we used geological structures in the Nagatoro area of the subduction-type Sanbagawa metamorphic belt in the Kanto mountains to estimate the stress and temperature conditions of the transition zone. Exhumed subducted rocks exposed in the study area show microstructures that indicate the simultaneous development of both brittle and ductile deformation indicating that this area is suitable to examine the nature of the transition zone. In this study we focus on the stresses, temperature and strain rates. Paleopiezometry applied to quartz microstructures of the ductilely deformed rocks allows stresses to be estimated and these can be correlated with the background stresses for the brittle deformation. The temperature of the metamorphism was estimated using carbonaceous material Raman spectroscopy. The results showed that the peak metamorphic temperature of Sanbagawa metamorphic rocks in Nagatoro area is ~350-400°C. Strain rates were then estimated using an appropriate quartz flow law incorporating the estimated stresses. The resulting strain rate was $\sim 10^{-13}$ /s. Independent estimates of pressure suggest that the Nagatoro study area preserves deformation relevant to depths somewhat shallower than the main domain of deep ETS region in modern SW Japan, and may corresponds to the upper-limit of the brittle-to-ductile transition zone. To understand the relationship between deep slow earthquakes and the deformation of Sanbagawa metamorphic rocks in Nagatoro area and surrounding Kanto mountains, we need further research of (i) comparison of subduction/exhumation process of recent subduction zones and the Sanbagawa belt and (ii) estimation of temperatures and strain rates in wider area.

Development of a machine learning model to detect short-term SSEs from tilt records

Tomoka Higa[1*], Hitoshi Hirose[2,1], Takeshi Kimura[3]

[1]Dept. Planetology, Kobe Univ., [2]RCUSS, Kobe Univ., [3]NIED
[*]Present address: Wakayama Local Meteorological Office

Short-term slow slip event (SSE) is one of slow earthquakes in which slow fault slip lasts for a few days to a month. It occurs mainly on plate boundary in subduction zones and is observed by geodetic methods such as tiltmeter, strain meter, and GNSS. Short-term SSEs which occur on plate boundary is considered to play an important role in strain buildup in megathrust fault zone where host huge earthquakes. However, it is possible that there are overlooked events in studied period because most short-term SSEs were detected by human inspection. A more complete SSEs catalog would make more quantitative discussion about how much accumulated strain is released by short-term SSEs. In this study, we develop a machine learning (ML) model to detect short-term SSEs from tilt records, with the ultimate goal of detecting events which analysts have overlooked.

The ML model developed in this study is that; when a single component of tilt time series data with sampling interval of an hour and a length of 30 days (1 channel, 721 data points) was inputted into the model, the model outputs probabilities of (1) SSE start time; (2) end time; and (3) noise; at each time epoch of input data. The machine learning model is a fully convolutional neural network based on PhaseNet (Zhu and Beroza, 2019) which picks P-wave and S-wave arrival times from seismograms and U-Net (Ronneberger et al., 2015) which performs image segmentation for biomedical images. We made synthetic dataset for training dataset that mimics tilt deformation by SSE and is created by adding random noise to a ramp function. The start and stop times of the rise and the amount of amplitude of the ramp function varied randomly. The number of observed cases of short-term SSEs with tiltmeters in southwest Japan is not enough to be used for a training dataset, so we use a synthetic dataset for training the ML model. In addition, we made a noise-only dataset without a signal (ramp function) considering to apply the ML model to real data. The model was trained on these two types of synthetic dataset. After training, to evaluate the performance of the trained model, we tested its prediction accuracy on a test dataset which consists of synthetic data, same as the training dataset. As a result, the ML model could detect 76% of the SSEs start time (the rise time of a ramp function) and 72% of the SSEs end time (the end time of a ramp function). For almost all noise-only data, the model could judge that the input data is noise data. Evaluating the trained model by S/N, accuracy of detecting SSE was reduced as S/N was reduced. It is considered that detecting SSE become difficult because the amplitude of signal is drowned out by the amplitude of the noise.

We applied the trained ML model to high-sensitivity accelerometer (tiltmeter) time-series records installed at National Research Institute for Earth Science and Disaster Resilience (NIED) Hi-net stations located in western Shikoku, Japan to confirm the applicability of this trained model to real data. We used 10 years (01 January 2003 to 31 December 2012) of the tilt time-series records. The time-series records were divided into intervals of each 30 days including overlaps, and were input into the trained model in sequence, then we obtained a catalog of start and end times of possible SSEs. Compared this catalog to the short-term SSEs catalog of Hirose and Kimura (2020), we succeeded to detect 20 of the start or end time of SSEs out of 32 events during the same period. Furthermore, we obtained 99 possible SSEs start or end time without the corresponding reported SSEs.

The reasons for the not-very-good 63% (=20/32) detection rate of known events might be that the number of observation points used for detection from real data is small, anomalies and missing measurements in real data are not processed, the structure of the machine learning model, and difference of characteristics of synthetic data used for training from the real data such as synthetic data does not contain drift and has the different S/N distribution.

If we can detect SSEs that have been overlooked by human inspection using this method, it is expected to be useful for further discussion on strain buildup in the subduction zone.

Effect of the thickness of gouge layer on the frictional weakening behavior of fault at high slip velocities

Akito Tsutsumi and Takumi Ogawa

Graduate School of Science, Kyoto University

Recent studies on friction velocity weakening behavior of faults at high-velocities discussed that the presence of gouge layer resulted in a remarkable difference in the high-velocity frictional weakening behavior (e.g., Platt et al., 2014; Mngadi et al., 2021). However, there have been few relevant experimental studies performed to understand the effect of fault gouge thickness on the frictional weakening behavior at high-velocities. Frictional velocity dependence of rock friction over a wide range of slip velocities is an important prerequisite to an understanding of slow to fast fault slip behavior. We report our results of a series of high-velocity friction experiments of quartz-dominated rocks. We will show that steady-state friction increases with the increase of the thickness of the simulated gouge layer.

Frictional experiments were conducted using a rotary-shear friction testing machine on the gouges prepared from the quartzite samples from Witwatersrand Basin, South Africa, which is the same sample as those used in the experiments of Mngadi et al. (2021). The gouges were crushed manually from the quartzite sample and then sieved to obtain grains smaller than ~120 μm. The experimental fault consists of a pair of quartize cylinders (24 mm diameter) with an intervening layer of the quartize gouge. A PTFE ring surrounds the fault to prevent gouge extrusion during the sliding. All of the experiments were done at a constant normal stress of 2 MPa and at a constant slip velocity v of 10 mm/s. Initial thickness of the gouge layer was changed by changing the initial weight of the gouge to be used as the following: 0.1, 0.15, 0.2 and 0.5 g. Experimental results show that the steady-state value of friction coefficient μ is low and it ranges from 0.25 to ~0.30 when the thickness of the gouge layer h is expected to be very thin with $t <$ ~0.1 mm. The low value of μ indicates that the slip velocity of the thin-gouge fault reaches the critical weakening velocity of flash heating. When the gouge thickness h is increased to exceed ~0.1 mm, the steady-state friction μ increases rapidly to attain almost constant value within the range of μ = 0.7–0.85.

Mngadi et al. (2021) performed high-velocity friction experiments on bare surfaces of quartzite rock samples and showed that generation of a gouge layer reduces the efficiency of flash heating. Their result is consistent to the theoretical discussion given by Platt et al. (2014). However, the detail of the relationships between the thickness of a gouge layer and the weakening behavior remains unclear. Our results reveal that formation of a very thin, h = ~0.1mm-thick gouge layer suppresses the efficiency of flash heating at this normal stress and slip rate condition. Slip velocity of v = 100 mm/s, which is an order of magnitude greater than the critical weakening velocity required for the thin gouge sample is needed for the thick gouge layer to cause high-velocity weakening. It is suggested that formation of just only a thin gouge layer on fault surface may have a stabilizing effect on fault slip, which otherwise resulted in significant weakening at high slip velocities.

Experimental study on fault weakening due to shear-induced pore pressure increase along a fault in shallow portion of accretionary prism

Keigo Tashiro[1], Akito Tsutsumi[1], Chao Huang[2], Chengrui Chang[2], Yuzuru Yamamoto[3], and Gonghui Wang[2]

[1]Graduate School of Science, Kyoto University, [2]DPRI, Kyoto University, [3]Graduate School of Science, Kobe University

The behavior of seismic slip in faults is essentially a process of fault strength weakening associated with slip. In order to elucidate the characteristics of strength weakening of the fault that develop in the shallow part of the accretionary body, we conducted large displacement shear tests under different drainage conditions. We used materials collected from the accretionary complex distributed in the Miura and Boso Peninsulas. The Miura-Boso accretionary complex is suitable for our experiments since the initial deformation of the accretionary body in the shallow part of the subduction zone is preserved due to its shallow burial depth (Yamamoto et al., 2005). In the faults that develop within this accretionary body, injection structure of fault gouge material into the hanging wall strata has been observed, which has been noted as evidence of high pore pressure generation during deformation (Yamamoto et al., 2005; Yamamoto, 2006). The process of pore water pressure increase during deformation in fault zones leads to a reduction in fault strength due to a decrease in effective stress. Therefore, understanding the mechanism of liquefaction is crucial for understanding the mechanism of fault strength weakening during earthquakes. The Misaki Formation in the Miura Peninsula is characterized by alternating layers of scoria sandstone and semi-pelagic siltstone. In our shear experiment, we used semi-pelagic siltstone as the sample. We utilized the large ring shear apparatus at the Disaster Prevention Research Institute, Kyoto University (Sassa et al., 2004; Agung et al., 2004) for the experiments. This apparatus allows shear tests under undrained conditions by applying a constant increase in shear stress. This enables the simulation of the entire rupture process, from the increase in pore water pressure under shear stress, reaching the rupture line, to the decrease in shear strength, and finally to steady-state slip. In this study, experiments were conducted by keeping the effective vertical stress constant in drained experiments and by controlling the discharge of water in undrained experiments. This allowed us to perform experiments that caused mechanical liquefaction and those that did not. Collected samples had weathered portions removed, were dried at 60°C for 24 hours, and were then crushed and sieved using a 150 mesh. Both the upper and lower sides of the sheared sections filled with semi-pelagic siltstone were filled with No. 8 silica sand. In both experiments, before starting the shear, the pore space (air) in the sample was replaced with carbon dioxide, then filled with water, and consolidated at 500 kPa for one day. After consolidation, the shear stress was increased at a rate of 0.1 kPa/sec. The undrained experiment was conducted twice with varying particle sizes.

The shear stress reached the rupture line at 251.8 kPa in the first undrained experiment, 209.4 kPa in the second, and 368.8 kPa in the drained experiment. In all three experiments, peak strength follows a same line connecting the rupture peak and the origin, indicating that the fault material's failure line are the same. In the undrained experiment, the effective stress decreases to approximately 325 kPa in the first trial and approximately 304 kPa in the second due to the increase in pore water pressure during the process of reaching the rupture line. After reaching the rupture line, macroscopic rotation (slip) begins, and pore water pressure rapidly increases. In the first undrained experiment, it increases to about 350 kPa, and in the second, it reaches about 360 kPa, becoming steady, while the shear stress decreases to about 40 kPa in the first trial and about 48 kPa in the second. Thus, due to the increase in pore pressure caused by shear slip, the fault strength was reduced by approximately 84% in the first trial and approximately 77% in the second, resulting in mechanical liquefaction. Comparing the decrease in shear stress with respect to slip displacement in both experiments, in the undrained experiment, with the help of increased pore water pressure, the decrease is rapid, with shear stress decreasing to a steady value after 100–200 mm of slip. In the drained experiment, since the shear stress reduction depends only on the nature of the fault material, it takes about 450 mm of slip to settle at a steady shear stress. It is assumed that natural faults may exhibit behavior in between these two cases. In the undrained experiment, a strong correlation was observed between the increase in pore water pressure and the reduction in shear stress. Furthermore, a correlation was seen between the reduction in vertical fault width and the increase in pore water pressure, suggesting that the reduction in fault width might influence the increase in pore water pressure. In the presentation, we will report on the structural differences observed in the particle arrangement.

The role of backthrust in the development of the Coulomb wedge from sandbox experiments

Satoshi Tonai[1], Motoharu Tsuboi[1], and Takami Tachibana[1]

[1]Kochi Univ.

Some shallow slow earthquakes observed at plate boundaries are thought to occur within the subduction wedge (e.g., Ito and Obara, 2006). Therefore, it is important to understand the deformation processes that occur inside the tip of the wedge to establish the mechanism of shallow slow earthquakes. In this study, we constructed a Coulomb wedge in a sandbox experiment and analyzed images of the developed wedge using digital image correlation (DIC). In particular, we traced the transitions of the backthrust and frontal thrust (FT), measuring the load to investigate the contribution of the backthrust to deformation of the wedge.

The experimental method was as follows. An adhesive sheet was placed inside an acrylic box with a load cell and an actuator. A 16-mm-thick layer of Toyoura sand covered the bottom of the box, and a camera was placed next to the sand layer. The actuator was pulled over a distance of 250 mm at a velocity of 0.4 mm/s to create a wedge. Based on the scaling law of the strength properties of the sample, the scale of the experiments relative to a natural subduction wedge is about 1/50,000. Up to 500 images were obtained at an interval of 1 image every 0.4 mm of sheet movement over a displacement of 50–250 mm. The snapshot interval of 0.4 mm corresponds to 500 years of real subduction, considering a natural plate convergence rate of 40 mm/year. The obtained images were imported into a PC and analyzed using DIC. The linear region with a principal strain of >1.0% and located close to the fixed wall was identified as the backthrust, and the distance from the intersection of the backthrust and FT to the fixed wall was measured. Results were compared with load data to investigate the correlation between the location of the backthrust and the load.

Our experiments reveal that the backthrust is repeatedly displaced between two main positions during the displacement of a single FT. Just before a new FT is formed and the load shows a single peak, the backthrust develops in front of the wedge, and the wedge is uplifted only in the front part between the FT and the backthrust. The backthrust then slowly recedes and subsequently abruptly moves near the fixed wall. After that, the position of the backthrust also moves within a certain width, forming a strain zone that is termed the “backstrain zone” (BSZ). Furthermore, the rate of increase in load tends to decrease just before the backthrust moves forward, although this change in rate is not always well defined. Overall, our results indicate that the displacement of the backthrust contributes substantially to intra-wedge deformation and that the deformation is not localized but occurs over a wide area.
In the future, we plan to further develop the DIC analysis, conduct experiments on sand layers with different initial conditions, and compare the results with natural deformation events such as shallow slow slip.

Objective clustering of GNSS velocities based on parallel translation and rotational motion for the identification of crustal blocks

Keisuke Yano[1], Atsushi Takahashi[2], Masayuki Kano[3]

1: The Institute of Statistical Mathematics;

2: RIKEN, Center for Advance Intelligence Project;

3: Tohoku University

Introduction

Dense Global Navigation Satellite System (GNSS) observation data have provided clearer pictures of plate motions. For instance, Thatcher (2007, 2009) identified more crustal blocks than previously known using GNSS observation data. Identifying these crustal blocks is important and has been utilized in earthquake disaster prevention assessments (e.g., Syu et al., 2016). As is widely recognized, the selection of crustal blocks heavily impacts on the results of block fault models (e.g., McCaffrey, 2007; Wallace et al., 2007; Floyd et al., 2010). Recently, objective methods for identifying crustal block structures have been proposed. Simpson et al. (2012), Savage and Simpson (2013a, 2013b), and Takahashi et al. (2018) used hierarchical clustering in the GNSS velocity vector space to identify crustal blocks in the San Francisco Bay, Mojave Desert, and Taiwan, respectively. Savage and Wells (2015), Savage (2018), and Takahashi and Hashimoto (2022) utilized non-hierarchical clustering with estimating Euler vectors to identify crustal blocks in the Pacific Northwest, Southwest Japan, and New Zealand, respectively. Clustering in the velocity vector space does not necessarily take rigid motions into account. On the contrary, clustering with Euler vectors is challenging to arrange hierarchically, and does not always consider the adjacency of observation sites. This study aims to address these issues by integrating both approaches and proposes a new identification method.

Data and Method

The proposed method utilizes the rotational motion by Euler vectors and the parallel translation of tangent vectors. First, using the GNSS position coordinates r_P, r_Q of two points P,Q and their velocity vectors v_P, v_Q, we estimate the Euler vector. We write this estimate by $\widehat{\omega}_{PQ}$. On the bases of fit of $\widehat{\omega}_{PQ}$, we define the dissimilarity between the velocity vectors at P,Q as:

$$d_{EV}(P,Q) \coloneqq \sqrt{||v_p - r_P \times \widehat{\omega}_{PQ}||^2 + ||v_Q - r_Q \times \widehat{\omega}_{QP}||^2}.$$

On the other hand, the differential geometry introduces ``parallel translation'' $\Pi_{\gamma(P,Q)}$ that maps a tangent vector at a point to a tangent vector at a different point. This allows us to define the dissimilarity between the velocity vectors of geographically separated points P and Q as:

$$d_{PT}(P,Q) \coloneqq ||v_P - \Pi_{\gamma(P,Q)} v_Q||.$$

Here, the concept of "parallel translation" enables us to explain the clustering in the velocity vector space proposed in previous studies. By using the sum of the two dissimilarities, we propose hierarchical clustering of GNSS velocity vectors that considers both parallel translation and rigid motion.

We checked our method by using the ITRF2008 plate model and the public data provided by Altamimi et al. (2012).

<u>Results</u>

Using the proposed hierarchical clustering method, we confirmed that the known plates are reconstructed without any reference other than velocity vectors and positional information. The reconstructed plates can be broadly categorized into North America and a group comprising Eurasia and Australia. Notably, within the latter group, several sub-blocks (Eurasia, India, Australia) were identified, providing an intuitive representation of the similarity in plate motions.

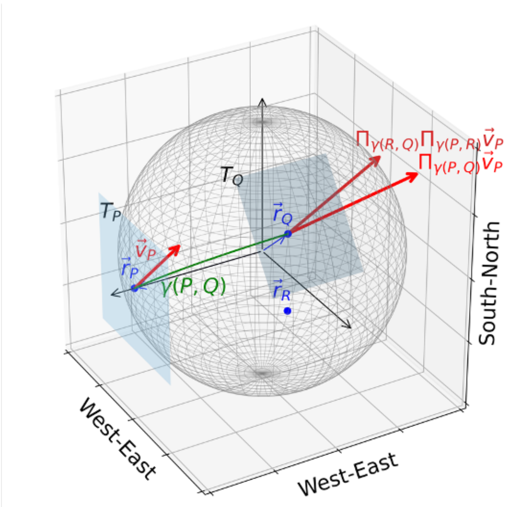

Figure 1：Result of parallel translation of a velocity vector v_P at a position r_P along the geodesic $\gamma(P,Q)$.

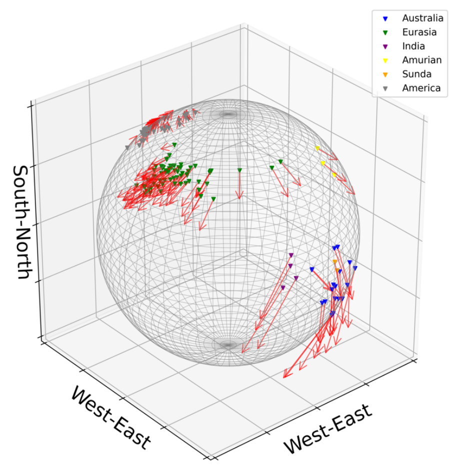

Figure 2: Public data used from Altamimi et al. (2012). Known plates are displayed with color.

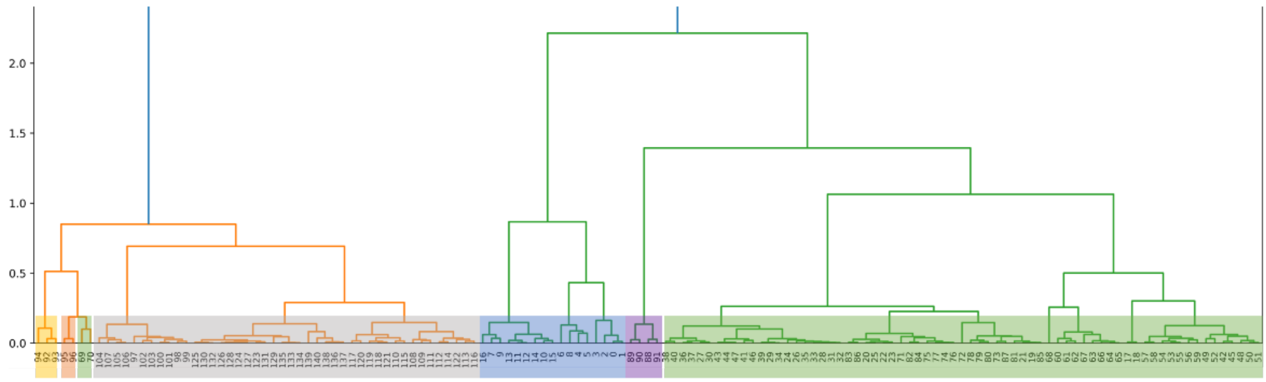

Figure 3: Results of agglomerative hierarchical clustering. Observation sites within the same known plate are displayed in the same color.

Examination of TEC anomalies in the ionosphere before large earthquakes

Kai Koyama[1], Yoshihiro Kaneko[1]

1. Graduate School of Science, Kyoto Univ.

Since the 2011 Mw9.0 Tohoku earthquake, the possibility of short-term earthquake forecasting based on total electron content (TEC) ionospheric monitoring of the Global Navigation Satellite System (GNSS) has been suggested by Heki (2011) and others. Heki (2011) reported that GNSS data for the 2011 Tohoku earthquake and other large earthquakes exhibit positive TEC anomalies 10 to 80 minutes before the earthquake origin times. In contrast, other studies (e.g., Eisenbeis and Occhipinti, 2021) argued that the positive TEC anomalies reported by Heki (2011) and others are artificial signals arising from their data analysis methods. In this study, we re-examine the presence of "pre-seismic TEC anomaly" before the Tohoku earthquake by comparing not only data from a limited number of stations shown by Heki (2011), but also data from many other GNSS station-satellite pairs. To remove noise specific to each station, we apply the stacking of the TEC data over a large area according to the latitude and longitude. We find that the time of the appearance of pre-seismic signals pointed out by Heki (2011) was earlier in the northeast (Hokkaido) region and later in the southwest (Kyushu) region. This suggests that the ‘pre-seismic anomaly’ did not spread outward from the epicentral region of the Tohoku earthquake and was likely unrelated to the earthquake itself. We present our ongoing efforts toward examining pre-seismic TEC signals for other large earthquakes worldwide.

"Giant" rock friction apparatus for understanding faulting processes on multi-spatio-temporal scales: A preliminary report

Futoshi Yamashita[1], Eiichi Fukuyama[2,1], Kurama Okubo[1], and Sumire Maeda[1]

[1]NIED, [2]Kyoto Univ.

Given that fault slip is a fundamental cause of earthquakes, a laboratory experiment that simulates the faulting process is one of the best ways to comprehensively understand the mechanisms of earthquakes and associated phenomena. It should be noted, however, that a big scale gap between the laboratory and nature can prevent us from properly understanding the natural phenomena. For example, some studies have revealed that there exists a spatial scale dependence of rock friction (e.g. Yamashita et al., 2015; Noda 2023); the dependence is caused by a stress heterogeneity on the fault resulting from self-evolved wear/heat heterogeneities in large-scale experiments, which is negligible on a small-scale laboratory fault. The large-scale experiments also showed that topographic heterogeneity on the fault can increase the fault strength and cause complicated faulting processes (Xu et al., 2023). Therefore, it is important to investigate how such heterogeneity peculiar to the large-scale fault area affects the whole faulting process, and then figure out how to extrapolate the knowledge obtained in the laboratory to natural phenomena. We considered that a larger scale experiment is essential for such an investigation, and then developed a new giant-scale rock friction apparatus.

Two rock specimens used for the giant-scale friction experiment are made from metagabbro blocks collected in India. The dimensions of the shorter one are 6.0 m long, 0.5 m wide, and 0.75m high, and those of the longer one are 7.5 m long, 0.5 m wide, and 0.75m high. The shorter one is stacked vertically on top of the longer one. Therefore, the contacting area, which is treated as a simulated fault, is 6.0 m long and 0.5 m wide. The contacting surfaces of the specimens have been polished so that the undulation over each surface is less than 50 µm. The normal load to the simulated fault is applied by six hydraulic jacks installed at the top of the upper specimen. The normal load applied by each jack is a maximum of 2 MN, and thus the maximum normal pressure on the fault area is an average of 4 MPa. The applied loads were measured individually with load cells connected in series to each jack, and then the amount of each load can be configured individually. The load to shear the simulated fault is applied to the side face of the lower specimen by a hydraulic jack capable of applying a maximum of 12 MN. The loading rate is controlled between 0.01 mm/s and 1 mm/s, and the simulated fault can be sheared up to 1 m in total. We conducted a preliminary experiment under the normal stress of 1 MPa with a constant loading rate of 0.01 mm/s. We observed many stick-slip events, and then roughly estimated the system stiffness as 2.7±0.2 GN/m from the amount of force drop and slip distance associated with each stick-slip event. We will investigate the spatio-temporal evolution of the fault slip associated with each stick-slip event in detail using dense measurement arrays of strain gauges and acoustic sensors, and its transition with the accumulated slip distance.

Two types of foreshocks generated by an artificial gouge patch on a 4-m-long laboratory fault

Kurama Okubo[1], Futoshi Yamashita[1], Eiichi Fukuyama[2, 1]

[1]NIED, [2] Graduate School of Engineering, Kyoto University

The generation of laboratory foreshocks can be enhanced due to the heterogeneities formed by fault gouges (Yamashita et al., 2021). Their source mechanisms are of great interest to be associated with the evolution of preslip towards the nucleation of dynamic ruptures. The source parameters such as location, slip, and stress state are crucial to address the source mechanisms, whereas the validation of them is challenging on the heterogeneous fault naturally formed during the stick-slip experiments. Therefore, we artificially set the circular gauge patches on the simulated fault of the 4-meter-long biaxial rock friction apparatus, which has been smoothed due to the iteration of stick-slip experiments, to validate the estimated source parameters with known characteristics of rupture patches, and to identify the source mechanisms of foreshocks.

We set the gouge patches with a diameter of 8mm along the simulated fault. The gouge is made by pulverizing metagabbro, the same as the host rock specimens. The median particle diameter is 8.2μm, and we put the patches using a sieve of 100μm and a circle ruler. We conducted the stick-slip experiment with the normal stress of 2MPa. We independently measured the stress state on the gauge patch using pressure measurement films (Prescale, FUJIFILM), showing the mean stress increased to 4MPa with the background stress of 2MPa.

The two types of foreshocks are generated around the preset gouge patches; one is the ordinal foreshocks showing clear P wave pulses with a corner frequency of ~300kHz. Another comprises prominent low-frequency components without the P and S pulses. The latter might be in analogy to low-frequency earthquakes, whereas we need to be careful with the frequency responses of the AE sensors to quantify the events and to investigate if the scaling is equivalent to natural earthquakes.

We used the AE sensors (V103-RM, Olympus) with a diameter of 13mm and a natural frequency of 1MHz. We calibrated the gain and frequency responses using the poles and zeros estimated with a laser Doppler vibrometer and the ball-drop test (Okubo et al., 2022AGU). We discerned the low-frequency events as the signal-to-noise is high enough for the detection, the moveout of the waveform is consistent, and the source location is most likely near the gouge patch. The dominant frequency of the raw waveform is around 30kHz, with which the AE sensor is sensitive (Wu and McLaskey 2018). As the lower limit of the frequency range in the sensor calibration is around 80kHz, the quantitative analysis of the low-frequency events remains to be performed. In this study, we focus on a given stick-slip event and foreshocks to evaluate the characteristics of those different types of foreshocks.

Both the ordinary and low-frequency foreshocks were preceded by the arrival of the preslip on the fault with a rupture velocity of 200m/s. The ordinary foreshock is generated with a time delay after the passage of the rupture, while the low-frequency event is observed just after the arrival of ruptures. It should be noted the ordinal foreshocks also contain the low-frequency components although their power spectrum is lower than the low-frequency events. The amplitude of waveforms is much larger with the low-frequency events, which would indicate the slip is caused in the surroundings of the gouge patch as well as on the patch similar to the model proposed by Das and Kostrov (1986). We further discuss the critical nucleation size of the gouge patches, which would be correlated to the pattern of the generation of foreshocks. This study contributes to linking the source properties estimated from the observations to the source mechanics of the slip events associated with various spectra.

Structural features revealed by multi-year seismic survey campaign and implication to seismic activities in the Nankai Trough

Kazuya Shiraishi[1], Yasuyuki Nakamura[1], Ryuta Arai[1], Gou Fujie[1],
Shuichi Kodaira[1], Gaku Kimura[1], and Paul Flores[1]

[1]JAMSTEC

To investigate detailed geological structures and their relationship with spatial variation of the earthquake activity, we are conducting multi-year seismic survey campaign, approximately a month every year, in the Nankai Trough. From 2018 to 2021, the multi-channel seismic surveys were conducted in the area from off the Kii Peninsula to the Hyuga-nada, and from 2022, the surveys are being continued from the southeast offshore of the Kii Peninsula to the off Tokai region. The dense 2D seismic data acquired at intervals of 4 km or 8 km between survey lines, including reprocessed legacy seismic data, reveal detailed structural features on the topographic relief of the subducting oceanic crust and heterogeneous structures within the overlying sediments. In this presentation, we show comparisons of typical seismic sections and the top of the oceanic crust in the southwest off the Kii Peninsula and off the Cape Ashizuri to Hyuga-nada using the dense 2D seismic data, and also off Kumano using a legacy 3D seismic dataset. We observed lateral variation of structural features and their spatial correlation with the activities of very low frequency earthquakes (VLFEs) and low frequency tremors.
Furthermore, we attempted to quantify the structural features in the southwest offshore of the Kii Peninsula. We have quantified the roughness of the top of the oceanic crust and the decollement surface, the thickness of subducted sediments beneath the decollement and overburden sediments of the accretionary prism, and the reflection characteristics on the decollement surface. We observed clear lateral variation of the topography on the oceanic crust with significant NNW-SSE trending depression and several local topographic highs; the middle part is smoother than the west and east parts. Also, the decollement surface is generally smoother than the oceanic crust surface. Comparing them with the distributions of VLFEs and tremors, which are observed so far with a spatial gap of the activity, we confirmed that there is a good correlation between the east-west variation of the structural features and the distribution of the seismic activity. The topographic roughness and underthrust sediment thickness may suggest that the Shikoku basin sediments filled the rift basin sufficiently thick before subduction to smoothen the potential decollement surface in the middle part, and thinly covered the topographically high part where the rough surfaces remain on both the oceanic crust and decollement in the present. The overburden sediment thickness and reflection characteristics imply the change of physical property and stress condition along the decollement. Thus, these structural features are possible major factors related to the activity of the slow and fast earthquakes. As a future study, combination of the quantified structural features, including other geological and geophysical factors undefined at this point, could be a quantitative index of spatial variation of seismic activities.

Frictional properties of the imbricate thrust material from the shallow part of the Miura accretionary prism, Southern Miura Peninsula, central Japan

Yuki Kasai[1], Akito Tsutsumi[1], Yuzuru Yamamoto[2]

[1]Graduate School of Science, Kyoto University, [2]Graduate School of Science, Kobe University

Fault material had been considered to have positive velocity dependence of friction under 10 km depth (Scholz, 1998). However, very low frequency earthquakes and low frequency tremor detected within shallow accretionary prism suggest that unstable slip occurs at shallow part of faults. The source faults of VLF are considered to be mega splay faults and out of sequence thrusts (OST) (Ito and Obara, 2006a). In this research, we focused on the Sengen thrust located in Southern Miura peninsula, central Japan. The Sengen thrust cuts accretionary prism named Misaki formation (Yamamoto et al., 2005). The Sengen thrust and OST have common characteristics that it branches from decollement of offscraped accretionary prism. In this research, we conducted microscopic observation, XRD analysis and frictional test of the fault samples for the purpose of investigating the structure, frictional properties and slip history of the Sengen thrust. In order to estimate parameters of the rate- and state-dependent friction law, we conducted velocity step friction test on the samples saturated with distilled water at a normal stress of 5 MPa with 0 MPa pore pressure within a range of slip velocities from few μm/s to several tens of μm/s. This velocity range is close to the lower limit of presumed slip velocity range of VLF observed at the Nankai subduction zone (50 μm/s–2 mm/s, Ito and Obara, 2006b).

We classified the fault rock of the Sengen thrust into fault gouge, fault breccia in hanging wall side and shear band zone in foot wall side. This classification is same as described in Yamamoto et al. (2005). The fault gouge is black colored and about 2 cm thick. Orientation of clay mineral and the long axis array of colorless minerals were found to be subparallel to the fault plane in fault gouge. The size of the clasts in fault breccia increases with the distance from fault gouge. The shear band zone was distinguished from host rock according to the intense and random cracks. The XRD analysis of gouge indicates that gouge contains smectite and illite.

It is revealed that the fault gouge sample exhibits positive velocity dependence of friction, and fault breccia and host rock exhibit negative velocity dependence of friction. The steady friction coefficient μ is measured to be in the range of 0.57-0.59 for gouge, 0.53-0.54 for fault breccia and 0.61-0.64 for host rock sample. The value of d_c of the fault rock is markedly different from the value of the host rock. The value d_c is 4.8 μm in host rock and about 20 μm in fault gouge. It is considered that the fault slip was inhibited in the velocity range of few μm/s to tens of μm/s if the deformation was localized into fault gouge. To examine the possibility that the slip velocity of the Sengen thrust reached the velocity range, we have to conduct friction test in lower velocity range. More detailed mineral analysis also needed to consider the difference of frictional properties of each sample.

References

Scholz, C. H (1998), *Nature* 391, 37-42, doi:10.1038/34097.

Ito, Y. and Obara, K., 2006a, Geophys. Res. Lett., 33, L02311, doi:10.1029/2005GL025270.

Yammoto Y., et al., 2005, Tectonics, 24(5), doi:10.1029/2005TC001823.

Ito, Y. and Obara, K., 2006b, Geophys. Res. Lett., 33(9), doi:10.1029/2006GL025883.

Origin of serpentinite in the Cretaceous Shimanto accretionary complex

Yusuke Shimura[1], Shunsuke Endo[2], Yoshihiro Asahara[3]

[1]Geological Survey of Japan, AIST, [2]Shimane University, [3]Nagoya University

Serpentinites in accretionary and high-*P* metamorphic complexes are classified into two types: those derived from oceanic lithosphere and those derived from mantle wedge. The former type is formed at a slow-spreading-ridge, where an oceanic crust may not be produced continuously and the lithospheric mantle is exposed on the seafloor. On the other hand, the latter type is formed at a forearc mantle wedge, where serpentinization proceeds by hydrous fluids supplied from a subducted oceanic slab.

The Cretaceous subduction zone in the eastern Asian continental margin had formed the Shimanto accretionary and Sanbagawa high-*P* metamorphic complexes in the shallow and deep parts, respectively. This subduction zone is characterized by a warm subduction environment, and thus, the two complexes are considered to be an analog for the Nankai subduction zone. Aoya et al. (*Geology*, 2013) proposed a mantle-wedge origin of the Sanbagawa serpentinites, based on their limited occurrences in the high-grade parts ($T \geqq 425$–470 °C; $P \geqq 8.0$–9.5 GPa), which correspond to depths greater than the crust–mantle boundary (30–35 km) or deeper, and therefore, proposed a mantle-wedge origin. However, in exceptional cases, the serpentinites are locally recognized in the shallower Sanbagawa metamorphic complex (Soda and Takagi, *Geol. Soc. Jpn.*, 2004) and the Shimanto accretionary complex (Takeuchi, *Bull. Geol. Surv. Jpn.*, 1996), and their origins are poorly understood. To address this issue, we conducted field and geochemical studies for the serpentinite enclosed in the Mugitani Formation of the Shimanto accretionary complex in the Kii Peninsula.

The Mugitani Formation in this study area is composed of dismembered beds of sandstone and pelitic phyllite along with mélange comprising sandstone, chert, and basalt blocks in a pelitic matrix, and is intruded by serpentinite. The serpentinite is locally foliated, and the foliation is subparallel to the main schistosity in the Mugitani Formation. The serpentinite consists of lizardite, talc, magnesite, and Cr-spinel without magnetite. Chemical compositions for Cr-spinel in the serpentinite are TiO_2 of <0.3 wt%, Cr/(Cr + Al) ratio of ~0.30–0.55, and Fe^{3+}/(Al + Cr + Fe^{3+}) ratio of <0.04, and these characteristics are similar to those originated from oceanic lithosphere. Along the contact boundary, the serpentinite and the host rocks in the Mugitani Formation are affected by metasomatism, and the serpentinite is altered to talc rock. Whole-rock geochemistry for the basalt and metasomatized basalt is characterized by REE patterns with flat middle to heavy REEs and a depletion in light REEs, which are typical of N-MORB.

In a subduction zone, the pre-subducting oceanic lithosphere bends and forms outer-rise faults, and the upper part of lithospheric mantle is serpentinized by seawater percolation through these faults (Ranero et al., *Nature*, 2003; Fujie et al., *Geophys. Res. Lett.*, 2013). Our field and geochemical constraints show that the serpentinite intruded after the mélange formation but before the peak metamorphism of the Mugitani Formation, and originated from the oceanic lithosphere rather than the mantle wedge. We therefore suggest that the studied serpentinite was upwelled from the slab mantle along the fossil outer-rise faults and across the plate boundary, and then intruded into the accretionary complex in the subduction zone.

Spatiotemporal evolution of Slow Slip Events along the Southern Ryukyu subduction zone during 2017-2022

Hiromu Sakaue[1], and Yoshiyuki Tanaka[1]

[1]Dept. EPS, Univ. Tokyo

Slow slip events (SSEs) are transient aseismic fault slip events, which are identified in the plate subduction zones along the Pacific Rim by Global Navigation Satellite System (GNSS) over the past two decades (e.g., Hirose et al. 1999; Dragart et al., 2001; Lowry et al., 2001; Douglas et al., 2005). SSEs with a moment magnitude (Mw) ranges of 6.6 to 6.7, with durations of ~1–2 months have been observed at an interval of approximately 6 months beneath the Yaeyama Islands along the southern Ryukyu subduction zone in the most southwestern part of Japan (e.g., Heki and Kataoka, 2008, Kano et al., 2018). The plate convergence rate beneath the Yaeyama Islands is 12–13 cm/year, consisting of the subduction of the Philippine sea plate northwestward at a rate of 8.0–8.5 cm/year (Sella et al., 2002) beneath the Ryukyu Arc and the southward back-arc spreading at a rate of 3.5–5.0 cm/year (Nishimura et al., 2004) along the Okinawa trough (Sibuet et al., 1998).
We use the daily coordinates at GNSS stations around the Yaeyama Islands, for the period from 2017 to 2022. These stations consist of 8 GEONET stations operated by GSI and 10 stations operated by Kyoto University and Kyushu University. The daily coordinates are analyzed by Prof. T. Nishimura of Disaster Prevention Research Institute, Kyoto University. We apply a modified Network Inversion Filter (Fukuda et al., 2008) to estimate daily slip and slip rate on the plate interface. The geometry of the upper surface of the Philippine Sea plate is given by Hayes et al. (2012).
Our results show 10 SSEs occurred for the period from May to July 2017, December 2017 to January 2018, August to October 2018, January to March 2019, July to September 2019, January to March 2020, August to October 2020, March to April 2021, September to November 2021, and June to August 2022, respectively. Total slip and moment magnitude are estimated to be ~6.0-11.3 cm and ~6.4-6.7, respectively. The spatial distribution of slip is quite similar, and the peak of slip located ~30 km Northwest of Iriomote Island at a depth of 50 km. We will present the spatiotemporal evolution of slip and slip rate during the 10 SSEs varies from event to event.

Acknowledgments
This research was supported by the JSPS KAKENHI grant JP16H06474 in Scientific Research on Innovative Areas “Science of Slow Earthquakes”; JP20J20413 in Grant-in-Aid for Transformative Research Areas (A) “Science of Slow-to-Fast Earthquakes”; 21340127 in Grant-in-Aid for Scientific Research (B); and the Ministry of Education, Culture, Sports, Science and Technology (MEXT) of Japan, under its Earthquake and Volcano Hazards Observation and Research Program.

Centroid moment tensor analysis for M6-class offshore earthquakes using long-period seismograms of the Seafloor Observation Network for Earthquakes and Tsunamis along the Japan Trench (S-net)

Lina Yamaya[1], Hisahiko Kubo[1], Katsuhiko Shiomi[1], and Shunsuke Takemura[2]

[1]NIED, [2]ERI, Univ. Tokyo

The Japan Trench subduction zone is one of the most active seismic regions in the world. In this region, the Seafloor Observation Network for Earthquakes and Tsunamis along the Japan Trench (S-net) has been operated since 2016. The use of offshore network data in addition to onshore network data increases the azimuthal coverage for offshore earthquakes and consequently has a potential to improve their spatial resolutions of hypocenter determination.
To conduct CMT analysis of long-period seismograms of S-net, we investigated the effect of 3-D heterogeneous seismic velocity structure. We calculated the synthetic. Waveforms using a 1-D seismic velocity structure model and compared those with a 3-D model (Koketsu et al., 2012). The synthetic waveforms for the 1-D model did not explain the data obtained from S-net even for long-period component. The result shows that the optimal 3-D seismic velocity structure model is necessary to analyze long-period seismograms in offshore regions, where thick oceanic sediments, seawater, and subducting oceanic plate exist.
We conducted CMT inversion for offshore earthquakes with magnitude (M) ~6 occurring at the Japan Trench subduction zone. We used acceleration waveforms filtered with 20–50 s from S-net and F-net. F-net is an onshore broadband seismograph network. We used the both of S-net and F-net to increase the azimuthal coverage for the target earthquakes. Green's functions were calculated assuming the 3-D seismic velocity structure. We used the simulation code provided by Maeda et al. (2017) to calculate the Green's functions. The CMT inversion was conducted at each grid for time and space.
We obtained the optimal CMT solutions with well-fitting waveform data with synthetics. For earthquakes that have thrust mechanisms, the centroid depths of the obtained CMT solutions are consistent with the depth of the plate interface. For earthquakes that occurred at the outer-rise region, the obtained centroid depths are concentrated at the top of the oceanic Moho. The combining use of the S-net and F-net stably provides better spatial resolutions of the centroid location determination than the only use of the S-net or F-net. Especially for the thrust earthquakes, the dip angles of the optimal CMT solutions are constrained better than those of the CMT solutions obtained from only using the F-net. The obtained CMT solutions will provide better information on earthquake source mechanisms and tectonic stress fields at the depth of the seismic zone.

On the network-MT surveys in the Kii Peninsula, southwestern Japan, aiming at obtaining deep 3-D electrical resistivity structure

Akira Watanabe[1], Makoto Uyeshima[1], Satoru Yamaguchi[2], Yoshiya Usui[1], Hideki Murakami[3], Tsutomu OGAWA[1], Naoto Oshiman[4], Ryokei Yoshimura[4], Koki Aizawa[5], Ichiro Shiozaki[6], Takafumi Kasaya[7]

[1]ERI, Univ. Tokyo, [2]Kobe Univ, Osaka City Univ, [3]Kochi Univ, [4]DPRI, Kyoto Univ., [5]SEVO, Kyushu Univ, [6]Tottori Univ, [7]JAMSTEC,

The Kii Peninsula in the forearc region of southwest Japan has distinct structural and tectonic features characterized by the subducting Philippine Sea slab, such as high seismicity in the crust, deep low-frequency tremors, high surface heat flow, and high-temperature hot springs. Therefore, in order to elucidate the mechanism of generating such tectonic features various geophysical surveys have been carried out on the Peninsula, including electromagnetic surveys. Some conventional MT surveys (NEDO 1994; Fuji-ta et al., 1997; Umeda et al., 2003; Kinoshita et al., 2018) and the Network-MT survey (Yamaguchi et al., 2009) have been performed. The Network-MT method (Uyeshima et al., 2001; Uyeshima, 2007) is characterized by employing a commercial telephone network to measure voltage differences with long dipole lengths ranging from 10 to several tens of kilometers. This method has three advantages; the first is wide spatial coverage (e.g., covering almost the entire Kii Peninsula), the second is a wide-period range, especially for the longer period (from 10 s to 50000 s), and the third is better quality data in terms of high S/N ratio and less susceptibility to static effects. Yamaguchi et al. (2009) deployed the Network-MT survey at 55 nets throughout the Kii Peninsula. One net consists of 3-5 channels with 4-6 electrodes, and we measured respective voltage differences at 10 s intervals for 50-400 days. Magnetic fields were also measured at three stations in the survey area. Using this data, Yamaguchi et al. (2009) showed a 2-D resistivity structure along a line crossing the central part of the Kii Peninsula. However, a 3-D model analysis is necessary to reveal the regional and deep structure of this region because the coastline and bathymetry are 3-D, and the strike of the igneous rocks (the Kumano acidic rocks) is not concordant with the direction of the subducting Philippine Sea slab.

Prior to determining the 3-D model, we re-analyzed the whole Network-MT data using the BIRRP code (Chave and Thomson, 2004) to yield the Network-MT response functions in the frequency domain (for the two-inputs (horizontal magnetic field) and one-output (electrical potential difference on each dipole) linear system). After careful selection of the good time series segments, we could successfully obtain sound and meaningful response functions. We confirmed that the spatial and period dependence is closely related to the spatial distribution of deep low-frequency tremors and the Philippine Sea plate subduction. We plan to obtain a deep and wide 3-D structure that successfully reproduces these response functions.

Expansion rates of aftershock zones for magnitude-7 class earthquakes around Japan possibly related to stress states

Yuta Mitsui[1], Yuya Utagawa[1], and Ayaka Miyamoto[1]

[1]Dept. Sci., Shizuoka Univ.

Earthquakes (mainshocks) trigger a series of aftershocks characterized by a power-law (Omori) decay. The aftershock zone logarithmically expands with time, and this expansion rate can be influenced by various factors, such as fault maturity, depth conditions, and local stress states. In this study, we assess the expansion rate of aftershock zones using a simplified isotropic model and investigate the controlling factors for magnitude-7 class earthquakes around the Japanese archipelago. Our findings reveal a negative correlation between the aftershock zone's expansion rate and the b-value of the aftershocks, indicating a positive correlation between aftershock expansion and the stress state following the mainshock. However, no significant results were observed regarding the effects of fault maturity or depth conditions. These results suggest that the expansion rate of aftershock zones primarily reflects the perturbed stress field resulting from the mainshock.

Ensemble estimation of seismic velocity and hypocenter in the Nankai Trough empowered by physics-informed neural network

Ryoichiro Agata[1], Kazuya Shiraishi[1], Gou Fujie[1]

[1]JAMSTEC

Hypocenter determination provides fundamental information for understanding the activities of slow and fast earthquakes. It is performed by solving a number of physical simulations of wave propagation (i.e., travel time calculation) to explore a solution that adequately explains the observations. Hypocenter determination is an ill-posed problem, and associated uncertainties are often quantified using Bayesian inversion. The subsurface velocity structure assumed in travel time calculation is often provided by active or passive seismic tomography. This tomographic information is also the output of ill-posed inverse analyses. Ignoring the uncertainties in the subsurface structure leads to over-fitting of the estimated model to the data and underestimation of uncertainties by not accounting for error propagation. One possible approach to address this problem is to quantify uncertainties in seismic velocity estimation, obtained as an ensemble velocity model using Bayesian inversion, for instance. Such an ensemble can be used as the multiple inputs of hypocenter determination, which allows for incorporating subsurface structure uncertainty in the estimation process (i.e., Bayesian multi-model inversion, Agata+2022JGR).

Recent advancements in deep learning techniques introduced new approaches to partial differential equations (PDEs) and PDE-based inverse problems. Among them, physics-informed neural networks (PINN) (Raissi+2019JCP) have been notably successful, by incorporating physical laws described by PDE in deep learning. Its mesh-free nature, flexibility, and scalability have drawn significant attention in various fields. It has also been successfully applied to both seismic tomography and hypocenter determination, including Bayesian inversion (e.g., Smith+2022GJI, Agata+2023IEEE-TGRS).

In the study, we aim to ensemble estimation of an earthquake's hypocenter and seismic velocity structures in a nearby active seismic survey line, using new techniques based on PINN as mentioned above. The target earthquake is the Mw 5.9 event that occurred on April 1, 2016, in the central part of the Nankai Trough region. Whether this earthquake occurred at the plate boundary was initially controversial. Subsequently, hypocenter determination with updated structural information and comparison with seismic reflection profile indicated that it occurred at the plate boundary. However, uncertainties in the structural models were not considered in both the hypocenter determination and the comparison. First, we use PINN-based Bayesian seismic refraction tomography to obtain an ensemble of velocity structures in the region. Hypocenter determination considering error propagation properly is then performed based on the velocity structure ensemble. We also consider uncertainty in seismic reflection profile when comparing it with the determined hypocenter location. These analyses demonstrate a novel approach to integrate estimation of subsurface structure and hypocenter using ensemble modeling, empowered by PINN.

Tectonic tremor distribution and migration at Kumano-nada: insights from ocean-bottom seismometer deployment between DONET1 and 2

Takeshi Akuhara[1], Yusuke Yamashita[2], Hiroko Sugioka[3], Atikul Haque Farazi[4], Shukei Ohyanagi[4], Yoshihiro Ito[2], Eiichiro Araki[5], Takashi Tonegawa[5], Takeshi Tsuji[6], Ryosuke Azuma[7], Ryota Hino[7], Kimihiro Mochizuki[1], Shunsuke Takemura[1], Tomoaki Yamada[1], and Masanao Shinohara[1]

[1]ERI, Univ. Tokyo, [2]DPRI, Kyoto Univ, [3]Graduate School of Science, Kobe Univ. [4]Dept. EPS, Kyoto Univ. [5]JAMSTEC, [6]School of Engineering, The Univ. of Tokyo, [7]RCPEVE, Tohoku Univ.

Accurate knowledge of tectonic tremor distribution is essential for better understanding the generation mechanisms of slow earthquakes. The Kumano-nada region, equipped with seafloor cabled seismometer networks (DONET1 and 2) and detailed subsurface structure models, provides a unique opportunity to study the structural factors influencing slow earthquake activities. To further augment this advantage, we deployed 15 ocean-bottom seismometers (OBSs) between DONET1 and 2 networks from September 2019 to June 2021 (Figure 1). During this observation period, an intense episode of slow earthquakes occurred on December 6th, 2020. The episode initiated beneath DONET1 network and migrated southwestwards to the middle of DONET1 and 2, where the OBSs were deployed. Akuhara et al. (2023, preprint in EarthArXiv) located tectonic tremors using data from these OBSs and DONET, employing on a Bayesian framework that allows formal estimates of the location uncertainty. The horizontal uncertainty (95% confidence interval) was found to be typically ±2–3 km.

This presentation provides a detailed distribution and migration pattern of tectonic tremors based on the tremor epicenters determined by the same Bayesian method. The tremors are primarily distributed in the trenchward side of the outer ridge, where the bathymetry is relatively flat, resulting in a source region with a nearly constant width along the dip direction. However, there is an exception at the eastern end, where the width narrows to about half. Interestingly, this region of tremor paucity coincides with the area of aftershocks from the 2004 off the Kii Peninsula earthquakes, which occurred within the Philippine Sea Plate. The cause of this coincidence, however, remains unresolved.

The tremors are clustered into three groups (Groups A–C in Figure 2), with Groups A and B separated by ~5 km and Groups B and C by ~10 km. Among those, no tremor activity has been identified within the region of Group B, at least since 2004. The tremor episode originated at the northeastern end of Group A, near the paleo Zenith Ridge and migrated southwestwards beyond the tremor gap to reach Group B. Notably, the migration speed appeared to increase when the migration front crossed the tremor gap. The southwestward migration continued to reach Group C, with a similar increase in migration speed observed at the tremor gap between Groups B and C. The acceleration at the tremor gaps may be attributed to the local heterogeneities on the plate interface, although the specific structural factors causing this phenomenon remain unknown. The integration of precise tremor epicenters and seismic reflection profiles in this region has the potential to elucidate the underlying cause in the future.

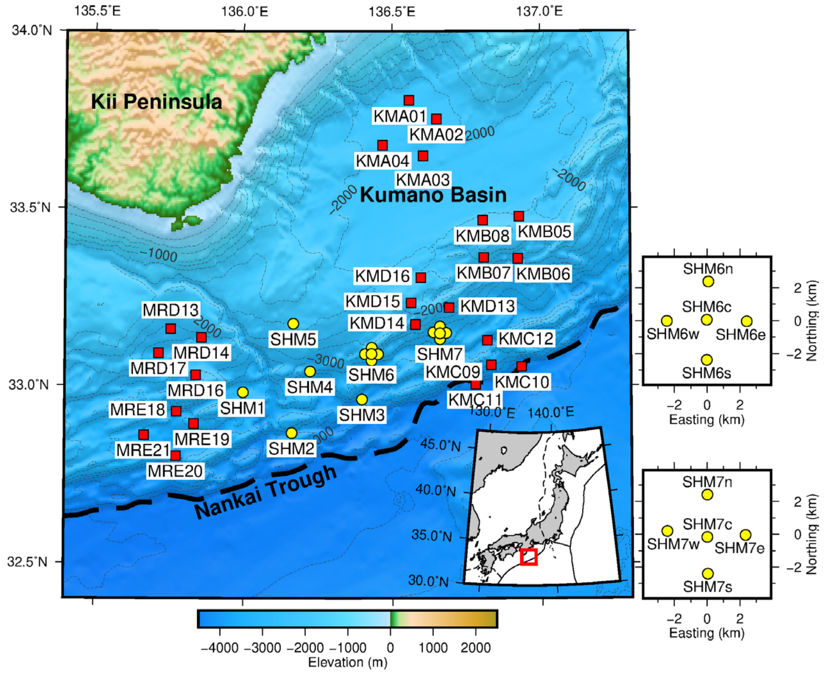

Figure 1. Station arrangement. The red squares are permanent DONET stations, and the yellow circles are temporary ocean-bottom seismometers (OBSs).

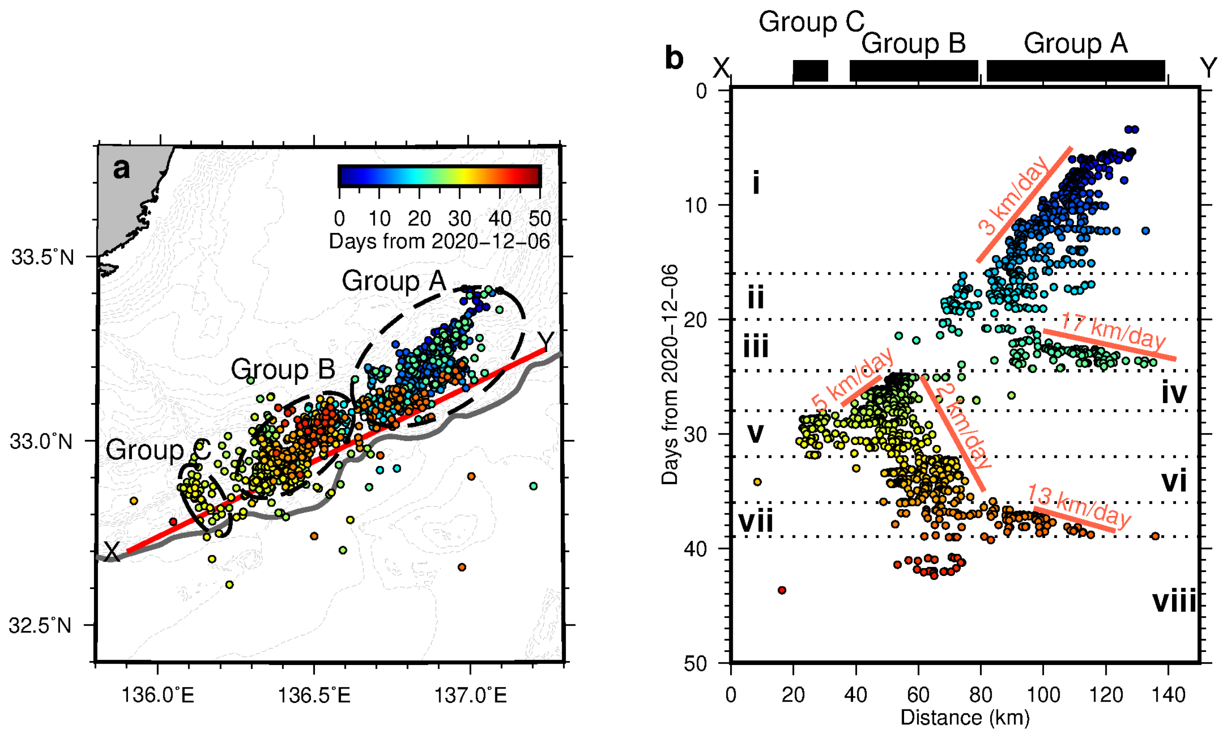

Figure 2. (a) Tectonic tremor distribution, with the color representing days of the study period. The gray line represents the deformation front. (b) Temporal evolution of tremors projected along the X–Y profile (red line in (a)). The color notation corresponds to that in (a). The red inclined lines delineate trench-parallel migration of tremors.

The characteristic of rupture propagation during earthquakes in Japanese crustal area

Ritsuya Shibata[1], and Naofumi Aso[1,2]

[1]Deptartment of Earth and Planetary Sciences, School of Science Tokyo Institute of Technology,
[2]Department of Applied Physics, Tokyo University of Science

During earthquakes, a shear rupture propagates along a finite fault, which radiates seismic waveforms. The shear-rupture propagation corresponds to the crack growth, which includes two rupture modes (Scholtz, 2019): the mode-II rupture and the mode-III rupture. The Griffith's theory (Griffith, 1920; 1924), where the rupture can propagate when the energy release rate exceeds the fracture energy, is the fundamental law for the crack growth. Therefore, the investigation of the rupture mode during earthquakes is important to understand the rupture propagation in the fracture mechanics considering the energy release rate depends on the rupture mode. To obtain the rupture mode at each spatio-temporal point, spatio-temporal information of the slip amount and the slip direction is required. In this regard, the slip-inversion images are useful to resolve this kind of the rupture characteristics.

In this study, we applied the waveform inversion with the radiation-corrected empirical Green's functions (Shibata et al., 2022) to the nine earthquakes in Japanese shallow crust with magnitude of 6–7, which provides the source processes involving the slip amounts and the slip directions. We also performed the bootstrapping test to investigate the robustness of the inversion results.

Then, we developed a method to extract rupture propagation directions from slip-inversion images. Specifically, we introduced the rupture propagation intensity as the angular function using a slip amount before and after a reference time at a reference location. In addition, to obtain the rupture mode at each point, we compared the direction of the largest rupture propagation intensity and the slip direction at every subfault at every 1 s, which allows us to discuss the rupture propagation stochastically. As a result, we could not confirm a significant preference of the rupture mode during the rupture propagation although several lateral-fault ruptures had more mode-II ruptures than mode-III ones.

Linking geometrical and physical property changes along Nankai Trough with slow earthquake activity using dense reflection survey

Paul Caesar M. Flores[1,2], Shuichi Kodaira[2,1], Gaku Kimura[2], Kazuya Shiraishi[2], Yasuyuki Nakamura[2], Gou Fujie[2], Tetsuo No[2], and Yuka Kaiho[2]

[1]Graduate School of Environment and Information Sciences, Yokohama National University, Yokohama, Japan, [2]Research Institute for Marine Geodynamics, Japan Agency for Marine-Earth Science and Technology, Yokohama, Japan

Very low frequency earthquakes (VLFEs) and tremors show a clustered distribution in the Nankai Trough. We examined the possible factors affecting the spatial distribution of slow earthquakes using a dense reflection survey covering 250 km x 100 km from off Tosa Bay to off Cape Shionomisaki with line intervals between 4 to 8 km. The decollement and oceanic crust horizons were tracked to map the thickness of the underthrust sediments. Taper angle was calculated by linear fitting of the seafloor and decollement. Decollement roughness was measured by the root mean square (RMS) of its height from a reference line that is parallel to the regression line and crossing the lowest point of the decollement horizon. The effective basal friction (μ_b) and pore pressure ratio (λ^*) were estimated using the critical taper theory. Empirical relationships between p-wave velocity, porosity, and effective mean stress were also used to calculate λ^*. Results showed high slow earthquake activity is associated with a rough decollement or a high standard deviation of the RMS (σ_{RMS} = 104 to 147 m) and variable thickness of the underthrust sediments, while a seismicity gap is observed in a smooth decollement (σ_{RMS} = 74 to 82 m). Decollement roughness is associated with multiple subducted seamounts off Muroto, and smaller scale bathymetric highs off Cape Shionomisaki. The high activity of VLFEs and tremors off Cape Muroto also aligns with a wide zone of low taper angle (3.8°), indicating low μ_b (0.1-0.4) and high λ^* (0.6-0.8). The λ^* calculated from p-wave velocity also shows an over pressured decollement off Muroto where the decollement shows a strong negative polarity reflection.

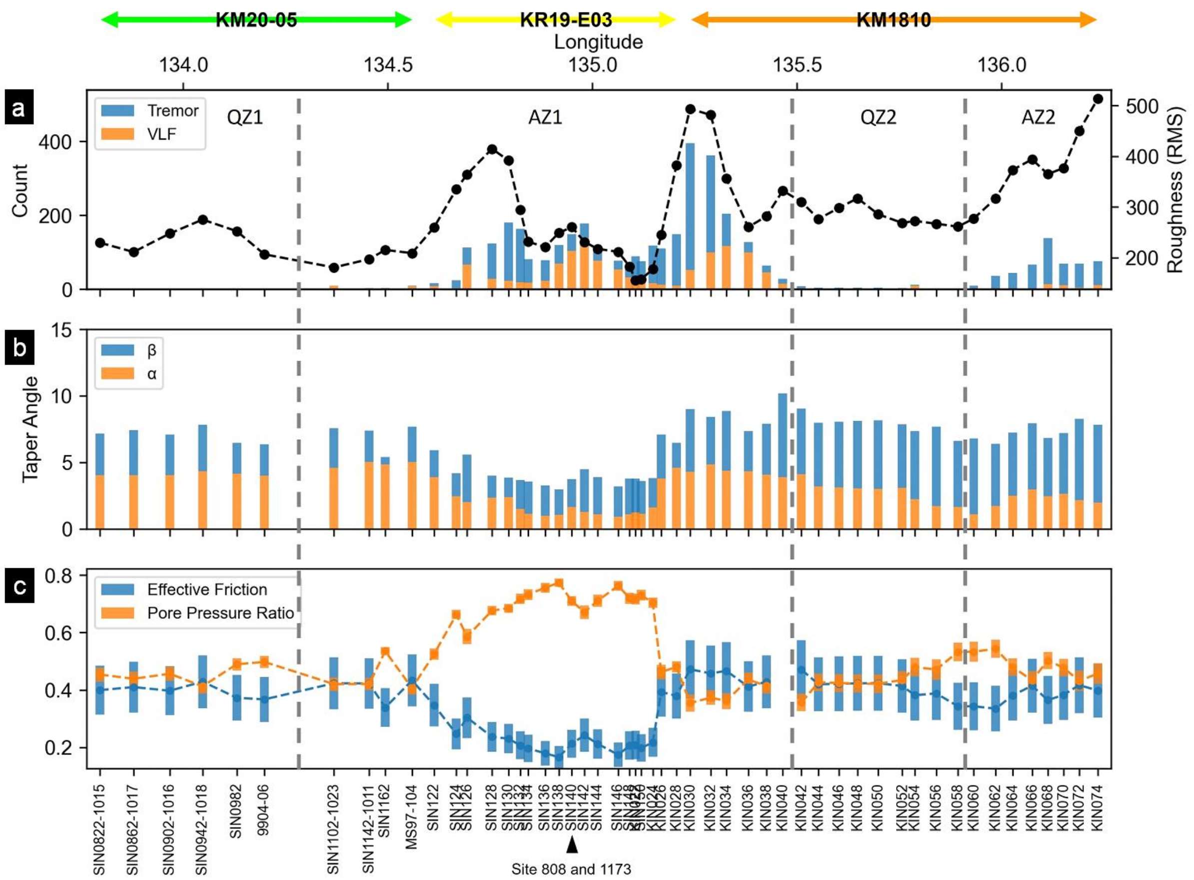

Figure 1. (a) The number of tremor and very low frequency earthquakes superimposed with the roughness of the decollement (black line). (b) The apparent seafloor slope (α) and basal slope (β) calculated from the seismic profiles. (c) The estimated effective basal friction (μ_b) and pore pressure ratio (λ^*) by applying the critical taper theory. The quiet (QZ) and active zones (AZ) are marked by the gray dashed vertical line.

Dynamic Rupture Simulation Reveals Fault Geometrical Effect on the 2023, Kahramanmaras and Ekinozu, Turkey, Earthquake Sequence

Ryosuke Ando[1], Ali Pinar[2], Doğan Kalafat[2], Haluk Ozener[2], Esref Yalcinkaya[3] and Yojiro Yamamoto[4]

[1]Dept EPS, Univ. Tokyo, [2]Bogazic Univ., [3]Istanbul Univ., [4]JAMSTEC

The 2023, M 7.8, Kahramanmaras earthquake (mainshock) occurred on February 6th, mainly along the plate interfaces called the East Anatolia fault ruptured toward NE (accommodating the motion between Anatolia and Arabia) and the Dead Sea Fault Zone ruptured toward SW (between Arabia and Africa). Followed in 9 hours, the M 7.6, Ekinozu earthquake (largest aftershock) was hosted by the subsidiary fault system called the Cardak – Surgu faults. This earthquake sequence presents significant complexity in fault geometry and rupture patterns. The observed hypocenter indicated that the mainshock rupture nucleated away from the East Anatolia fault (EAF) and was probably located on a subsidiary fault called the N-S striking Narli fault. The Narli fault is close to the area called Maras Tripple Junction (MTJ) where Anatolian, Arabian and African plates meet.

We performed a set of stress tensor inversions and dynamic rupture simulations. We used the FDP-BIEM developed by Ando, 2016, for the fully-dynamic rupture simulation. The 3-D fault geometry is built based on the previously compiled surface fault traces with constant dip angles. Based on the stress inversion using the aftershock focal mechanisms (M>4), we find that the maximum horizontal principal stress axis around the Cardak – Surgu faults is slightly rotated clockwise from that around EAF. The Narli fault and EAF are favorably oriented.

The simulation can reproduce a number of coseismic features determined by seismic and geodetic observations. Such features include 1) the rupture propagated from the Narli fault to EAF; 2) initially propagated towards the northeast on EAF, and eventually to the southwest; 3) the rupture to the south is posed at a bend (MTJ) before entering into the Dead Sea Fault zone (the Amanos Fault), further delaying the southwest rupture; 4) the possible super-shear on the Amanos Fault; 5) the locations of large slip areas determined by the SAR data. Moreover, the positive dynamic Coulomb stress change (~ 2MPa) is simulated in the middle of the Cardak Fault, while the Surgu Fault experienced the smaller amplitude. These characteristics are understandable as the primary effect of the fault geometry.

Acknowledgment: This work used computational resources of Earth Simulator provided by JAMSTEC through the HPCI System Research Project (Project ID: hp220105).

Advancements in Paleoseismology through Coastal Landforms and Coral Records in Subduction Zones

Junki Komori[1], Aron J. Meltzner[1,2], Noelynna T. Ramos[3]

[1]Earth Observatory of Singapore, Nanyang Technological University,

[2]Asian School of Environment, Nanyang Technological University,

[3]National Institute of Geological Sciences, University of the Philippines

Understanding the recurrence of great earthquakes carries significant implications for various fields, including disaster mitigation and earthquake physics. The recurrence interval of these seismic events often extends over centuries, necessitating the analysis of millennia of data to discern underlying patterns. Despite advancements in recent seismic observation, comprehensive understanding of these recurrence patterns remains challenging due to the limitation in timeframes of instrumental and historical observations. Consequently, geological datasets play an essential role in reconstructing long-term earthquake records.

Paleo-seismological investigations along subduction zones frequently focus on the coastal landforms and fossils, as the evidence of relative sea-level (RSL) changes. Holocene marine terraces, formed through abrupt uplift events, provide valuable insights including their formation ages and accumulated RSL changes since their formations. These data provided evaluations of recurrence of past megathrust earthquakes along global subduction zones. Additionally, coral growth records are known as RSL proxies in tropical regions. The elevational growth limits of coral microatolls approximately correspond to the lowest tide levels, enabling precise estimation of annual RSL changes.

Our ongoing research is targeting such coastal geology of Luzon Island, the Philippines. The central portion of the island's western coast is characterized by Holocene marine terraces, indicative of past coseismic uplifts. In addition, Pleistocene terraces are identified, documenting longer-term deformation over the past hundred thousand years, and coral microatolls also provide insights into finer-scale RSL changes. Our investigation involves remote sensing terrain interpretation employing digital elevation models (DEM), complemented by a simulation-based approach to reconstruct past RSL changes. These deformation patterns provide insight into the underlying mechanism associated with subduction structures.

Recent advancements in geological surveying underscore that records across various timescales cannot be treated as simple extrapolations or interpolations of other observations. To fully grasp the recurrence of past earthquakes, it becomes necessary to establish connections between observations across different timescales, rather than fixating on isolated phenomena.

Failure of relatively weaker blocks within a stronger matrix as origin of non-volcanic tremor

Jason P. Morgan[1], Paola Vannucchi[2]

[1]SUSTech, China, [2]University of Florence, Italy

Here we report on geological observations and numerical model results that support the hypothesis that non-volcanic tremor at subduction megathrusts is often created by conditions involving the seismic failure of relatively weaker blocks within a stronger matrix. In shallow portions of the subduction megathrust, pre-subduction and subduction-linked diagenesis and metamorphism can lead to a strength-inversion from what initially formed as a weak matrix with relatively stronger blocks to a stronger matrix with embedded relatively weaker blocks. Tremor with the observed characteristic of nearly constant source durations for all observed magnitudes will naturally occur when the now-weaker blocks fail seismically while their surrounding matrix has not yet reached a state of general seismic failure. At deeper levels within the subduction megathrust, compositionally-dependent-metamorphism of compositionally distinct 'blocks' and 'matrix' in a subduction shear channel can induce a similar rheological strength inversion, as can the build-up of dehydration-linked fluids within blocks in a less permeable matrix. Each of these distinct geological scenarios implies similar tremor behaviour that is linked to a characteristic block scale within the subduction shear channel.

Matrix stresses will be enhanced by block failure resulting in periods of tremor-rich slow-slip events, with a non-linear matrix rheology this tendency will be enhanced. Shear channel stresses will only diminish significantly after seismic failure occurs in the stronger matrix, e.g. after a micro-earthquake or earthquake, not due to the effects of tremor alone thus slow-slip events and tremor will tend to be correlated as observed. Numerical results for simple and 'geological' block-matrix patterns show similar stress and tremor evolution. We propose that this simple mechanical hypothesis can be fruitfully explored as an enhancement and alternative to mechanisms linked to asperities or fluid generation. The weak blocks do not act as asperities, instead their tremorgenic failure is being induced by aseismic matrix creep. Fluid generation and migration may preferentially occur within both the higher permeability blocks (where both fluids and high-permeability conditions may be generated during p-T conditions associated with dehydration reactions) and in post-earthquake fault zones after the matrix fails seismically.

Quantitative Detection of Tectonic Tremor Migration Events Using Characteristics of Tremors and Seismicity

Seiya Yano[1], Satoshi Ide[1]

[1]Dept. EPS, Univ. Tokyo

Tectonic tremors have been detected mainly in plate boundaries, and thought to be related to giant earthquakes. The spatial distribution of tremors consists of characteristic structures over a wide scale range, from ~100 km segments to ~km clusters, in which various migration patterns have been reported (e.g., Shelly et al., 2007; Ghosh et al., 2010; Houston et al., 2011; Yabe & Ide, 2014). Such structures and migration patterns may reflect the physical properties and status on the plate interface. If we regard each migration series as one event, its magnitude and duration are intermediate between those of tremors and slow slip events (e.g., Wech et al., 2010; Bletery et al., 2017; Gombert & Hawthorne, 2023), which supports the hypothesis that various slow earthquakes are different manifestations of a single broadband phenomenon (Ide et al., 2007; Ide & Beroza, 2023). Since the definition of migration events have yet been uncertain, we try to develop a scheme to quantitatively characterize migration events, based on characteristic metrics of tremors and seismicity.

This scheme uses tremor-candidate events detected by the envelope correlation method. From these candidates, we extract tremors by a density-based clustering, based on the nearest-neighbor distances (Zaliapin & Ben-Zion, 2013) and event characteristics, such as magnitude, duration, and depth. Then we apply another clustering using the nearest-neighbor distances among the extracted tremors, and systematically identify migration events. This scheme detected more than twice as many tremors as the previous catalog in western Japan (Mizuno & Ide, 2019), including short-duration events, which have been identified as low-frequency earthquakes. We confirmed that many migration events occurred repeatedly at almost the same locations, and that cluster-scale migration events occur in succession, leading to a larger segment-scale scale migration.

Mapping the source of shallow tremors and VLFEs commonly using Source-Scanning Algorithm

Motoki NEGISHI[1], Kazushige OBARA[1], Shunsuke TAKEMURA[1], Takeshi AKUHARA[1] , Yusuke YAMASHITA[2], Hiroko SUGIOKA[3], Masano SHINOHARA[1]

1. ERI, Univ. of Tokyo, 2. DPRI, Kyoto Univ., 3. Kobe Univ.

Shallow slow earthquakes actively occurred from December 2020 to January 2021 in the shallow part of the plate boundary near the Nankai Trough off the southeast coast of the Kii Peninsula, Japan. Shallow tremors and very low-frequency earthquakes (VLFEs) have been observed by permanent seismic networks of F-net and DONET, and their activity patterns and source parameters have been studied (e.g., Ogiso & Tamaribuchi, 2022; Takemura et al., 2022). During this episode, shallow tremors and VLFEs migrated from DONET1 to DONET2 areas however, there is an observational gap for shallow slow earthquake activity between DONET1 and DONET2 areas. In this study, therefore, we performed Source-Scanning Algorithm (SSA) (Kao and Shan, 2004) to image the spatiotemporal distribution of sources of the shallow tremors and VLFEs using waveforms observed by a high-density ocean bottom seismometer (OBS) array and DONET.

The dense OBS array used in the study consisted of 15 three-component seismometers with a natural frequency of 1 Hz installed in the region between DONET1 and DONET2 during the period September 20, 2019, to June 1, 2021(Akuhara et al.,2023). It includes two sets of cross-shaped arrays composed of five seismometers with a station spacing of approximately 2 km. We used this OBS array and DONET to achieve comprehensive detection of shallow tremors and VLFEs during the episode from December 2020.

Continuous waveform data from OBS array and DONET were filtered by different bandpass filters of 2-8 Hz and 0.1-0.15 Hz for tremor and VLFE, respectively. Then SSA method was commonly applied to these waveforms to image sources of shallow tremors and VLFEs. Both tremors and VLFEs show similar results as in the previous catalogs like a general migration pattern from northeast to southwest in December 2020. For the VLFEs, we detected events not listed in the catalogs of previous studies by visual inspection and imaged their source locations consistent with the migration pattern of pre-known shallow slow earthquake episodes.

International Joint Workshop on Slow-to-Fast Earthquakes 2023

General Information for on-site participants

Open hours
Ito Hall, Ito International Research Center, workshop venue, will be open at 9:00 on Day 1 (Sep. 13) and 8:30 on Day 2 and 3 (Sep. 14-15). Registration desk opens at the same time.

Language
The official conference language is English. No simultaneous interpretation will be provided.

Badges
The participant name badge will be provided at the registration desk. All participants are requested to wear the badge throughout the workshop.

Social party fee (advance registration only)
Beverage fee (3,000 JPY) will be collected at the registration desk when you receive the participant name badge.

Wi-Fi
Wi-Fi (including eduroam and UTokyo Wi-Fi) is available at the venue.

Campus tour
Walking tour on Hongo campus, UTokyo will be conducted by students on Day 3 (Sep. 15) after the morning session (English/Japanese). No reservation is required.
Meet: in front of the entrance after the morning session on Day 3
Duration: approx. 1hr.

Field trip (advance registration only)
Meet at: 8:00 a.m., Sep. 16th (Sat), at Univ. Tokyo (Hongo Campus)
Breakup: around 18:00 p.m. at JR Soga station

Mobile phone policy
Using mobile phones during the session is prohibited. Please turn off or set to silent mode.

Photography
Photographing / recording sessions are strictly prohibited.
Notice: Please note that the organizer will be taking photos in the venue for the purpose to use in conference report /website / other media.
Group photo will be taken after the oral session of Day 2 (Sep. 14).

Lost and found
Contact the registration desk in case of personal belongings being lost or found. Belongings not picked up during the workshop will be handed over to the venue.

Refreshments
Coffee / tea during the breaks will be served daily. Bringing your own food and drink (=anything that has not been served at the venue or purchased from the vending machine in

the building) is prohibited.

Meal
Meals will not be served during the workshop.
Hongo street where many restaurants are located is right behind the venue.
For location and open hours of on-campus cafeterias, please refer to the following link.
https://www.utcoop.or.jp/en/shops/hongo/

Baggage
In case you need your baggage to be stored on Day 3 (Sep. 15), please contact the registration desk.

Smoking
No smoking allowed on the premises.

COVID-19
“Guidelines for preventing of the spread of COVID-19 infection” by the University of Tokyo” is applied to all the participants.
https://www.u-tokyo.ac.jp/content/400214248.pdf
https://www.u-tokyo.ac.jp/content/400214358.pdf (in Japanese)

*Please contact the secretariat (sfeq-office-group@g.ecc.u-tokyo.ac.jp) in case a participant feels unwell, including having a fever while the workshop or field trip is taking place.

Presentation Guideline

*Please contact sfeq-office-group@g.ecc.u-tokyo.ac.jp for inquiries on presentation.

For oral presenters
Screen aspect ratio: 16:9 is preferred.
Presentation duration is 45 minutes including 10-minute discussion for the keynote speakers and 15 minutes including 3-minute discussion for other speakers. Bell rings at 30, 35 and 45 minutes for keynote speakers and 10, 12, 15 minutes for 15-minute speakers.
Presenters will use their own PCs for presentation. The connector type is HDMI. Presenters are recommended to check the connection and compatibility with the video projector in the session room during the break before their presentation.

For poster presenters
Poster board size: W900mm, H2400mm (A0 841*1189mm is preferred).
All the posters should be PORTRAIT style.
The poster layout map and pins will be supplied.
Posters are to be posted on the assigned boards by lunch time of Day 1 (Sep. 13) and to be removed by 16:00 on Day 3 (Sep. 15). Posters remained on the boards after 16:00 of Sep. 15 will be disposed by LOC.

International Joint Workshop on Slow-to-Fast Earthquakes 2023

Information for on-line participants

Oral session will be broadcasted using Zoom. Meeting ID will be informed to the registered participants before the workshop starts. Please do not distribute meeting ID.

Organizers

“Science of Slow-to-Fast Earthquakes”
Grant-in Aid for Transformative Research Area, MEXT, Japan.
Secretariat at Earthquake Research Institute, the University of Tokyo
1-1-1 Yayoi, Bunkyo-ku, Tokyo, JAPAN 113-0032
Email: sfeq-post-group@g.ecc.u-tokyo.ac.jp

Co-organized by:

Workshop " Toward a comprehensive understanding of all seismic phenomena from slow earthquakes to fast ruptures" supported by ERI Joint Usage/Research Center Program

Workshop " Workshop on Slow-to-fast earthquake and understanding its process and circumstance for disaster mitigation of megathrust earthquakes" supported by DPRI Joint Usage/Research Center Program

Supported by:

The Second Earthquake and Volcano Hazards Observation and Research Program (Earthquake and Volcano Hazard Reduction Research)

Workshops in the past

2022, Nara Kasugano International Forum I-RA-KA, Nara, Nara, Japan
2021, online
2020, online
2019, Sakura Hall, Tohoku University, Sendai, Miyagi, Japan
2018, Across Fukuoka, Fukuoka, Japan
2017, Hotel Mystays Matsuyama, Ehime, Japan
2016, Earthquake Research Institute, the University of Tokyo, Tokyo, Japan
2015, Graduate School of Environmental Studies, Nagoya University, Nagoya, Japan
2014, Uji campus, Kyoto University, Uji, Kyoto, Japan
2013, ERI, University of Tokyo, Tokyo, Japan
2012, ERI, University of Tokyo, Tokyo, Japan

Time Schedule (Overview)

Sep.13		Activity/Presenter	Chair
9:00		Registration	
10:00		Opening Session/General Instructions	
10:05	O01	Saeko KITA (Building Research Institute)	Ito / Ide
10:50	O02	Zahra ZANDVAKILI (JAMSTEC X-star Kochi)	
11:05	O03	Novia ANGGRAINI (Hokkaido Univ.)	
11:20		Break (coffee)	
11:50	O04	Kate Huihsuan CHEN (National Taiwan Normal Univ.)	
12:35	O05	Satoshi IDE (Univ. of Tokyo)	
12:50	O06	Kuo-En CHING (National Cheng Kung Univ.)	
13:05		Lunch	
14:00		Poster Core Time (coffee)	
16:00	O07	Asaf INBAL (Tel Aviv Univ.)	Baba / Inoue
16:15	O08	Yoshihiro ITO (Kyoto Univ.)	
16:30	O09	Eiichiro ARAKI (JAMSTEC)	
16:45	O10	Yoshitaka HASHIMOTO (Kochi Univ.)	
17:00	O11	Masaoki UNO (Tohoku Univ.)	
17:15	O12	Diana MINDALEVA (Tohoku Univ.)	
17:30		General Discussion	
18:00		Close/Party	

Sep.14		Activity/Presenter	Chair
9:00	O13	Atsushi OKAMOTO (Tohoku Univ.)	Hamada / Yamaguchi
9:45	O14	Matt IKARI (Univ. of Bremen)	
10:00	O15	Hiroyuki NODA (Kyoto Univ.)	
10:15		Break (coffee)	
10:45	O16	Michael STRASSER (Univ. of Innsbruck)	
11:30	O17	Paola VANNUCCHI (Univ. of Florence)	
11:45	O18	Takeshi TSUJI (Univ. of Tokyo)	
12:00		Group Photo	
12:05		Breakout Session	
13:00		Lunch	
14:00		Poster Core Time (coffee)	
16:00	O19	Gaku KIMURA (JAMSTEC)	Fukuchi / Shimura
16:15	O20	Asuka YAMAGUCHI (Univ. of Tokyo)	
16:30	O21	Hanaya OKUDA (JAMSTEC X-star Kochi)	
16:45	O22	Ken-ichi HIRAUCHI (Shizuoka Univ.)	
17:00		General Discussion / Breakout Summary	
18:00		Close	

Sep.15		Activity/Presenter	Chair
9:00	O23	Ross STEIN (Temblor / Stanford Univ.)	Kato / Tanaka
9:45	O24	Ryo KURIHARA (Hot springs research institute of Kanagawa Pref.)	
10:00	O25	Ahmed ELBANNA (Univ.of Illinois Urbana Champaign)	
10:15		Break (coffee)	
10:45	O26	Anne SOCQUET(Univ. Grenoble Alpes)	
11:30	O27	Nelson PULIDO (NEID)	
11:45	O28	Rikuto FUKUSHIMA (Kyoto Univ.)	
12:00		Bussiness Meeting for SFEQ (in Japanese) Campus Tour by Students	
13:00		Lunch	
14:00	O29	Alexandre SCHUBNEL (ENS Paris)	Matsuzawa / Yamaya
14:30	O30	Yoshihiro KANEKO (Kyoto Univ.)	
14:30	O31	Zhu-Yuan LIN (Osaka Univ.)	
14:45	O32	Chengrui CHANG (Univ. of Tokyo)	
15:00		Break (coffee)	
15:30	O33	Takehito SUZUKI (Aoyama Gakuin Univ.)	
15:45	O34	Takanori MATSUZAWA (NEID)	
16:00	O35	Tomoaki NISHIKAWA (Kyoto Univ.)	
16:15	O36	Adnan BARKAT (The Chinese Univ. of Hong Kong)	
16:30		General Discussion	
17:00		Closing Session	

Day 1 (13 Sep.)					
Registration	9:00	10:00	1:00		
Opening Session/ General Instructions	10:00	10:05	0:05		
O01	10:05	10:50	0:45	Saeko KITA (Building Research Institute)	M~7 inland earthquakes at anomalously deep focal depth and their relationship with seismic velocity and attenuation structure beneath Hidaka collision zone, northern Japan
O02	10:50	11:05	0:15	Zahra ZANDVAKILI (JAMSTEC XSTAR Kochi)	Geofluid behavior prior to 2018 Hokkaido eastern Iburi earthquake based on groundwater geochemistry
O03	11:05	11:20	0:15	Novia ANGGRAINI (Hokkaido Univ.)	Searching for Very Low Frequency Earthquakes (VLFE) around Western Kuril Trench
Break	11:20	11:50	0:30		
O04	11:50	12:35	0:45	Kate Huihsuan CHEN (National Taiwan Normal Univ.)	The interplay between fast and slow earthquakes and its relation with fluid pressure cycling in a collisional mountain belt
O05	12:35	12:50	0:15	Satoshi IDE (Univ. of Tokyo)	Tectonic tremors in Taiwan, 2012-2022
O06	12:50	13:05	0:15	Kuo-En CHING (National Cheng Kung Univ.)	Mud Tectonics and Creeping Faults in SW Taiwan
Lunch	13:05	14:00	0:55		
Poster Core Time	14:00	16:00	2:00		
O07	16:00	16:15	0:15	Asaf INBAL (Tel Aviv Univ.)	Dynamic triggering along the Dead Sea Transform uncovers tremor source physics
O08	16:15	16:30	0:15	Yoshihiro ITO (Kyoto Univ.)	Effects of subducting seamount on slow and fast seismicity in the Guerrero Seismic Gap, Mexico
O09	16:30	16:45	0:15	Eiichiro ARAKI (JAMSTEC)	Fiber optic sensing experiments in the seafloor and seafloor borehole in the Nankai Trough
O10	16:45	17:00	0:15	Yoshitaka HASHIMOTO (Kochi Univ.)	Geological constraints on slip duration and slip rate in exhumed accretionary complexes for a comparison in a scaling law of slow earthquakes
O11	17:00	17:15	0:15	Masaoki UNO (Tohoku Univ.)	Physical conditions of magmatic-hydrothermal fracturing in deep crust: Records of subvolcanic deep low-frequency earthquakes?
O12	17:15	17:30	0:15	Diana MINDALEVA (Tohoku Univ.)	Geological tracers of temporal evolution of fluid flow in high-grade metamorphic rocks related to seismic events in the middle crust
General Discussion	17:30	18:00	0:30		
Close / Party	18:00	20:00	2:00		

Day 2 (14 Sep.)					
O13	9:00	9:45	0:45	Atsushi OKAMOTO (Tohoku Univ.)	Fluid flow and fluid-rock interactions at shallow mantle wedge
O14	9:45	10:00	0:15	Matt IKARI (Univ. of Bremen)	The potential use of laboratory SSEs as stick-slip precursors in simulated fault gouges
O15	10:00	10:15	0:15	Hiroyuki NODA (Kyoto Univ.)	High-velocity friction experiments for samples of various size
Break(coffee)	10:15	10:45	0:30		
O16	10:45	11:30	0:45	Michael STRASSER (Univ. of Innsbruck)	Major fast megathrust earthquake recurrence in the Japan Trench? Long-term (> 17 000 years) perspectives from submarine paleoseismology
O17	11:30	11:45	0:15	Paola VANNUCCHI (Univ. of Florence)	Shallow transient fault slip and frictional instabilities at the Sumatra-Andaman subduction zone
O18	11:45	12:00	0:15	Takeshi TSUJI (Univ. of Tokyo)	Spatiotemporal variation of pore pressure and stress state in the plate subduction zone
Group Photo	12:00	12:05	0:05		
Breakout Session	12:05	13:00	0:55		
Lunch	13:00	14:00	1:00		
Poster Core Time	14:00	16:00	2:00		
O19	16:00	16:15	0:15	Gaku KIMURA (JAMSTEC)	Frontal Thrust ramp-up and slow Earthquakes due to Underthrust of Basement high Relief in the Nankai Trough
O20	16:15	16:30	0:15	Asuka YAMAGUCHI (Univ. of Tokyo)	Preliminary results of R/V Yokosuka YK23-10S cruise: submersible survey along the Shionomisaki submarine canyon in the Nankai Trough
O21	16:30	16:45	0:15	Hanaya OKUDA (JAMSTEC XSTAR Kochi)	Weakening of clayey gouge at intermediate velocities and its potential effect on slow earthquakes
O22	16:45	17:00	0:15	Ken-ichi HIRAUCHI (Shizuoka Univ.)	Frictional and mechanical properties of episodic tremor and slip zone: A brief review
General Discussion / Breakout Summary	17:00	18:00	1:00		
Close	18:00				

Day 3 (15 Sep.)					
O23	9:00	9:45	0:45	Ross STEIN (Temblor / Stanford Univ.)	Central shutdown and surrounding activation of aftershocks from megathrust earthquake stress transfer
O24	9:45	10:00	0:15	Ryo KURIHARA (Hot springs res.inst.of Kanagawa Pref.)	Lower dominant frequencies of fast earthquakes at the east of Izu peninsula
O25	10:00	10:15	0:15	Ahmed ELBANNA (Univ.of Illinois Urbana Champaign)	Revealing The Dynamics of the Feb 6th 2023 M7.8 Kahramanmaraş/Pazarcik Earthquake: Near-Field Records and Dynamic Rupture Modeling
Break(coffee)	10:15	10:45	0:30		
O26	10:45	11:30	0:45	Anne SOCQUET(Univ. Grenoble Alpes)	Exploring aseismic slip beyond typical sizes and durations, and their potential link to earthquakes
O27	11:30	11:45	0:15	Nelson PULIDO (NEID)	Megathrust earthquake potential in Central Peru (Lima region) based on stress accumulation rates and the earthquake energy balance at the subduction interface
O28	11:45	12:00	0:15	Rikuto FUKUSHIMA (Kyoto Univ.)	Physics-Informed Neural Networks for fault slip monitoring: simulation, frictional parameter estimation, and prediction on slow slip events in a spring-slider system
Bussiness Meeting for SFEQ	12:00	13:00	1:00	(Campus Tour by Students)	
Lunch	13:00	14:00	1:00		
O29	14:00	14:15	0:15	Alexandre SCHUBNEL (ENS Paris)	Nucleation of Laboratory Earthquakes: Quantitative Analysis and Scalings
O30	14:15	14:30	0:15	Yoshihiro KANEKO (Kyoto Univ.)	Physical mechanism of the temporal decrease of a Gutenberg-Richter b-value prior to a large earthquake
O31	14:30	14:45	0:15	Zhu-Yuan LIN (Osaka Univ.)	Rheology and structure of model smectite clay from coarse-grained molecular dynamics
O32	14:45	15:00	0:15	Chengrui CHANG (Univ. of Tokyo)	The Effect of a Fluid Phase on Rheological Properties of a Sheared Granular System
Break(coffee)	15:00	15:30	0:30		
O33	15:30	15:45	0:15	Takehito SUZUKI (Aoyama Gakuin Univ.)	Condition of transition between slow and fast earthquakes in terms of fluid pressure and porosity
O34	15:45	16:00	0:15	Takanori MATSUZAWA (NEID)	Tremor activity in April 1988 revealed from analog seismograms of the Kanto-Tokai Observation Network
O35	16:00	16:15	0:15	Tomoaki NISHIKAWA (Kyoto Univ.)	Comparison of statistical seismicity models of low-frequency earthquakes (LFEs) and its implications for the mechanisms governing LFE activity
O36	16:15	16:30	0:15	Adnan BARKAT (The Chinese Univ. of Hong Kong)	Deciphering the interplay between permeability and seismicity rate changes at Axial Seamount caused by dynamic stresses
General Discussion	16:30	17:00	0:30		
Closing Session	17:00				

45-min talks: Keynote speakers

Poster		
In-Person (P01-P79)		
P01	Mamoru NAKAMURA	Changes in very low frequency earthquake activity in the South Ryukyu Trench over 23 years
P02	Mari HAMAHASHI	Shallow fault-related folding and late Quaternary slip rate of the Osaka Bay Fault, western Japan
P03	Syed Idros BIN ABDUL RAHMAN	New seismicity catalog and Site characterization from a regional array in Bangladesh: possible correlation of seismicity and seasonal monsoon
P04	Taku UEDA	Shear strain energy change estimated by the current crustal deformation in Japan and spatial correlation with the crustal seismicity
P05	Akemi NODA	Mechanical plate coupling along the Sagami trough estimated from GNSS data and implication for the generation mechanism of great thrust-type earthquakes and slow slip events
P06	Takuro IMADERA	Detection of immediate aftershocks following the 2011 Tohoku Earthquake using a seismic array in the Kanto region
P07	Amane SUGII	Development of a method for determining the epicenter of tectonic tremors using a deep learning decision basis method
P08	Yuya JINDE	Extraction of deep tectonic tremor waveforms using deep learning: Application to Hi-net stations in the Shikoku region
P09	Akiko TAKEO	Current situation of onshore broadband seismic observation for slow earthquakes in Japan and worldwide, 2023
P10	Yohei HAMADA	Controlled Shear Stress Experiments for Spontaneous Generation of Slow Earthquakes using a Rotating Shear Apparatus
P11	Suguru YABE	Evaluating uncertainties in CMT inversion to estimate non-double couple components of earthquakes
P12	Takane HORI	Numerical experiments using a friction law both for rapid and slow sliding with radiation damping effect
P13	Ryoko NAKATA	Numerical simulation with a multiscale circular patch model in the northern segment along the Japan Trench (IV)
P14	Miki TAKAHASHI	Runaway slip in fault rock analog
P15	Takahiro HOSOKAWA	Geological constraint on fluid pressure ratio during mélange formation in a shallow ductile-to-brittle transition zone along a subduction plate interface
P16	Rina FUKUCHI	Comparison between the porosity of gravels of submarine landslide deposit and that of accretionary prism sediment in the off-Kumano Nankai Trough
P17	Taizo UCHIDA	Exothermic events in the fossil seismogenic fault yielded as the secondary magnetization; Cretaceous accretionary complex, Shimanto Belt
P18	Gaspard FARGE	Along-strike segmentation of tremor and its relationship with the hydraulic structure of the subduction zone
P19	Takashi TONEGAWA	Temporal variation of the physical property of the plate boundary in the Nankai subduction zone
P20	Kazunori MURAMATSU	Evaluation of the dip angle of the Median Tectonic Line active fault system by quasi-dynamic earthquake sequence simulation
P21	Ching-Chieh SU	The role of afterslip in the stress interaction between repeating earthquakes and microseismicity in Parkfield
P22	Keisuke ARIYOSHI	Extension of Aseismic Slip Propagation Theory to Slow Earthquake Migration
P23	Ryoya MATSUSHIMA	3D viscoelastic earthquake sequence simulation of subduction zone with inland faults
P24	Yuki SHINOHARA	Repeated viscoelastic fracturing under shear as an analog of slow to fast earthquakes
P25	Ryo MIZUSHIMA	Model for heterogeneous faults with randomly distributed frictional parameters
P26	Edward VINIS	Systematic Changes in Quartz Precipitation on Granite Surfaces Revealed by Hydrothermal Experiments
P27	Rie NAKATA	Seismic imaging for seamount subduction at Hyuga-Nada using active and passive OBS data
P28	Yanhan CHEN	New insight of low frequency earthquakes (LFEs) in continuous ocean bottom seismometers at the Guerrero Seismic Gap, Mexico
P29	Ketzallina FLORES	Identification of Possible Tsunami Earthquakes along the Mexican Subduction Zone
P30	Madison FRANK	Deformation mechanisms and rheology of mélange shear zones associated with seamount subduction
P31	Ruyu YAN	Tidal sensitivity of tectonic tremors in Hikurangi subduction zones
P32	Yusuke YOKOTA	Development of UAV technology to realize high-frequency GNSS-A observation: experimental verification
P33	Tomohiro INOUE	Spatiotemporal evaluations for configuration of a sensor network to detect slow slip events from the seafloor deformation signal in the Hikurangi subduction zone
P34	Shun ADACHI	Adjoint tomography of an accretionary wedge and shallow slow-slip regions in the North Island of New Zealand
P35	Sando SAWA	b values dependency on olivine grain size in phase transformation faulting: Implication for deep-focus earthquakes
P36	Sambuddha DHAR	Illuminating low-viscosity zone beneath Quaternary volcanoes by numerical simulation of postseismic deformation of the 2011 Tohoku-oki earthquake
P37	Satoru BABA	Seismological observation by distributed acoustic sensing using automatic phase picking method around the Tsugaru Strait, northeastern Japan
P38	Thomas YEO	Kilometre-scale ductile fractures instigated by deformation-induced nanocavities
P39	Daisuke SATO	Interlocking asperities revealed inside the focal zones of Bungo-Channel slow slip events and massive earthquakes along the Nankai Trough, Japan
P40	Shukei OHYANAGI	Periodic swarm of shallow earthquake and tremor near the Japan Trench, Off Fukushima

P41	Shunsuke TAKEMURA	Effects of site amplification and high-frequency seismic wave propagation on seismic energy estimation for shallow tremors
P42	Akifumi TAKAYAMA	Preparation for an estimation of seismic structures around slow earthquake areas in the Nankai subduction zone using receiver functions in multi-frequency bands
P43	Kazutoshi IMANISHI	Analysis of slow-to-fast earthquakes using strain and rotational observations
P44	Kentaro KUNIYOSHI	Slow and fast seismic activity in the southeastern Guerrero seismic gap from 2022 to 2023
P45	Minoru IDENO	Identification of Eruptive Activity Anomalies at Mt. Aso Based on the Gradient Boosting Method of Multimodal Observation Data from Seismographs and GPS
P46	Reiju NORISUGI	Machine learning predicts earthquakes in the continuum model of a rate-and -state fault with frictional heterogeneities
P47	Yuto KANO	Seismic source spectral properties of dynamic rupture with a self-similar, self-healing slip pulse
P48	Kazuki SAWAYAMA	Direct investigations of the fracture flow with asperity contact, and its relationship to the geophysical properties
P49	Francesco GRIGOLI	Waveform-based methods for the analysis of Distributed Acoustic Sensing(DAS) data
P50	Kodai SAGAE	Fine-scale hypocenter migration of earthquake swarms beneath the northeastern Noto Peninsula, Japan
P51	Osamu SANDANBATA	Tsunamigenic faulting events in submarine calderas: Observations and physics
P52	Samriddhi PRAKASH MISHRA	Towards adjoint tomography of the Nankai and Kyushu subduction zones
P53	Yusuke MUKUHIRA	Scaling Microseismic Cloud Shape during Hydraulic Stimulation using In-situ Stress and Permeability
P54	Koki MASUDA	New Single-station Detection Method for Seismic Slow Earthquakes
P55	Seiya MAEHARA	Stress and temperature estimation for Sanbagawa metamorphic rocks in Kanto Mountains: A possibility of occurrence of deep slow earthquakes
P56	Hitoshi HIROSE	Development of a machine learning model to detect short-term SSEs from tilt records
P57	Akito TSUTSUMI	Effect of the thickness of gouge layer on the frictional weakening behavior of fault at high slip velocities
P58	Keigo TASHIRO	Experimental study on fault weakening due to shear-induced pore pressure increase along a fault in shallow portion of accretionary prism
P59	Satoshi TONAI	The role of backthrust in the development of the Coulomb wedge fromsandbox experiments
P60	Keisuke YANO	Objective clustering of GNSS velocities based on parallel translation and rotational motion for the identification of crustal blocks
P61	Kai KOYAMA	Examination of TEC anomalies in the ionosphere before large earthquakes
P62	Futoshi YAMASHITA	"Giant" rock friction apparatus for understanding faulting processes on multi-spatio-temporal scales: A preliminary report
P63	Kurama OKUBO	Two types of foreshocks generated by an artificial gouge patch on a 4-m-long laboratory fault
P64	Kazuya SHIRAISHI	Structural features revealed by multi-year seismic survey campaign and implication to seismic activities in the Nankai Trough
P65	Yuki KASAI	Frictional properties of the imbricate thrust material from the shallow part of the Miura accretionary prism, Southern Miura Peninsula, central Japan
P66	Yusuke SHIMURA	Origin of serpentinite in the Cretaceous Shimanto accretionary complex
P67	Hiromu SAKAUE	Spatiotemporal evolution of Slow Slip Events along the Southern Ryukyu subduction zone during 2017-2022
P68	Lina YAMAYA	Centroid moment tensor analysis for M6-class offshore earthquakes using long-period seismograms of the Seafloor Observation Network for Earthquakes and Tsunamis along the Japan Trench (S-net)
P69	Akira WATANABE	On the network-MT surveys in the Kii Peninsula, southwestern Japan, aiming at obtaining deep 3-D electrical resistivity structure
P70	Yuta MITSUI	Expansion rates of aftershock zones for magnitude-7 class earthquakes around Japan possibly related to stress states
P71	Ryoichiro AGATA	Ensemble estimation of seismic velocity and hypocenter in the Nankai Trough empowered by physics-informed neural network
P72	Takeshi AKUHARA	Tectonic tremor distribution and migration at Kumano-nada: insights from ocean-bottom seismometer deployment between DONET1 and 2
P73	Ritsuya SHIBATA	The characteristic of rupture propagation during earthquakes in Japanese crustal area
P74	Paul Caesar M. FLORES	Linking geometrical and physical property changes along Nankai Trough with slow earthquake activity using dense reflection survey
P75	Ryosuke ANDO	Dynamic Rupture Simulation Reveals Fault Geometrical Effect on the 2023, Kahramanmaras and Ekinozu, Turkey, Earthquake Sequence
P76	Junki KOMORI	Advancements in Paleoseismology through Coastal Landforms and Coral Records in Subduction Zones
P77	Jason MORGAN	Failure of relatively weaker blocks within a stronger matrix as origin of non-volcanic tremor
P78	Seiya YANO	Quantitative Detection of Tectonic Tremor Migration Events Using Characteristics of Tremors and Seismicity
P79	Motoki NEGISHI	Mapping the source of shallow tremors and VLFEs commonly using Source-Scanning Algorithm

Participants's list			
P34	ADACHI	Shun	Kyoto University
	ADITIYA	Arif	Nagoya University
P71	AGATA	Ryoichiro	Japan Agency for Marine-Earth Science and Technology (JAMSTEC)
	AIDA	Koki	Department of Earth and Planetary Environmental Science, Faculty of Science, The University of Tokyo
	AIKEN	Chastity	French Research Institute for the Exploitation of the Sea
	AKISHIBA	Manato	Kochi University
P72	AKUHARA	Takeshi	ERI, the University of Tokyo
	AMEZAWA	Yuta	Geological Survey of Japan, AIST
P75	ANDO	Ryosuke	The University of Tokyo
O03	ANGGRAINI	Novia	Institute of Seismology and Volcanology, Hokkaido University
	AOKI	Shigeki	Japan Meteorological Agency
	AOYAMA	Towako	ERI, the University of Tokyo
	ARAI	Ryuta	Japan Agency for Marine-Earth Science and Technology (JAMSTEC)
	ARAKAWA	Hinako	Tokyo University of Science
O09	ARAKI	Eiichiro	Japan Agency for Marine-Earth Science and Technology (JAMSTEC)
P22	ARIYOSHI	Keisuke	Japan Agency for Marine-Earth Science and Technology (JAMSTEC)
	ASO	Naofumi	Tokyo University of Science
	AZUA	Kellen	Department of Geophysics, University of Chile
P37	BABA	Satoru	Japan Agency for Marine-Earth Science and Technology (JAMSTEC)
	BANNISTER	Stephen	GNS Science, New Zealand
O36	BARKAT	Adnan	The Chinese University of Hong Kong
	BECKER	Thorsten	The University of Texas at Austin
P03	BIN ABDUL RAHMAN	Syed Idros	Kyushu University
O32	CHANG	Chengrui	The University of Tokyo
P28	CHEN	Yanhan	Kyoto University
O04	CHEN	Kate Huihsuan	National Taiwan Normal University
O06	CHING	Kuo-En	National Cheng Kung University
	CHOULI	Audrey	ISTerre, University Grenoble Alpes
	COSTANTINO	Giuseppe	ISTerre, Université Grenoble Alpes (FR)
P36	DHAR	Sambuddha	Tohoku University
	DOKE	Ryosuke	Hot Springs Research Institute of Kanagawa Prefecture
	EL YOUSFI	Zaccaria	ISTerre, University of Grenoble
O25	ELBANNA	Ahmed	University of Illinois Urbana Champaign
	ESSING	David	Alfred Wegener Institute for Polar and Marine Research
P18	FARGE	Gaspard	University of California Santa Cruz
P29	FLORES	Ketzallina	Kyoto University
P74	FLORES	Paul Caesar M.	Yokohama National University
P30	FRANK	Madison	University of Tsukuba
	FUJIE	Gou	JAMSTEC
	FUJII	Harumi	Kobe University
	FUJINAKA	Tatsuya	Marine Earthquakes
	FUJISAWA	Hironobu	Tokyo University of Science
P16	FUKUCHI	Rina	Naruto University of Education
	FUKUDA	Kota	ERI, the University of Tokyo
O28	FUKUSHIMA	Rikuto	Graduate School of Science, Kyoto University
	FUKUSHIMA	SHUN	ERI
	FUNAKOSHI	Minoru	Japan Meteorological Agency
	GABRIEL	Alice-Agnes	Scripps, UCSD & LMU Munich
P49	GRIGOLI	Francesco	University of Pisa
P10	HAMADA	Yohei	Japan Agency for Marine-Earth Science and Technology (JAMSTEC)
P02	HAMAHASHI	Mari	Yamaguchi University
O10	HASHIMOTO	Yoshitaka	Kochi University
	HIGAKI	Anca	IFREMER, France
	HIGUCHI	Tomoyo	Tokyo University of Science
	HINO	Ryota	Tohoku University

O22	HIRAUCHI	Ken-ichi	Shizuoka University
P56	HIROSE	Hitoshi	Kobe University
	HIROSE	Takehiro	JAMSTEC
P12	HORI	Takane	Japan Agency for Marine-Earth Science and Technology (JAMSTEC)
P15	HOSOKAWA	Takahiro	Kochi University
	HOSONO	Hinako	Geological Survey of Japan, AIST
	HSIAO	Shih-Han	National Chengkung Universuty
	HU	Gui	ERI, the University of Tokyo
O05	IDE	Satoshi	The University of Tokyo
P45	IDENO	Minoru	The University of Tokyo
O14	IKARI	Matt	Marum, University of Bremen
	IKEHARA	Ken	Geological Survey of Japan, AIST
P06	IMADERA	Takuro	ERI, the University of Tokyo
P43	IMANISHI	Kazutoshi	Geological Survey of Japan, AIST
O07	INBAL	Asaf	Department of Geophysics, Tel Aviv University
P33	INOUE	Tomohiro	Institute of Industrial Science, The University of Tokyo
	ISHIKAWA	Tadashi	Japan coast guard
	ITABA	Satoshi	Geological Survey of Japan, AIST
O08	ITO	Yoshihiro	DPRI, Kyoto University
	ITOH	Yuji	ERI, University of Tokyo; ISTerre, Université Grenoble Alpes
	IWAKIRI	Kazuhiro	Japan Meteorological Agency
P08	JINDE	Yuya	Kanazawa University
	KAKIUCHI	Yusuke	School of Engineering, the University of Tokyo
	KAMATA	Shunichi	Hokkaido University
	KANEKI	Shunya	Geological Survey of Japan, AIST
O30	KANEKO	Yoshihiro	Kyoto University
P47	KANO	Yuto	Kyoto University
	KANO	Masayuki	Tohoku University
P65	KASAI	Yuki	Graduate School of Science, Kyoto University
	KATAYAMA	Hiroaki	Japan Meteorological Agency
	KATO	Aitaro	ERI, the University of Tokyo
O19	KIMURA	Gaku	Japan Agency for Marine-Earth Science and Technology (JAMSTEC)
	KINOSHITA	Yohei	University of Tsukuba
O01	KITA	Saeko	Building Research Institute
	KODAIRA	Shuichi	Japan Agency for Marine-Earth Science and Technology (JAMSTEC)
P76	KOMORI	Junki	Earth Observatory of Singapore, NTU
	KOYAMA	Yukinojo	The University of Tokyo
P61	KOYAMA	Kai	Graduate School of Science, Kyoto University
	KUBOTA	Tatsuya	National Research Institute for Earth Science and Disaster Resilience
P44	KUNIYOSHI	Kentaro	Graduate School of Science, Kyoto University
	KUO	Szu-Ting	National Central University, Taiwan
O24	KURIHARA	Ryo	Hot springs research institute of Kanagawa Prefecture
O31	LIN	Zhu-Yuan	Osaka University, Graduate school of Science
	MA	Yanxue	ERI, Utokyo
	MAEDA	Yuta	Nagoya University
	MAEDA	Sumire	National Research Institute for Earth Science and Disaster Resilience
P55	MAEHARA	Seiya	The University of Tokyo
P54	MASUDA	Koki	The University of Tokyo
	MATSUO	Ryo	Graduate School of Science, Kyoto University
P23	MATSUSHIMA	Ryoya	Department of Earth and Planetary Science, The University of Tokyo
O34	MATSUZAWA	Takanori	National Research Institute for Earth Science and Disaster Resilience(NEID)
	MENDO	Gerardo	Earthquake Research Institute, The University of Tokyo
O12	MINDALEVA	Diana	Tohoku University
P70	MITSUI	Yuta	Faculty of Science, Shizuoka University
	MIYAJIMA	Takumi	The University of Tokyo
	MIYAZAWA	Masatoshi	Kyoto Univ.
P25	MIZUSHIMA	Ryo	Osaka University, Graduate school of Science

	MOCHIZUKI	Kimihio	Earthquake Research Institute, Univ. of Tokyo
	MOORE	Gregory	University of Hawaii/AORI Utokyo
P77	MORGAN	Jason	SUSTech
P53	MUKUHIRA	Yusuke	Tohoku University
	MÜNCHMEYER	Jannes	ISTerre Grenoble
P20	MURAMATSU	Kazunori	The University of Tokyo
	NAGAE	Koya	JCG
	NAGAYA	Takayoshi	Tokyo Gakugei University
	NAKAJO	Sota	Osaka Metropolitan University
P01	NAKAMURA	Mamoru	University of the Ryukyus
	NAKAMURA	Masaki	MRI
	NAKAMURA	Yasuyuki	JAMSTEC
	NAKANO	Masaru	Japan Agency for Marine-Earth Science and Technology (JAMSTEC)
P27	NAKATA	Rie	ERI, the University of Tokyo
P13	NAKATA	Ryoko	The University of Tokyo
P79	NEGISHI	Motoki	ERI, the University of Tokyo
O35	NISHIKAWA	Tomoaki	DPRI, Kyoto University
	NISHIMOTO	Michelle	Japan Women's University
	NISHIO	Yoshiro	Kochi University
O15	NODA	Hiroyuki	Kyoto University
P05	NODA	Akemi	Meteorological Research Institute, Japan Meteorological Agency
	NOMURA	Shunichi	Waseda University
P46	NORISUGI	Reiju	Kyoto University
	OBANA	Koichiro	JAMSTEC
	OHTAKE	Kazuki	ERI, the University of Tokyo
P40	OHYANAGI	Shukei	Kyoto University
O13	OKAMOTO	Atsushi	Tohoku University
P63	OKUBO	Kurama	National Research Institute for Earth Science and Disaster Resilience(NEID)
O21	OKUDA	Hanaya	Japan Agency for Marine-Earth Science and Technology (JAMSTEC)
	OLIVIER	Djiogang Francis	University of DSCHANG Cameroon
	OTSUBO	Makoto	Geological Survey of Japan, AIST
	OTSUKA	Hideto	Tohoku University
	PARK	Jin-Oh	AORI, University of Tokyo
	PALGUNADI	Kadek	King Abdullah University of Science and Technology
	PECCI	Davide	University of Pisa
	PLATA-MARTINEZ	Raymundo	JAMSTEC
P52	PRAKASH MISHRA	Samriddhi	Graduate School of Science, Kyoto University
O27	PULIDO	Nelson	National Research Institute for Earth Science and Disaster Resilience(NEID)
	RADIGUET	Mathilde	ISTerre, Université Grenoble Alpes
	RAPAGNANI	Giacomo	University of Pisa
	RUAN	Yihuan	Kyoto University
P50	SAGAE	Kodai	Geological Survey of Japan, AIST
	SAISHU	Hanae	AIST
P67	SAKAUE	Hiromu	The University of Tokyo
P51	SANDANBATA	Osamu	ERI, the University of Tokyo
P39	SATO	Daisuke	Japan Agency for Marine-Earth Science and Technology (JAMSTEC)
P35	SAWA	Sando	Tohoku University
	SAWAKI	Yasunori	Geological Survey of Japan, AIST
P48	SAWAYAMA	Kazuki	Kyoto University
O29	SCHUBNEL	Alexandre	Laboratoire de Géologie de l'ENS PARIS, France
	SEO	Min-Seong	Seoul National University, South Korea
	SHANKER	Daya	Indian Institute of Technology Roorkee
	SHELLY	David	USGS
P73	SHIBATA	Ritsuya	Tokyo Institute of Technology
	SHIBAZAKI	Bunichiro	Building Research Institute
	SHIGEMATSU	Norio	Geological Survey of Japan, AIST
P66	SHIMURA	Yusuke	Geological Survey of Japan, AIST

P24	SHINOHARA	Yuki	Tokyo University of Science
	SHIOMI	Katsuhiko	NIED
P64	SHIRAISHI	Kazuya	Japan Agency for Marine-Earth Science and Technology (JAMSTEC)
	SIEGEL	Cristián Ed.	Universidad de Chile
O26	SOCQUET	Anne	University Grenoble Alpes
O23	STEIN	Ross	Temblor / Stanford University
O16	STRASSER	Michael	University of Innsbruck
P21	SU	Ching-Chieh	National Taiwan Normal University
P07	SUGII	Amane	Kanazawa University
	SUGIOKA	Hiroko	Kobe University
	SUMINO	Yutaka	Tokyo University of Science
O33	SUZUKI	Takehito	Aoyama Gakuin University
P14	TAKAHASHI	Miki	Geological Survey of Japan, AIST
P42	TAKAYAMA	Akifumi	Graduate School of Science, Kyoto University
P41	TAKEMURA	Shunsuke	ERI, the University of Tokyo
P09	TAKEO	Akiko	The University of Tokyo
	TAMARIBUCHI	Koji	Meteorological Research Institute
	TANAKA	Yoshiyuki	The University of Tokyo
	TANAKA	Yusuke	Tohoku University
	TANAKA	Sachiko	National Research Institute for Earth Science and Disaster Resilience
	TANIKAWA	Wataru	Japan Agency for Marine-Earth Science and Technology
	TARUMI	Yurika	The Mainichi Newspapers
P58	TASHIRO	Keigo	Graduate School of Science, Kyoto University
	TOH	Akiko	The University of Tokyo
P59	TONAI	Satoshi	Kochi University
P19	TONEGAWA	Takashi	Japan Agency for Marine-Earth Science and Technology (JAMSTEC)
O18	TSUJI	Takeshi	The University of Tokyo
	TSUSHIMA	Hiroaki	Meteorological Research Institute, Japan Meteorological Agency
P57	TSUTSUMI	Akito	Kyoto University
P17	UCHIDA	Taizo	Kochi University
	UCHIDE	Takahiko	Geological Survey of Japan, AIST
P04	UEDA	Taku	DPRI, Kyoto University
	UEDA	Mizuki	University of Tsukuba
	UJIIE	Kohtaro	University of Tsukuba
O11	UNO	Masaoki	Tohoku University
O17	VANNUCCHI	Paola	University of Florence
	VEEDU	Deepa Mele	Indian Institute of Technology Kanpur, India
	VILLEGAS	Juan-Carlos	Geophysical Institute of Peru
P26	VINIS	Edward	Tohoku University
	WALLIS	Simon	The University of Tokyo
	WANG	Lu	Tohoku University
P69	WATANABE	Akira	ERI, the University of Tokyo
	XIE	Qifeng	GFZ Potsdam
P11	YABE	Suguru	Geological Survey of Japan, AIST
O20	YAMAGUCHI	Asuka	Atmosphere and Ocean Research Institute, the University of Tokyo
	YAMAGUCHI	Tetsuo	The University of Tokyo
	YAMAMOTO	Akane	Nihon University
	YAMASAKI	Yuto	University of Tsukuba
P62	YAMASHITA	Futoshi	National Research Institute for Earth Science and Disaster Resilience(NEID)
P68	YAMAYA	Lina	National Research Institute for Earth Science and Disaster Resilience(NEID)
P31	YAN	Ruyu	University of Chinese Academy of Sciences
	YANG	Yuyun	The Chinese University of Hong Kong
P60	YANO	Keisuke	The Institute of Statistical Mathematics
P78	YANO	Seiya	The University of Tokyo
P38	YEO	Thomas	The University of Tokyo / GSJ
	YOKOBIKI	Takashi	JAMSTEC
P32	YOKOTA	Yusuke	Institute of Industrial Science, The University of Tokyo

	YOSHIOKA	Shoichi	Kobe University
O02	ZANDVAKILI	Zahra	Marine Core Research Institute, Kochi University
	ZHANG	Junli	MARUM, University of Bremen
	ZHANG	Hang	Earthquake Research Institute
	ZHAO	Yang	Atmosphere and Ocean Research Institute, the University of Tokyo
	ZHU	Weiling	Institute of Tibetan Plateau Research, Chinese Academy of Sciences